

Towards a reconstruction of the SUSY seesaw model

Dissertation zur Erlangung des
naturwissenschaftlichen Doktorgrades
der Bayerischen Julius-Maximilians-Universität Würzburg

vorgelegt von
Frank Deppisch
aus Ochsenfurt

Würzburg 2004

Eingereicht am: 6. August 2004
bei der Fakultät für Physik und Astronomie

1. Gutachter: Prof. Dr. R. Rückl
2. Gutachter: Prof. Dr. H. Fraas
der Dissertation.

1. Prüfer: Prof. Dr. R. Rückl
2. Prüfer: Prof. Dr. H. Fraas
3. Prüfer: Prof. Dr. J. Geurts
im Promotionskolloquium.

Tag des Promotionskolloquiums: 17. März 2005

Doktorurkunde ausgehändigt am:

Written materials miss the essence of reality [1].

Contents

1	Introduction	7
2	Supersymmetry	9
2.1	Beyond the Standard Model	9
2.2	The MSSM	12
2.3	Minimal supergravity	15
3	Slepton flavor violation	19
3.1	Low energy loop processes	19
3.1.1	$l_i \rightarrow l_j \gamma$	19
3.1.2	Other rare LFV processes	21
3.1.3	Electric dipole moments	22
3.2	Slepton pair production	23
3.2.1	e^+e^- collider	23
3.2.2	e^-e^- collider	31
3.2.3	Precision mass measurements	33
4	Supersymmetric seesaw	37
4.1	Theoretical framework	37
4.2	Renormalization group evolution	40
4.3	Bi-unitary parameterization	42
4.4	Leptogenesis	44
4.5	Neutrino data	47
5	Results for degenerate right-handed neutrinos	51
6	Results for hierarchical right-handed neutrinos	71
7	Bottom-up approach	81
8	Conclusions	87
A	Numerical parameters	99

B	MSSM notation and conventions	101
B.1	Neutralinos	101
B.2	Charginos	102
B.3	Charged Sleptons	102
B.4	Sneutrinos	103
B.5	Vertices	104
C	Renormalization Group Equations	107
C.1	SM	107
C.2	MSSM	108
C.3	SUSY seesaw	110
D	Processes	113
D.1	$l_i \rightarrow l_j \gamma$	113
D.2	$e^+ e^- \rightarrow \tilde{l}_j^+ \tilde{l}_i^-$	114
D.3	$e^- e^- \rightarrow \tilde{l}_i^- \tilde{l}_j^-$	115
D.4	$\tilde{l}_i^\pm \rightarrow l_\alpha^\pm \tilde{\chi}_a^0$	115

Chapter 1

Introduction

The discovery of neutrino masses and mixing by a combination of solar and atmospheric neutrino observations, as well as reactor and accelerator experiments [2–16] has now firmly established the incompleteness of the Standard Model (SM). This experimental progress is accompanied by a strong effort from theorists to explain the nature and source of the neutrino masses and their flavor transitions. The most elegant model for neutrino mass generation is the seesaw mechanism [17–19], in which very heavy right-handed neutrinos are introduced to the particle spectrum of the Standard Model. The seesaw mechanism can naturally explain the puzzling smallness of the left-handed neutrino masses, which are suppressed by the heavy masses of the right-handed neutrinos, $m_\nu = (100 \text{ GeV})^2/M_R$. With neutrino masses of the order $m_\nu \approx 0.1 \text{ eV}$, the mass scale M_R of the right-handed neutrinos is expected to be around 10^{14} GeV , i.e. close to the scale $M_{\text{GUT}} \approx 10^{16} \text{ GeV}$ of Grand Unified Theories (GUTs). This means that the low energy neutrino observables can act as an indirect probe to physics at the GUT scale.

A major drawback of the seesaw model is that it contains many free parameters, which can not be constrained by measurements of the light neutrino sector. In principle, neutrino mixing also implies charged lepton flavor violation (LFV), but this is strongly suppressed if only right-handed neutrinos are added to the Standard Model. In the seesaw mechanism, lepton flavor violating processes, like the decay $\mu \rightarrow e\gamma$, are vanishingly rare. Thus, charged lepton flavor violating processes can not be used to probe the seesaw mechanism, leaving the neutrino sector as the only source of information.

This picture changes dramatically if we supersymmetrize the theory. Independent from neutrino physics, supersymmetry (SUSY) is a fascinating theoretical concept, and is generally considered as the most promising candidate for a theory of physics above the TeV scale. Among many other virtues, SUSY provides an answer to the potential Higgs mass instability of the Standard Model and naturally permits the unification of gauge couplings at the GUT scale. Upcoming and planned future colliders, like the Large Hadron Collider (LHC) at CERN or TESLA, are designed to look for SUSY signals and, if found, to test the properties of the supersymmetric particles.

Combining supersymmetry and seesaw mechanism crucially affects the renormalization group equations (RGEs) of the theory. The slepton mass and trilinear coupling matrices

receive flavor violating corrections due to virtual effects of the right-handed neutrinos. The lepton flavor violation apparent in the neutrino sector is transmitted to the slepton sector, or to put it more appropriately, both are generated by the same mechanism. Generically, decay rates of the processes $\mu \rightarrow e\gamma$ and $\tau \rightarrow \mu\gamma$ can be expected close to their current experimental limits. This is particularly interesting, since some of the existing bounds will be improved significantly in the near future. The above LFV processes have been studied [20–48] in the context of the SUSY seesaw model, all pointing out that rare decays, especially $\mu \rightarrow e\gamma$, can considerably constrain the seesaw parameter space.

Rare decays are not the only possible observables for LFV, though. A main virtue of experiments at an e^+e^- linear collider (LC) is the clean environment allowing studies of the production and decay of new particles with low background. This not only enables precision measurements of particle properties, but also searches for very rare processes and small effects. Phenomenological investigations have indicated how tests of LFV at a high-energy LC could nicely complement searches for lepton flavor violating rare decays such as $\mu \rightarrow e\gamma$. Previous work [49–63] has mainly focussed on slepton pair production assuming two-generation slepton mixing, whereas we include the full three-generation flavor transitions in all our calculations. There also exist correlations between LFV in the high-energy $e^\pm e^-$ collisions and the radiative lepton decays, which are relatively weakly affected by the parameters of the neutrino sector, but very sensitive to the SUSY parameters. Consequently, they could play an important role in probing the class of models of LFV studied here. In addition, slepton masses can be measured with very high precision. Although not a lepton flavor violating effect, the inclusion of right-handed neutrinos modifies the slepton masses. Their determination can provide important information on the seesaw parameter space.

The main goals of this thesis are: First, to provide a reliable computational scheme for the calculation of slepton mass corrections and their impact on the most important experimental observables. To this end, we implement the full minimal supersymmetric seesaw model renormalization group equations to one-loop order. This basis is then used to analyze in detail the connection between neutrino parameters, SUSY parameters of the mSUGRA constrained minimal supersymmetric Standard Model (MSSM), theoretical assumptions on the high energy seesaw model and the measurable observables. Emphasis is put on the rare decays $l_i \rightarrow l_j\gamma$, slepton pair production processes at $e^\pm e^-$ colliders and precision slepton mass measurements, especially on their different sensitivities and correlations. The ultimate goal is to use all this information to determine the high energy seesaw parameters from observables at or below collider energies.

Following this introduction, we present in Chapter 2 the basics of the the minimal supersymmetric Standard Model as far as needed for our discussion. In Chapter 3, we discuss the LFV observables and experiments, most importantly low energy rare decays and slepton pair production at linear colliders. Chapter 4 contains the theoretical framework of the supersymmetric seesaw model, together with a short review of leptogenesis and neutrino physics. These general results are then applied in Chapters 5 and 6 to two interesting cases, namely (quasi-)degenerate and hierarchical right-handed neutrino masses. In Chapter 7, we present a general scheme that can be used to reconstruct the high energy seesaw parameters from low energy observables. Finally, a conclusion is given in Chapter 8.

Chapter 2

Supersymmetry

2.1 Beyond the Standard Model

The Standard Model of elementary particle physics is a highly successful theory of the known particles and their interactions. The SM is a gauge theory, in which the gauge group $SU(3)_c \times SU(2)_L \times U(1)_Y$ is spontaneously broken to $SU(3)_c \times U(1)_{EM}$ by the nonvanishing vacuum expectation value (VEV) of a fundamental scalar field, the Higgs boson, at energies of the order $100 \text{ GeV} - 1 \text{ TeV}$. Despite its success to describe non-gravitational and microscopic phenomena, there are a number of theoretical and phenomenological issues that the SM fails to address properly:

Hierarchy problem. The mass of the Higgs boson associated with electroweak symmetry breaking has to be in the electroweak range. However, radiative corrections to the Higgs mass are quadratically dependent on the ultraviolet cutoff scale Λ , since the masses of fundamental scalar fields are not protected by chiral or gauge symmetries. The natural value of the Higgs mass is therefore of $\mathcal{O}(\Lambda)$ rather than $\mathcal{O}(100 \text{ GeV})$, leading to a destabilization of the mass scales hierarchy in the SM, if the scale Λ of new physics is much larger than the electroweak scale. In other words, to achieve $m_h \approx \mathcal{O}(100 \text{ GeV})$ it is necessary to fine-tune the scalar mass-squared parameter $m_0^2 \approx \Lambda^2$ of the fundamental ultraviolet theory to a precision of m_h^2/Λ^2 ($= 10^{-28}$ for $\Lambda = 10^{16} \text{ GeV}$ and $m_h = 100 \text{ GeV}$).

Electroweak symmetry breaking (EWSB). In the SM, electroweak symmetry breaking is parameterized by the Higgs boson h and its potential $V(h)$. However, the parameters of the Higgs sector are not fixed within the Standard Model, and they must be put into the theory by hand.

Gauge coupling unification. Precise measurements of the low energy values of the gauge couplings have demonstrated that the SM cannot describe gauge coupling unification [64] accurately enough. Unification would be desirable to embed the SM gauge theory into a larger gauge group of a Grand Unified Theory (GUT), like $SO(10)$.

Generation structure and fermion masses. The SM does not explain the existence of three generations and can only parameterize the strongly hierarchical values of the fermion masses. The discovery of neutrino masses implies that the theory has to be extended, as the neutrinos in the SM are strictly left-handed and massless.

Cosmological problems. Several difficulties are encountered when trying to build cosmological models based solely on the SM particle content. The SM cannot explain the baryon asymmetry of the universe; although the Sakharov criteria [65] for baryogenesis can be met, the baryon asymmetry generated at the electroweak phase transition is too small. The SM also does not provide a viable candidate for the cold dark matter of the universe.

Therefore, the Standard Model has to be extended. Theories with low energy supersymmetry have emerged as the strongest candidates for physics beyond the SM. There are various reasons to expect that low energy supersymmetry is the probable outcome of experimental progress and that it will be directly confirmed at an upcoming collider.

In the simplest supersymmetric world, each particle has a superpartner which differs in spin by $1/2$ and is related to the original particle by a supersymmetry transformation. Since supersymmetry relates the scalar and fermion sectors, the chiral symmetries which protect the masses of the fermions also protect the masses of the scalars from quadratic divergences, leading to a solution of the hierarchy problem.

Supersymmetry is defined as a symmetry relating bosonic and fermionic degrees of freedom,

$$Q|B\rangle \rightarrow |F\rangle, \quad Q|F\rangle \rightarrow |B\rangle, \quad (2.1)$$

where Q denotes the spin $1/2$ generator of the supersymmetry algebra. In $N = 1$ supersymmetry (i.e. there is one such generator) in four dimensional spacetime, the supersymmetry algebra is given by the anti-commutator

$$\{Q_\alpha, \bar{Q}_\beta\} = 2\sigma_{\alpha\beta}^\mu P_\mu, \quad (2.2)$$

with the Pauli matrices σ^μ , spinor indices α, β and particle momentum P_μ . This shows that the supersymmetry algebra includes the Poincare algebra of spacetime (momentum and angular momentum generators have vanishing commutators with the supersymmetry generators). The irreducible representations of the supersymmetry algebra are called supermultiplets, the two most important being:

Chiral supermultiplets, containing one complex scalar ϕ , one two-component chiral fermion ψ , and an auxiliary scalar field F .

Vector supermultiplets, containing a spin 1 vector gauge boson V_μ^a , a Majorana spinor λ^a (called gaugino) and a scalar auxiliary field D^a (a is the adjoint representation index of the respective gauge group).

In the construction of supersymmetric theories, these supermultiplets (or their field theoretical counterparts, the superfields) are very convenient.

Supersymmetry must be a broken symmetry, because exact SUSY would dictate that every superpartner is degenerate in mass with its corresponding SM particle, which is clearly ruled out by experiment. Possible ways to achieve a spontaneous breaking of supersymmetry depend on the form of the high energy theory. Supersymmetry may even be explicitly broken without losing its ability to solve the hierarchy problem as long as the breaking is of a certain type known as soft breaking. If supersymmetry is broken softly, the superpartner masses can be lifted to a phenomenologically acceptable range. The scale of the mass splitting between the two partners should be of the order of $100 \text{ GeV} - 1 \text{ TeV}$ because it then can be tied to the scale of electroweak symmetry breaking. In any case, the effective Lagrangian at the electroweak scale is expected to be parameterized by a general set of soft supersymmetry-breaking (SSB) terms if the attractive features of supersymmetry are to be maintained, and the Lagrangian can be separated as

$$\mathcal{L} = \mathcal{L}_{\text{SUSY}} + \mathcal{L}_{\text{soft}}, \quad (2.3)$$

with the supersymmetric part $\mathcal{L}_{\text{SUSY}}$ and the SUSY violating part $\mathcal{L}_{\text{soft}}$. If low energy supersymmetry indeed offers the solution to the hierarchy problem, direct evidence of the existence of the superpartners should be discovered within the next decade, either at current experiments at the upgraded $p\bar{p}$ Fermilab Tevatron collider or at the upcoming LHC at CERN.

Low energy supersymmetry has long been considered the best-motivated possibility for new physics at the TeV scale not only for theoretical reasons, but also for its successful explanations and predictions:

Hierarchy problem. The SM Higgs sector has two 'naturalness' problems. One is the technical naturalness problem associated with the absence of a symmetry protecting the Higgs mass at the electroweak scale when the natural cutoff scale is at or above the GUT scale, as already mentioned above. The second problem is associated with explaining the origin of the electroweak scale, when a more fundamental embedding theory such as a GUT or string theory is typically defined at a scale about 10^{14} times larger than the electroweak scale. This is often referred to as the gauge hierarchy problem.

Supersymmetry provides a solution to the technical hierarchy problem, as the Higgs mass parameter is not renormalized as long as SUSY is unbroken. Supersymmetry also softens the gauge hierarchy problem by breaking the electroweak symmetry radiatively through logarithmic running, mitigating the effect of the large number $\approx 10^{14}$.

Radiative EWSB. With plausible boundary conditions at a high scale, low energy supersymmetry can provide the explanation of the origin of electroweak symmetry breaking [66]. Schematically, the SM effective Higgs potential has the form $V(h) = m^2 h^2 + \lambda h^4$. First, supersymmetry requires that the quartic coupling λ is a function of the $U(1)_Y$ and $SU(2)$ gauge couplings, $\lambda = (g_1^2 + g_2^2)/2$. Second, the m^2 parameter runs to negative values at the electroweak scale, driven by the large top quark Yukawa coupling. Thus the 'Mexican hat' potential with a minimum away from $h = 0$ emerges naturally.

Gauge coupling unification. In contrast to the SM, the minimal supersymmetric Standard Model presented in the next section allows for the unification of the gauge couplings [67, 68]. The extrapolation of the low energy values of the gauge couplings using renormalization group equations of the MSSM particle content show that the gauge couplings unify at the scale $M_{\text{GUT}} \approx 2 \cdot 10^{16}$ GeV [69, 70]. Gauge coupling unification and electroweak symmetry breaking depend on essentially the same physics since each needs the SUSY breaking parameters and the Higgs mixing term μ to be of the order of the electroweak scale.

Cold dark matter. In supersymmetric theories, the lightest superpartner (LSP) can be stable. It then provides a suitable cold dark matter candidate [71]. Estimates of its relic density are of the right order of magnitude to provide the observed amount.

2.2 The Minimal Supersymmetric Standard Model

The MSSM is defined to be the minimal supersymmetric extension of the SM, and hence is a $SU(3)_c \times SU(2)_L \times U(1)_Y$ supersymmetric gauge theory together with the most general set of soft supersymmetry-breaking terms. The known matter and gauge fields of the SM are promoted to superfields in the MSSM: each known particle has a presently unobserved superpartner. The superpartners of the SM chiral fermions are spin zero sfermions. The superpartners of the gauge bosons are the spin 1/2 gauginos.

The Higgs sector of the MSSM differs from that of the SM. It consists of two Higgs doublets H_u and H_d , which couple at tree level to up and down type chiral fermions separately. Both are required for the theory to be anomaly free and the superpotential to be holomorphic.

The complete particle content of the MSSM is shown in Table 2.1. In the following, symbols with hats denote superfields while those with tildes denote superpartner fields. The MSSM superpotential is [72]

$$\mathcal{W} = \hat{u}^{cT} \mathbf{Y}_u \hat{Q} \cdot \hat{H}_u - \hat{d}^{cT} \mathbf{Y}_d \hat{Q} \cdot \hat{H}_d - \hat{e}^{cT} \mathbf{Y}_e \hat{L} \cdot \hat{H}_d + \mu \hat{H}_u \cdot \hat{H}_d, \quad (2.4)$$

where the dot stands for $SU(2)$ index contraction, $A \cdot B = \epsilon_{\alpha\beta} A^\alpha B^\beta$, with the antisymmetric tensor $\epsilon_{\alpha\beta}$ ($\epsilon_{12} = +1$). The lepton and quark fields in (2.4) are three component objects in flavor space, e.g. $\hat{L}^T = (\hat{L}_e, \hat{L}_\mu, \hat{L}_\tau)$. Consequently, the Yukawa terms $\mathbf{Y}_u, \mathbf{Y}_d, \mathbf{Y}_e$ are 3×3 matrices. There are additional renormalizable couplings [72]

$$\mathcal{W}_{\mathcal{R}} = \lambda_{ijk} \hat{L}_i \hat{L}_j \hat{e}_k^c + \lambda'_{ijk} \hat{L}_i \hat{Q}_j \hat{d}_k^c + \lambda''_{ijk} \hat{u}_i^c \hat{d}_j^c \hat{d}_k^c, \quad i, j, k = 1, 2, 3, \quad (2.5)$$

allowed by gauge invariance, which violate baryon and lepton number. Such couplings could lead to rapid proton decay and certain combinations are strongly constrained. In the MSSM a discrete symmetry called R -parity (B : baryon number, L : lepton number, S : spin),

$$R = (-1)^{3(B-L)+2S}, \quad (2.6)$$

Superfield	Boson	Fermion	Description
\hat{g}	g	\tilde{g}	gluons/gluinos
\hat{W}	W	\tilde{W}	W bosons/winos
\hat{B}	B	\tilde{B}	B boson/bino
\hat{L}	$(\tilde{\nu}, \tilde{e})_L$	$(\nu, e)_L$	l.h. (s)neutrinos, ch. (s)leptons
\hat{e}^c	\tilde{e}_R^*	e_L^c	r.h. charged (s)leptons
\hat{Q}	$(\tilde{u}, \tilde{d})_L$	$(u, d)_L$	l.h. (s)quarks
\hat{u}^c	\tilde{u}_R^*	u_L^c	r.h. up-type (s)quarks
\hat{d}^c	\tilde{d}_R^*	d_L^c	r.h. down-type (s)quarks
\hat{H}_d	$(h_d^0, h_d^-)_L$	$(\tilde{h}_d^0, \tilde{h}_d^-)_L$	down-type Higgs(inos)
\hat{H}_u	$(h_u^+, h_u^0)_L$	$(\tilde{h}_u^+, \tilde{h}_u^0)_L$	up-type Higgs(inos)

Table 2.1: Particle content of the MSSM.

is imposed which forbids all couplings in (2.5). The usual Standard Model particles have even R -parity, $R = +1$, while their superpartners have odd R -parity, $R = -1$. The conservation of R has very important consequences:

- The lightest sparticle with $R = -1$ (the LSP) is stable, and hence a possible candidate for cold dark matter.
- Sparticles can only be produced in even numbers.
- Each sparticle other than the lightest supersymmetric particle (LSP) must finally decay into a state with an odd number of LSPs.

The necessity of supersymmetry being broken at low energies implies the appearance of supersymmetry-breaking terms in the Lagrangian. In order not to reintroduce the hierarchy problem only a certain subset of all possible SUSY-breaking terms should be implemented. One then arrives at the soft SUSY-breaking (SSB) Lagrangian [72–74],

$$\begin{aligned}
-\mathcal{L}_{\text{soft}} &= \frac{1}{2}(\tilde{M}_1 \tilde{B} \tilde{B} + \tilde{M}_2 \tilde{W} \tilde{W} + \tilde{M}_3 \tilde{g} \tilde{g}) \\
&+ \left(\tilde{u}^{c\top} \mathbf{A}_u \tilde{Q} \cdot H_u - \tilde{d}^{c\top} \mathbf{A}_d \tilde{Q} \cdot H_d - \tilde{e}^{c\top} \mathbf{A}_e \tilde{L} \cdot H_d + B H_u \cdot H_d + \text{h.c.} \right) \\
&+ \tilde{Q}^\dagger \mathbf{m}_Q^2 \tilde{Q} + \tilde{u}^{c\dagger} \mathbf{m}_u^2 \tilde{u}^c + \tilde{d}^{c\dagger} \mathbf{m}_d^2 \tilde{d}^c + \tilde{L}^\dagger \mathbf{m}_L^2 \tilde{L} + \tilde{e}^{c\dagger} \mathbf{m}_e^2 \tilde{e}^c \\
&+ m_{h_d}^2 |H_d|^2 + m_{h_u}^2 |H_u|^2, \tag{2.7}
\end{aligned}$$

where $\tilde{M}_1, \tilde{M}_2, \tilde{M}_3$ are bino, wino and gluino masses, respectively (the adjoint representation gauge indices of the wino fields are omitted). The second line in (2.7) consists of trilinear (scalar)³ couplings with arbitrary matrices $\mathbf{A}_u, \mathbf{A}_e, \mathbf{A}_d$ and the SSB Higgs mixing parameter B . The third line contains soft SUSY-breaking contributions to the sfermion masses with the 3×3 hermitian matrices $\mathbf{m}_Q^2, \mathbf{m}_u^2, \mathbf{m}_d^2, \mathbf{m}_L^2, \mathbf{m}_e^2$. Explicit Higgs mass contributions are found in the last line. All parameters are completely arbitrary within the MSSM. If for example the

entries of \mathbf{m}_L^2 are all of comparable size, the induced lepton flavor and CP violation would be disastrously large. This makes the need for an additional theoretical framework apparent.

The terms in (2.7) explicitly contribute to masses and interactions of the superpartners but not to their SM counterparts. The underlying supersymmetry breaking is assumed to be spontaneous, presumably taking place in a hidden sector as in the supergravity framework to be discussed in Section 2.3. All the quantities in $\mathcal{L}_{\text{soft}}$ receive radiative corrections and thus are scale dependent, satisfying known renormalization equations, which are given in Appendix C.2 (for the MSSM without right-handed neutrinos).

The soft parameters clearly have a significant impact on the MSSM mass spectrum and mixing. The mass matrices of the sfermions are generally not diagonal in the fermion mass basis, giving rise to flavor violating terms. Gauginos and higgsinos with equal electric charges mix, the mass eigenstates of the charged ones denoted as charginos and the neutral ones as neutralinos. Details on the construction and diagonalization of particle mass matrices can be found in Appendix B.

One of the most important successes of supersymmetry is that it can provide a natural mechanism for understanding Higgs physics and electroweak symmetry breaking [66, 74]. This mechanism requires correlations among the Higgs soft SUSY-breaking parameters and the supersymmetric Higgs mass parameter μ . The two electroweak Higgs doublets in the MSSM are

$$H_u = \begin{pmatrix} h_u^+ \\ h_u^0 \end{pmatrix}, \quad H_d = \begin{pmatrix} h_d^0 \\ h_d^- \end{pmatrix}, \quad (2.8)$$

with hypercharges $\pm 1/2$, respectively. For successful electroweak symmetry breaking, the neutral components of the doublets acquire nonzero vacuum expectation values,

$$\langle H_u \rangle = \begin{pmatrix} 0 \\ v_u \end{pmatrix}, \quad \langle H_d \rangle = \begin{pmatrix} v_d \\ 0 \end{pmatrix}, \quad (2.9)$$

where v_d and v_u can be chosen real and positive. The connection to the SM requires that

$$v_d^2 + v_u^2 = v^2 = \frac{2m_Z^2}{g_1^2 + g_2^2} \approx (174 \text{ GeV})^2. \quad (2.10)$$

The important SUSY parameter $\tan \beta$ is defined as the ratio of the VEVs,

$$\tan \beta = \frac{v_u}{v_d}. \quad (2.11)$$

Electroweak symmetry breaking takes place when the Higgs potential is minimized for nonzero v_d and v_u . At tree level, the condition for this to happen can be expressed as [72, 75]

$$\begin{aligned} |\mu|^2 &= \frac{1}{2} (\tan 2\beta (m_{h_u}^2 \tan \beta - m_{h_d}^2 \cot \beta) - m_Z^2), \\ B &= \frac{\sin 2\beta}{2} (m_{h_d}^2 + m_{h_u}^2 + 2|\mu|^2). \end{aligned} \quad (2.12)$$

Although it is not necessary nor sufficient, EWSB generically occurs if $m_{h_u}^2$ in (2.7) is negative. A feature of the MSSM is that this up-type Higgs soft (mass)² parameter is driven to negative values due to the large top quark Yukawa coupling even if it is positive at some high energy scale. This is known as radiative electroweak symmetry breaking.

2.3 Minimal supergravity

For the theoretical treatment of spontaneous SUSY breaking it is generally assumed that the theory can be split into two sectors with no direct renormalizable couplings between them [76–78]:

- *An observable sector*, containing the SM fields plus superpartners.
- *A hidden sector*, in which SUSY is spontaneously broken.

Within such a framework, supersymmetry breaking is communicated from the hidden sector to the observable sector via suppressed interactions.

As gravitational interactions are shared by all particles, gravitation is a popular candidate for the mediation of supersymmetry breaking. Also, promoting global SUSY to local SUSY naturally leads to supergravity, an effective field theory of gravitation. Supergravity interactions are suppressed by $M_{\text{Planck}} \approx 10^{18}$ GeV, leading to a gravitino (the spin 3/2 partner of the spin 2 graviton) mass of the order

$$m_{3/2} \approx \frac{M_S^2}{M_{\text{Planck}}}, \quad (2.13)$$

where M_S is the scale of spontaneous supersymmetry breaking. Generically, $m_{3/2}$ sets the scale of all soft SUSY-breaking parameters, m_{soft} . For viable phenomenology, this infers $m_{3/2} \approx m_{\text{soft}} \approx \mathcal{O}(1 \text{ TeV})$ and $M_S \approx 10^{11}$ GeV.

In the minimal supergravity framework one assumes that the Kähler potential (an ingredient from which the supergravity Lagrangian is constructed) has canonical form,

$$K(\hat{\Phi}_i) = \sum_i |\hat{\Phi}_i|^2, \quad (2.14)$$

where the $\hat{\Phi}_i$ are all MSSM chiral superfields and those hidden superfields that participate in SUSY breaking. This leads to a common soft scalar mass m_0 , a common gaugino mass $m_{1/2}$, and a common trilinear coupling A_0 in the soft SUSY-breaking Lagrangian $\mathcal{L}_{\text{soft}}$ (2.7)¹,

$$\begin{aligned} m_{\tilde{Q}}^2 &= m_{\tilde{d}}^2 = m_{\tilde{u}}^2 = m_{\tilde{L}}^2 = m_{\tilde{e}}^2 = m_0^2 \mathbb{I}, \\ m_{\tilde{h}_u}^2 &= m_{\tilde{h}_d}^2 = m_0^2, \\ \mathbf{A}_u &= A_0 \mathbf{Y}_u, \quad \mathbf{A}_d = A_0 \mathbf{Y}_d, \quad \mathbf{A}_e = A_0 \mathbf{Y}_e, \\ \tilde{M}_1 &= \tilde{M}_2 = \tilde{M}_3 = m_{1/2}, \end{aligned} \quad (2.15)$$

at the Planck scale, highly constraining the MSSM parameter space. It is common practice to adopt the above conditions at M_{GUT} rather than M_{Planck} , because the physics above the GUT scale is not known without specifying a GUT group. Thus, the soft scalar mass matrices are all diagonal, flavor degenerate and even universal among all sfermion species at M_{GUT} . The

¹Throughout this work, the 3×3 identity matrix is denoted by \mathbb{I} .

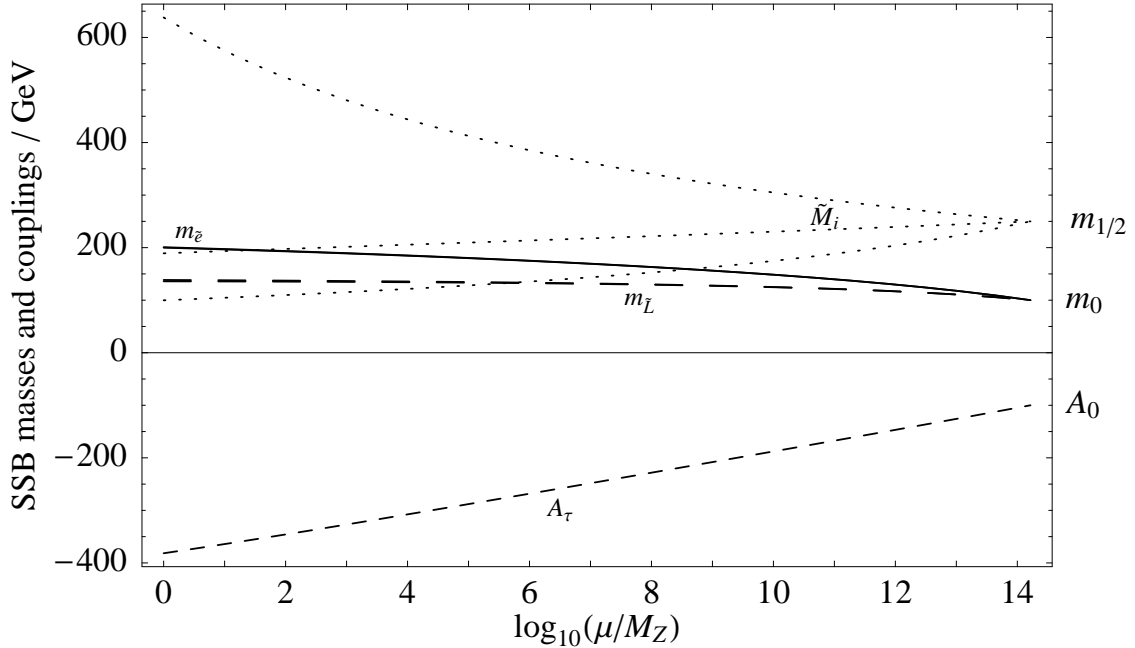


Figure 2.1: Running of the SUSY breaking parameters \tilde{M}_i , $m_{\tilde{L}}$, $m_{\tilde{e}}$, $A_\tau = (A_e)_{33}$ in the mSUGRA scenario SPS1a.

universality and flavor degeneracy of the sfermion masses is not conserved at the electroweak scale due to the MSSM RGEs in Appendix C.2. As an example, this is shown in Figure 2.1 for one of the mSUGRA scenarios used in this work. On the other hand, the MSSM RGEs do conserve the lepton flavor.

Through successful radiative electroweak symmetry breaking (2.12), it is possible to trade the Higgs parameters μ and B for the EW breaking parameter $\tan \beta$ and the sign of μ (we are assuming that all parameters are real, otherwise, the phase of μ would remain undetermined). This leaves us with the following set of independent parameters,

$$m_0, m_{1/2}, A_0, \tan \beta, \text{sign } \mu, \quad (2.16)$$

in the mSUGRA constrained MSSM.

In this work we use mSUGRA benchmark scenarios proposed in [79] and one Snowmass scenario [80]. The sparticle spectra corresponding to these scenarios are consistent with all experimental and cosmological constraints, in particular with

- direct sparticle searches,
- $b \rightarrow s\gamma$,
- cosmological relic density, with the lightest neutralino as lightest SUSY particle and dark matter candidate,
- Higgs searches.

	B'	C'	G'	I'	SPS1a
$m_{1/2}$	250	400	375	350	250
m_0	60	85	115	175	100
A_0	0	0	0	0	-100
$\tan\beta$	10	10	20	35	10
μ	+333	+503	+471	+439	+352
h_0	113	116	117	116	114
$\tilde{e}_R, \tilde{\mu}_R$	121	180	189	224	143
$\tilde{\tau}_1$	112	172	162	155	133
$\tilde{e}_L, \tilde{\mu}_L$	188	289	285	300	202
$\tilde{\tau}_2$	192	291	291	310	206
$\tilde{\nu}_{e,\mu}$	171	278	273	289	186
$\tilde{\nu}_\tau$	187	277	270	277	185
$\tilde{\chi}_1^0$	98	163	153	143	96
$\tilde{\chi}_2^0$	181	310	289	270	176
$\tilde{\chi}_3^0$	346	519	489	464	358
$\tilde{\chi}_4^0$	365	535	504	478	377
$\tilde{\chi}_1^\pm$	180	309	290	270	176
$\tilde{\chi}_2^\pm$	367	535	505	479	378

Table 2.2: Fundamental parameters and particle masses in the mSUGRA benchmark scenarios used. All values are in GeV except for the dimensionless parameter $\tan\beta$.

The values of the mSUGRA parameters (2.16) in the benchmark scenarios used are listed in Table 2.2, along with the most important particle masses at low energies. The masses have been calculated using the procedures presented in Appendix B. We constrain ourselves to those scenarios which lead to sufficiently light sleptons, so that the production of slepton pairs containing a large admixture of at least one left-handed \tilde{l}_L component is possible at $\sqrt{s} = 500$ GeV or at most 800 GeV. Also, we will mainly concentrate on the scenario SPS1a which has become a standard within the SUSY collider physics community. Its sparticle mass spectrum is shown in Figure 2.2. The other scenarios will be used to highlight possible alternatives.

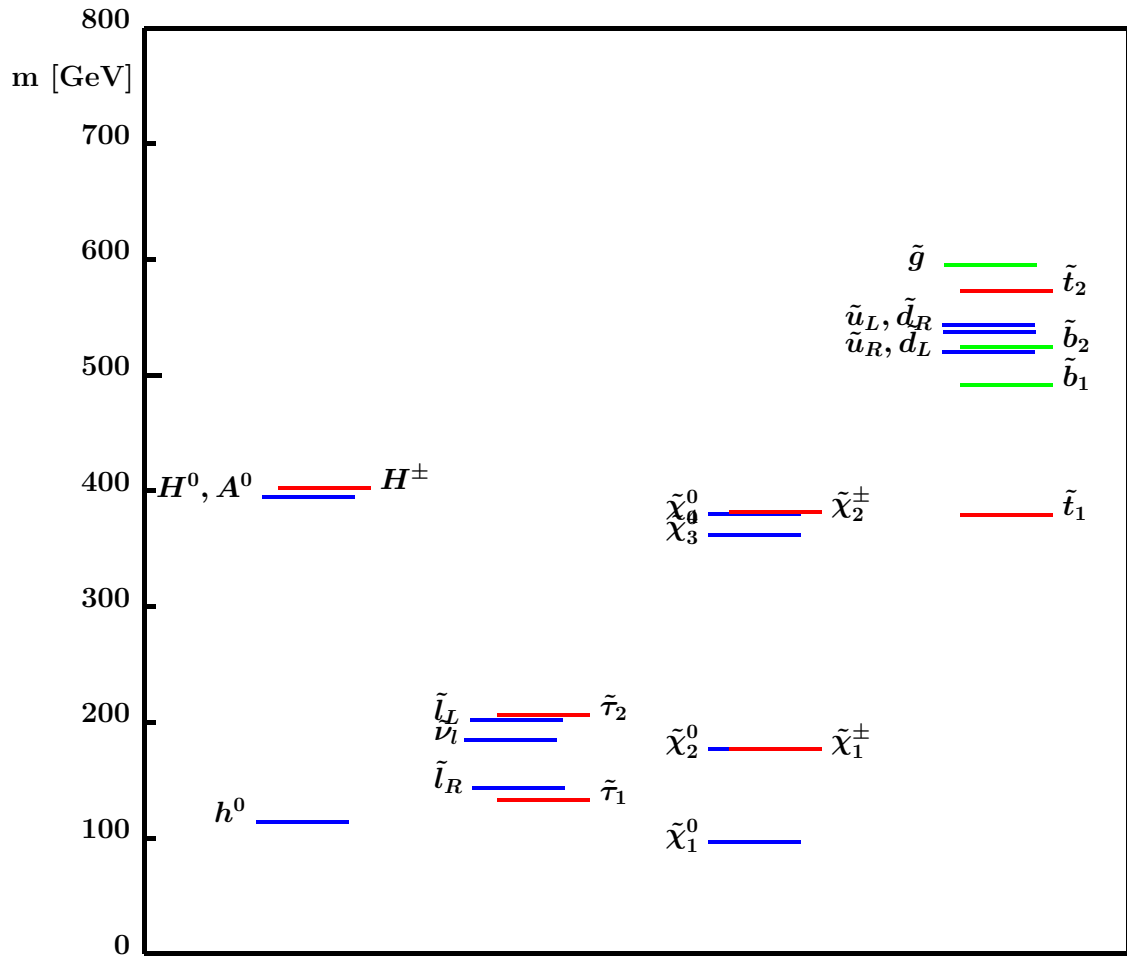


Figure 2.2: Sparticle mass spectrum of the mSUGRA scenario SPS1a, taken from [80].

Chapter 3

Slepton flavor violation

As has been noted in the preceding chapter, there exist in general many possible sources of lepton flavor violation in the MSSM, in the form of flavor non-diagonal slepton mass terms and trilinear couplings. Potentially, they can lead to disastrously large LFV process rates. The introduction of the mSUGRA constrained parameter space with its universal and flavor-diagonal masses cured this problem by removing all off-diagonal terms. In this chapter we introduce small deviations $(\delta m_{\tilde{X}}^2)_{ij}$, concentrating on the left-handed slepton sector,

$$\mathbf{m}_{\tilde{L}}^2 = \text{diag}((\mathbf{m}_{\tilde{L}}^2)_{11}, (\mathbf{m}_{\tilde{L}}^2)_{22}, (\mathbf{m}_{\tilde{L}}^2)_{33}) + \begin{pmatrix} (\delta \mathbf{m}_{\tilde{L}}^2)_{11} & (\delta \mathbf{m}_{\tilde{L}}^2)_{12} & (\delta \mathbf{m}_{\tilde{L}}^2)_{13} \\ (\delta \mathbf{m}_{\tilde{L}}^2)_{12}^* & (\delta \mathbf{m}_{\tilde{L}}^2)_{22} & (\delta \mathbf{m}_{\tilde{L}}^2)_{23} \\ (\delta \mathbf{m}_{\tilde{L}}^2)_{13}^* & (\delta \mathbf{m}_{\tilde{L}}^2)_{23}^* & (\delta \mathbf{m}_{\tilde{L}}^2)_{33} \end{pmatrix}. \quad (3.1)$$

Here, $(\mathbf{m}_{\tilde{L}}^2)_{ii}$ are the diagonal terms of the flavor-conserving mSUGRA framework. The additional terms in (3.1) anticipate the contributions from adding right-handed neutrinos to the MSSM particle content in the supersymmetric seesaw mechanism, as will be outlined in Chapter 4. Constraints from LFV processes naturally lead to bounds on the quantities $(\delta \mathbf{m}_{\tilde{L}}^2)_{ij}$. In the following we review the most important processes that can be used to limit or determine these parameters.

It should be noted that the results of this chapter are model independent. We only assume that the charged lepton flavor violation is generated by off-diagonal left-handed slepton mass terms as in (3.1). The actual process calculations do not even depend on this assumption but hold for arbitrary slepton mixing as described in Appendices B.3 and B.4.

3.1 Low energy loop processes

3.1.1 $l_i \rightarrow l_j \gamma$

The classical probes, yielding the most stringent bounds, in the search for flavor changing neutral currents (FCNC) have been the processes $\mu \rightarrow e \gamma$, $\tau \rightarrow \mu \gamma$ and $\tau \rightarrow e \gamma$. The current

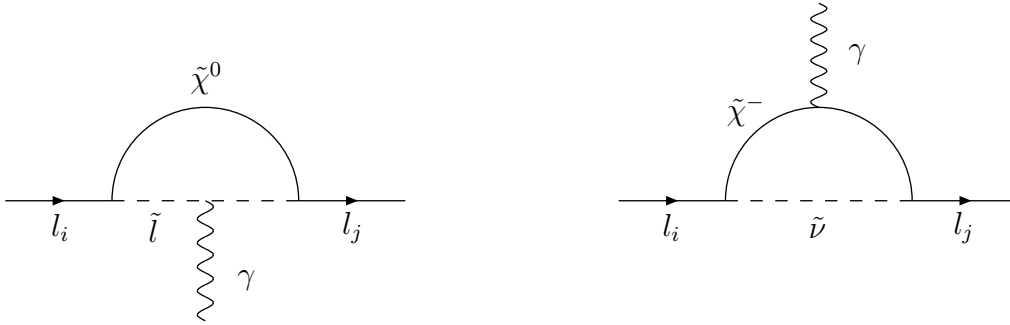


Figure 3.1: Diagrams for $l_i^- \rightarrow l_j^- \gamma$ in the MSSM

limits on the branching ratios of these processes are:

$$\begin{aligned} Br(\mu \rightarrow e\gamma) &< 1.2 \cdot 10^{-11} && [81, 82], \\ Br(\tau \rightarrow \mu\gamma) &< 3.1 \cdot 10^{-7} && [83, 84], \\ Br(\tau \rightarrow e\gamma) &< 3.7 \cdot 10^{-7} && [81]. \end{aligned} \quad (3.2)$$

The MEG experiment at PSI and data from B-factories are expected to improve the sensitivities on $Br(\mu \rightarrow e\gamma)$ and $Br(\tau \rightarrow \mu\gamma)$, respectively, in the near future:

$$\begin{aligned} Br(\mu \rightarrow e\gamma) &\approx 10^{-13} && [85], \\ Br(\tau \rightarrow \mu\gamma) &\approx 10^{-8} && [84, 86]. \end{aligned} \quad (3.3)$$

In addition, searches for $\tau \rightarrow \mu\gamma$ at the LHC or SUPERKEKB may reach a level of $Br \approx 10^{-9}$.

In the MSSM, contributions to these processes can arise from diagrams with charged sleptons or sneutrinos in the loop if there is a non-vanishing flavor mixing in the slepton sector. The Feynman diagrams for the process $l_i \rightarrow l_j \gamma$ are shown in Figure 3.1, from which one obtains the following decay rate [35, 48],

$$\Gamma(l_i \rightarrow l_j \gamma) = \frac{e^2}{16\pi} m_{l_i}^5 (|A_{ij}^L|^2 + |A_{ij}^R|^2), \quad m_{l_i} \gg m_{l_j}, \quad (3.4)$$

where the coefficients A^L and A^R are given in Appendix D.1. Because $m_{l_i} \gg m_{l_j}$ and $\mathbf{m}_{\tilde{e}}^2$ is assumed to be diagonal (this will hold to a very high degree in the SUSY seesaw, see Chapter 4), one has $A^R \gg A^L$ [21, 22]. The dominant contribution in (3.4) can then be

approximated by¹ [87]

$$A_{ij}^R = \frac{1}{m_{l_i}} (A_{ij}^{CR} + A_{ij}^{NR}), \quad (3.5)$$

$$A_{ij}^{CR} \approx \frac{1}{32\pi^2} \frac{g^2 m_{l_i}}{\sqrt{2} m_W c_\beta} \sum_{a=1}^2 \sum_{k=1}^3 \frac{m_{\tilde{\chi}_a^-}}{m_{\tilde{\nu}_k}^2} (\mathbf{O}_1)_{a1} (\mathbf{O}_2)_{a2} (\mathbf{U}_{\tilde{\nu}}^*)_{jk} (\mathbf{U}_{\tilde{\nu}})_{ik} F_2^C \left(\frac{m_{\tilde{\chi}_a^-}^2}{m_{\tilde{\nu}_k}^2} \right), \quad (3.6)$$

$$A_{ij}^{NR} \approx -\frac{1}{32\pi^2} g^2 t_W \sum_{a=1}^4 \sum_{k=1}^6 \frac{m_{\tilde{\chi}_a^0}}{m_{\tilde{l}_k}^2} \mathbf{N}_{a1} (\mathbf{N}_{a2} + \mathbf{N}_{a1} t_W) (\mathbf{U}_{\tilde{l}}^*)_{jk} (\mathbf{U}_{\tilde{l}})_{(i+3)k} F_2^N \left(\frac{m_{\tilde{\chi}_a^0}^2}{m_{\tilde{l}_k}^2} \right), \quad (3.7)$$

the two parts A^{CR} , A^{NR} corresponding to charginos/sneutrinos or neutralinos/charged sleptons in the loop, respectively. $F_2^C(x)$ and $F_2^N(x)$ are loop functions (also given in Appendix D.1), which are of order unity in the mSUGRA scenarios used. $\mathbf{O}_{1/2}$, \mathbf{N} , $\mathbf{U}_{\tilde{l}}$ and $\mathbf{U}_{\tilde{\nu}}$ are the chargino, neutralino, charged slepton and sneutrino mixing matrices, respectively. Their definitions can be found in Appendix B. The numerical calculations discussed later are performed with the full expressions for A_{ij}^L and A_{ij}^R of Appendix D.1.

Note that there is no difference between the rates of $l_i^- \rightarrow l_j^- \gamma$ and $l_i^+ \rightarrow l_j^+ \gamma$ at the one-loop level [45, 46]. We therefore do not distinguish between $Br(l_i^- \rightarrow l_j^- \gamma)$ and $Br(l_i^+ \rightarrow l_j^+ \gamma)$ in the following.

For rough order of magnitude estimates, the branching ratio to (3.4) can be further approximated through the mass-insertion technique (an off-diagonal mass term in the flavor basis is described by a two-leg vertex and inserted only to lowest order in a Feynman diagram [21, 22]), yielding

$$Br(l_i \rightarrow l_j \gamma) \approx \alpha^3 \tan^2 \beta \frac{m_{l_i}^4 m_{l_i}}{\tilde{m}^4 \Gamma_i} \frac{|(\delta \mathbf{m}_{\tilde{l}}^2)_{ij}|^2}{\tilde{m}^4}, \quad (3.8)$$

where \tilde{m} is the typical mass scale of SUSY particles in the loop and Γ_i is the total width of lepton l_i . This approximation is applicable if the off-diagonal mass terms are small compared to the diagonal masses, $(\delta \mathbf{m}_{\tilde{l}}^2)_{ij} \ll (\mathbf{m}_{\tilde{l}}^2)_{ii}$ ($i \neq j$).

3.1.2 Other rare LFV processes

The processes $l_i^- \rightarrow l_j^- l_j^- l_j^+$ and $\mu^- \mathbf{N} \rightarrow e^- \mathbf{N}$ ($\mu - e$ conversion in nuclei) are generated in the MSSM by photon penguin diagrams (the photon in Figure 3.1 decays into $l_j^- l_j^+$ or $q_j^- q_j^+$, respectively), Z penguins and box diagrams [20, 48, 88, 89]. Current bounds are:

$$\begin{aligned} Br(\mu^+ \rightarrow e^+ e^+ e^-) &< 1.0 \cdot 10^{-12} & [81], \\ R(\mu^- \text{Ti} \rightarrow e^- \text{Ti}) &< 6.1 \cdot 10^{-13} & [81, 82], \end{aligned} \quad (3.9)$$

with R denoting the cross section normalized to the total muon capture rate. The MECO experiment aims at a sensitivity for $\mu^- \text{Al} \rightarrow e^- \text{Al}$ below $R \approx 10^{-16}$ [90]. In the farther future, the PRISM project plans to provide beams of low energy muons with an intensity increased

¹Throughout this work, trigonometric functions will often be abbreviated by their initials, $s_\beta \equiv \sin \beta$, $c_\beta \equiv \cos \beta$, $t_W \equiv \tan \theta_W$, with the electroweak mixing angle θ_W .

by several orders of magnitude, so that it may become possible to reach $Br(\mu \rightarrow e\gamma) \approx 10^{-15}$ [91], $Br(\mu^+ \rightarrow e^+e^+e^-) \approx 10^{-16}$ [92] and $R(\mu^- \text{Ti} \rightarrow e^- \text{Ti}) \approx 10^{-18}$.

In the case of conserved R -parity, as considered in this work, the main contributions to the above processes arise from photon penguin diagrams. As a consequence, one has the following model-independent relations [21, 48],

$$\frac{Br(\mu \rightarrow 3e)}{Br(\mu \rightarrow e\gamma)} \approx \frac{\alpha}{8\pi} \frac{8}{3} \left(\ln \frac{m_\mu^2}{m_e^2} - \frac{11}{4} \right) \approx 7 \cdot 10^{-3}, \quad (3.10)$$

$$\frac{R(\mu^- \text{N} \rightarrow e^- \text{N})}{Br(\mu \rightarrow e\gamma)} \approx 16\alpha^4 \frac{\Gamma_\mu}{\Gamma_{\text{cap}}} Z_{\text{eff}}^4 Z |F(q^2)|^2 \quad (3.11)$$

$$\approx 6 \cdot 10^{-3} \quad \text{for Titanium}, \quad (3.12)$$

where $F(q^2)$ is a nuclear form factor, Z (Z_{eff}) is the (effective) electric charge of the nucleus and Γ_{cap} the total muon capture rate [93–95]. From these relations and by comparing the experimental limits in (3.2) and (3.9), one can see that the present limits on $Br(\mu \rightarrow 3e)$ and $R(\mu^- \text{N} \rightarrow e^- \text{N})$ are considerably less sensitive than the current bound on $Br(\mu \rightarrow e\gamma)$. However, a future measurement in the range of $R(\mu^- \text{Ti} \rightarrow e^- \text{Ti}) \approx 10^{-18}$ [96] could provide a more sensitive test than the corresponding future sensitivity $Br(\mu \rightarrow e\gamma) \approx 10^{-15}$.

3.1.3 Electric dipole moments

Although lepton flavor conserving observables, electric dipole moments (EDMs) of the electron and muon are correlated with LFV decays such as $\mu \rightarrow e\gamma$. The electric dipole moment of lepton l_i is given by [46, 48]

$$d_i = \frac{e}{2} m_{l_i} (A_{ii}^R - A_{ii}^L), \quad (3.13)$$

with the same coefficients A^R and A^L as in (3.4) given in Appendix D.1. Neglecting the lepton mass one arrives at [48]

$$d_i = \frac{e}{32\pi^2} \sum_{k,a} \left(\text{Im} (C_{ik,a}^L C_{ik,a}^{R*}) \frac{m_{\tilde{\chi}_a^-}}{m_{\tilde{\nu}_k}^2} F_2^C \left(\frac{m_{\tilde{\chi}_a^-}^2}{m_{\tilde{\nu}_k}^2} \right) - \text{Im} (N_{ik,a}^L N_{ik,a}^{R*}) \frac{m_{\tilde{\chi}_a^0}}{m_{l_k}^2} F_2^N \left(\frac{m_{\tilde{\chi}_a^0}^2}{m_{l_k}^2} \right) \right), \quad (3.14)$$

where the sum extends over the appropriate slepton/sneutrino and chargino/neutralino mass eigenstates. The factors $\text{Im}(C_{ik,a}^L C_{ik,a}^{R*})$ and $\text{Im}(N_{ik,a}^L N_{ik,a}^{R*})$ show that EDMs are CP violating observables, sensitive to the imaginary parts of the slepton mass matrices (see Appendix B.5 for the definition of the vertex factors $C^{L/R}$, $N^{L/R}$). The main emphasis in this work is on lepton flavor violation rather than CP violation, though. Furthermore, EDMs are not able to give significant constraints on the SUSY seesaw parameter space, as will be seen in Chapters 5 and 6. Their current (expected future) limits being to large,

$$\begin{aligned} d_e &< 1.5 \cdot 10^{-27} (10^{-33}) \text{ ecm} \quad [97, 98], \\ d_\mu &< 1.5 \cdot 10^{-18} (10^{-26}) \text{ ecm} \quad [92]. \end{aligned} \quad (3.15)$$

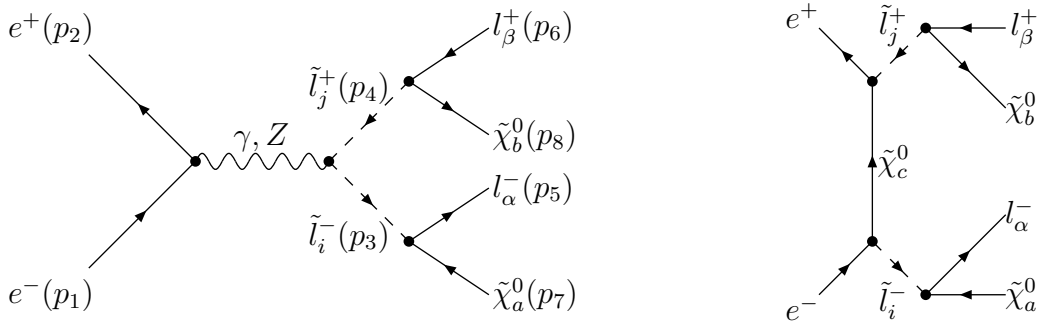


Figure 3.2: Feynman diagrams for $e^+e^- \rightarrow \tilde{l}_j^+\tilde{l}_i^- \rightarrow l_\beta^+l_\alpha^-\tilde{\chi}_b^0\tilde{\chi}_a^0$. The arrows on scalar lines refer to the lepton number flow.

Nevertheless, as CP and lepton flavor violation are closely related, we will briefly comment on these observables in the context of the SUSY seesaw model. For a more thorough discussion of EDMs in the context of the SUSY seesaw model, the reader is referred to [48].

3.2 Slepton pair production

Future linear colliders, such as TESLA, will be able to measure sparticle properties to a very high precision. Among many other things, a LC has the ability to constrain or determine the off-diagonal parts of the slepton mass matrix, complementing the search for LFV via rare decays as outlined in the previous section. A natural channel to do this is the production of slepton pairs, which decay into various Standard Model particles and two or more LSPs (in our case, the LSP is always the lightest neutralino).

3.2.1 e^+e^- collider

The slepton flavor mixing induced by off-diagonal slepton mass matrix entries (3.1) gives rise to the lepton flavor violating processes $e^+e^- \rightarrow \tilde{l}_j^+\tilde{l}_i^- \rightarrow l_\beta^+l_\alpha^-\tilde{\chi}_b^0\tilde{\chi}_a^0$, ($i, j = 1, \dots, 6$). The lowest-order Feynman diagrams are shown in Figure 3.2. More specifically, the lepton flavor violation in these processes is caused by the slepton mixing matrix $U_{\tilde{l}}$ (B.19), which enters both the slepton production and the decay vertices. As a consequence, factorization in production cross section times branching ratios is not always appropriate. One rather has to coherently sum over all intermediate slepton states. In the following, we summarize our analytical results on the amplitudes and cross sections for the above processes. The detailed calculations have been carried out in [99].

The sleptons are produced either via s-channel exchange of a photon or Z boson, or t-channel exchange of neutralinos. The sleptons then decay into two leptons of differing flavor and two neutralinos. From now on, we will concentrate on two lightest neutralinos $\tilde{\chi}_1^0$ as they constitute a stable final state. The signature of our processes is then $e^+e^- \rightarrow l_\beta^+l_\alpha^- + \cancel{E}$, as the

neutralinos are not observable. Note that in the mSUGRA scenarios defined in Table 2.2, the heavier neutralino states $\tilde{\chi}_a^0$, $a = 2, 3, 4$, do not contribute to these signals; either they are too heavy and hence not or only rarely produced in the slepton decays, or they are too light in order to decay invisibly via $\tilde{\chi}_a^0 \rightarrow \tilde{\nu} \nu \rightarrow \tilde{\chi}_1^0 \nu \nu$. Other open channels such as $\tilde{\tau} \tau$ lead to more complicated final states which are not considered here.

As already mentioned, the flavor violation can take place in the production and the decay, caused by the LFV vertices of the type lepton-slepton-neutralino and Z -slepton-slepton (Appendix B.5). The effect of the lepton flavor violating Z vertex is rather subdominant as it is additionally suppressed by left-right mixing of the sleptons. In addition, t-channel exchange is roughly one order of magnitude larger than s-channel exchange.

Signal cross section The helicity amplitudes for our process, separated into production and decay, can be found in the Appendices D.2 and D.4. It is then straightforward to derive the cross sections for the complete $2 \rightarrow 4$ process $e^+ e^- \rightarrow \tilde{l}_j^+ \tilde{l}_i^- \rightarrow l_\beta^+ l_\alpha^- \tilde{\chi}_1^0 \tilde{\chi}_1^0$. For the square of the amplitudes summed over all possible intermediate slepton states one finds [61]

$$|\mathcal{M}|^2 = \sum_{ijkl} (\mathcal{M}_{ij} \mathcal{M}_{kl}^*) (\mathcal{M}_i^- \mathcal{M}_k^{-*}) (\mathcal{M}_j^+ \mathcal{M}_l^{+*}) C_{ik} \frac{\pi}{2\langle m\Gamma \rangle_{ik}} C_{jl} \frac{\pi}{2\langle m\Gamma \rangle_{jl}} \times \left[\delta(p_3^2 - m_{\tilde{l}_i}^2) + \delta(p_3^2 - m_{\tilde{l}_k}^2) \right] \left[\delta(p_4^2 - m_{\tilde{l}_j}^2) + \delta(p_4^2 - m_{\tilde{l}_l}^2) \right], \quad (3.16)$$

with

$$C_{ik} = \frac{1}{1 + i \frac{\Delta \tilde{m}_{ik}^2}{2\langle m\Gamma \rangle_{ik}}}, \quad \langle m\Gamma \rangle_{ik} = \frac{1}{2} (m_{\tilde{l}_i} \Gamma_{\tilde{l}_i} + m_{\tilde{l}_k} \Gamma_{\tilde{l}_k}), \quad \Delta \tilde{m}_{ik}^2 = m_{\tilde{l}_i}^2 - m_{\tilde{l}_k}^2. \quad (3.17)$$

\mathcal{M}_{ij} , \mathcal{M}_i^- and \mathcal{M}_j^+ are the amplitudes for the slepton production, and the positive and negative slepton decay, respectively. As one can see in (3.16), we have used the narrow width approximation for the slepton propagators, which is well justified since the slepton widths $\Gamma_{\tilde{l}_i}$, of order 1 GeV or less, are much smaller than the slepton masses of order 100 GeV. For the product of two slepton propagators, this approximation yields [49]

$$\left(\frac{1}{p^2 - m_{\tilde{l}_i}^2 + im_{\tilde{l}_i} \Gamma_{\tilde{l}_i}} \right) \left(\frac{1}{p^2 - m_{\tilde{l}_k}^2 + im_{\tilde{l}_k} \Gamma_{\tilde{l}_k}} \right)^* \approx C_{ik} \frac{\pi}{2\langle m\Gamma \rangle_{ik}} \left[\delta(p^2 - m_{\tilde{l}_i}^2) + \delta(p^2 - m_{\tilde{l}_k}^2) \right]. \quad (3.18)$$

In principle, it is necessary to include the interference between the identical outgoing neutralinos (which are Majorana particles). This effect is negligible in the case of small slepton decay widths. We checked this during the Monte-Carlo simulation of the signal.

Integrating over the slepton momenta squared, p_3^2 and p_4^2 , and using the definitions (the

particle four-momenta are defined in Figure 3.2)

$$\begin{aligned}
d\sigma_{ijkl} &= (2\pi)^4 \delta(p_1 + p_2 - p_3 - p_4) \frac{d^3 p_3}{(2\pi)^3 2E_3} \frac{d^3 p_4}{(2\pi)^3 2E_4} \frac{\mathcal{M}_{ij} \mathcal{M}_{kl}^*}{2s}, \\
dB_{ik} &= (2\pi)^4 \delta(p_3 - p_5 - p_7) \frac{d^3 p_5}{(2\pi)^3 2E_5} \frac{d^3 p_7}{(2\pi)^3 2E_7} \frac{C_{ik}}{2\langle m\Gamma \rangle_{ik}} \mathcal{M}_i^- \mathcal{M}_k^{-*}, \\
dB_{jl} &= (2\pi)^4 \delta(p_4 - p_6 - p_8) \frac{d^3 p_6}{(2\pi)^3 2E_6} \frac{d^3 p_8}{(2\pi)^3 2E_8} \frac{C_{jl}}{2\langle m\Gamma \rangle_{jl}} \mathcal{M}_j^+ \mathcal{M}_l^{+*},
\end{aligned} \tag{3.19}$$

the differential cross sections can be expressed in the intuitive form

$$d\sigma(e^+ e^- \rightarrow l_\beta^+ l_\alpha^- + 2\tilde{\chi}_1^0) = \frac{1}{4} \sum_{ijkl} \sum_{\substack{p_3^2=m_l^2, m_k^2 \\ p_4^2=m_l^2, m_l^2}} d\sigma_{ijkl} dB_{ik} dB_{jl}. \tag{3.20}$$

As expected on general grounds, for large mass differences, $\Delta\tilde{m}_{ik}^2 \gg \langle m\Gamma \rangle_{ik}$, $i \neq k$, the factors C_{ik} in (3.17) approach δ_{ik} . Consequently, the coherent sum in (3.20) reduces to an incoherent sum over products of production cross sections times branching ratios,

$$d\sigma(e^+ e^- \rightarrow l_\beta^+ l_\alpha^- + 2\tilde{\chi}_1^0) \approx \sum_{ij} d\sigma(e^+ e^- \rightarrow \tilde{l}_j^+ \tilde{l}_i^-) dBr(\tilde{l}_i^- \rightarrow l_\alpha^- \tilde{\chi}_1^0) dBr(\tilde{l}_j^+ \rightarrow l_\beta^+ \tilde{\chi}_1^0). \tag{3.21}$$

Using the full slepton mixing matrix $U_{\tilde{l}}$ and summing over all intermediate slepton states, (3.20) takes into account all possible flavor transitions. If the off-diagonal entries in the slepton mass matrix (or alternatively, the mixing angles in $U_{\tilde{l}}$) are small, the cross section is dominated by one flavor transition. This is most easily formulated within the mass-insertion approximation, leading to

$$d\sigma(e^+ e^- \rightarrow l_\beta^+ l_\alpha^- + 2\tilde{\chi}_1^0) \approx \frac{|(\delta\mathbf{m}_{\tilde{L}}^2)_{\alpha\beta}|^2}{m_{\tilde{l}}^2 \Gamma_{\tilde{l}}^2} \sigma(e^+ e^- \rightarrow \tilde{l}_i^+ \tilde{l}_i^-) Br(\tilde{l}_i^- \rightarrow l_\alpha^- \tilde{\chi}_1^0) Br(\tilde{l}_i^+ \rightarrow l_\beta^+ \tilde{\chi}_1^0), \tag{3.22}$$

for $\alpha \neq \beta$, with the flavor-diagonal production cross section $\sigma(e^+ e^- \rightarrow \tilde{l}_i^+ \tilde{l}_i^-)$ and decay branching ratios $Br(\tilde{l}_{i/j}^\pm \rightarrow l_{\alpha/\beta}^\pm \tilde{\chi}_1^0)$. Care must be taken to include only those channels that allow the flavor transition at hand through one mass insertion only, e.g. for $\alpha = \mu$ and $\beta = \tau$ at least two flavor transitions would be necessary in the t-channel. Hence, only the s-channel flavor diagonal production cross section should be taken into account in the $\tau^+ \mu^-$ case. Comparing (3.22) with the analogous approximation for $Br(l_\alpha \rightarrow l_\beta \gamma)$ (3.8), one immediately sees that both observables are highly correlated with each other through the off-diagonal slepton mass terms,

$$Br(l_\alpha \rightarrow l_\beta \gamma) \propto \sigma(e^+ e^- \rightarrow l_\beta^+ l_\alpha^- + 2\tilde{\chi}_1^0) \propto |(\delta\mathbf{m}_{\tilde{L}}^2)_{\alpha\beta}|^2. \tag{3.23}$$

As is apparent in (3.17), the flavor correlation is highly sensitive to the masses and total widths of the sleptons. Whereas previous studies often used only generic values of these

quantities, we calculate the slepton decay widths $\Gamma_{\tilde{l}_i^-}$ in each scenario including the effects of LFV. For all mSUGRA benchmark scenarios used, the dominant slepton decay channels are

$$\begin{aligned}\tilde{l}_i^- &\rightarrow l_\alpha^- \tilde{\chi}_a^0 \\ &\rightarrow \bar{\nu}_\alpha \tilde{\chi}_a^- \\ &\rightarrow \tilde{l}_j^- Z \\ &\rightarrow \tilde{l}_j^- h_0,\end{aligned}\tag{3.24}$$

with a combined branching ratio always larger than 99%. The inclusion of these decays is essential for the numerical stability of the flavor correlation factors (3.17). The calculation of the two-body decays (3.24) is straightforward. The respective vertices can be found in [100].

Background analysis After having discussed the lepton flavor violating signals leading to the signatures $l_\beta^+ l_\alpha^- + \cancel{E}$, we now turn to the Standard Model and lepton flavor conserving SUSY background. For the dominant SM reactions we also illustrate the efficiency of angular and energy cuts in reducing this background. We are going to assume that at the time these searches for LFV will be performed, SUSY has already been discovered and the lighter sparticle masses and main decay channels are known. In this case, one will be able to design very specific cuts optimized to each channel of interest.

The background calculation was performed using the software package CompHEP [101]. For the Standard Model and lepton flavor conserving SUSY background processes the existing CompHEP model files were used. In order to study the impact of cuts on the signal, we implemented our own left-handed slepton flavor violating SUSY model, i.e. enhancing the standard SUSY model file with LFV vertices generated by off-diagonal mass terms (3.1).

The dominant Standard Model background is produced by the following lepton flavor conserving processes,

$$\begin{aligned}\text{B1)} \quad &e^+ e^- \rightarrow W^+ W^- \rightarrow l_\beta^+ \nu_\beta l_\alpha^- \bar{\nu}_\alpha, \quad \alpha \neq \beta, \\ \text{B2)} \quad &e^+ e^- \rightarrow W^+ e^- \bar{\nu}_e \rightarrow l_\beta^+ \nu_\beta e^- \bar{\nu}_e, \quad \beta \neq 1, \\ \text{B3)} \quad &e^+ e^- \rightarrow \tau^+ \tau^- \rightarrow \tau^+ \nu_\tau l_\alpha^- \bar{\nu}_\alpha, \quad \alpha = 1, 2,\end{aligned}$$

all with the signature $l_\beta^+ l_\alpha^- + \cancel{E}$. It will turn out that these processes cause the dominant background to our signals. In order to reduce it we adopt three different types of cuts:

Beam-pipe cuts: $|\cos(e^\pm, l_{\beta/\alpha}^\pm)| < 0.966$ ($\sim 15^\circ$)

Cutting away small angles of the outgoing leptons partially eliminates the large contributions from the t -channel photon exchange in (B2), and small angle W^\pm (B1) and τ (B3) production. The angular distributions of the final leptons in the signal are relatively flat as the leptons are decay products of the heavy sleptons. The value of 15° roughly optimizes the signal to background ratio for all mSUGRA scenarios used. The signal rates themselves are only reduced by $\approx 15\%$. Optimizing the angular cut for each scenario is possible but does not have a large impact.

Lepton-energy cuts: $E_{\alpha/\beta}^{\min} \leq E_{l_{\alpha/\beta}^{\pm}} \leq E_{\alpha/\beta}^{\max}$

We require that the lepton energies lie within the intervals corresponding to the decay $\tilde{l}^{\pm} \rightarrow l_{\alpha/\beta}^{\pm} \tilde{\chi}_1^0$ in the signal,

$$E_{\alpha/\beta}^{\min} = \frac{m_{\tilde{l}}^2 - m_{\tilde{\chi}_1^0}^2}{2(E_{\tilde{l}} + p_{\tilde{l}})}, \quad E_{\alpha/\beta}^{\max} = \frac{m_{\tilde{l}}^2 - m_{\tilde{\chi}_1^0}^2}{2(E_{\tilde{l}} - p_{\tilde{l}})}, \quad (3.25)$$

where \tilde{l} is the appropriate mother-slepton, and the momentum and energies are given by

$$p_{\tilde{l}} = \sqrt{\frac{1}{4s} \lambda(s, m_{l_3}^2, m_{l_4}^2)}, \quad E_{\tilde{l}} = \sqrt{m_{\tilde{l}}^2 + p_{\tilde{l}}^2}, \quad (3.26)$$

in the center of mass frame. The ideal lepton energy distributions of the signal are flat between the limits E^{\min} , E^{\max} , and vanish outside. The only problem is that there can be up to six sleptons in the intermediate state, each with a differing mass, contributing to the signal coherently. Conservatively, the minimum (maximum) value of E^{\min} (E^{\max}) of all sleptons would be used to achieve full conservation of the signal cross section. To enhance the signal to background ratio we go a step further. As noticed in the previous section, the signal is dominated by one flavor transition and thus a certain combination of intermediate sleptons. In the μ^+e^- t -channel, the dominant intermediate states are $\tilde{e}_L^+ \tilde{e}_R^-$ and $\tilde{\mu}_L^+ \tilde{e}_R^-$, as the flavor of the negatively charged lepton is conserved, and the right-handed selectrons couple more strongly to neutralinos. They are also favored due to their smaller masses (see Table 2.2). This allows the usage of a more narrow energy interval without cutting too much of the signal, optimized for each scenario and flavor channel $l_{\beta}^+ l_{\alpha}^-$.

Missing-energy cut: $2m_{\tilde{\chi}_1^0} \leq \cancel{E} \leq \sqrt{s} - E_{\alpha}^{\min} - E_{\beta}^{\min}$

The outgoing neutralinos of the signal are neutral and not observable. They can only be traced through their missing energy, which must be larger than $2m_{\tilde{\chi}_1^0}$ but small enough to allow production of two leptons with their minimal energies. As in the lepton energy cut, we optimize $E_{\alpha/\beta}^{\min}$ for each scenario and flavor channel.

In Tables 3.1 and 3.2 we summarize the SM background cross sections to $e^+e^- \rightarrow \mu^+e^- + \cancel{E}$ and $e^+e^- \rightarrow \tau^+\mu^- + \cancel{E}$, respectively, that remain after applying the above cuts. The lepton flavor violating mass term $(\delta m_L^2)_{ij}$ is adjusted in each channel and scenario such that the uncut signal cross section amounts to 1 fb, allowing an easy determination of the cut efficiencies, which are also given in Tables 3.1 and 3.2. We do not consider the channel $e^+e^- \rightarrow \tau^+e^- + \cancel{E}$, as it will normally be unobservably small in the SUSY seesaw model to be discussed later. Requiring a signal to background ratio $S/\sqrt{B} \gtrsim 2$ leads to a minimal uncut and observable signal of roughly 0.2–0.3 fb in the μ^+e^- -channel and 0.1–0.3 fb in the $\tau^+\mu^-$ -channel for $\sqrt{s} = 500$ GeV and a luminosity of 1000 fb⁻¹. An additional background suppression may be achieved by applying selectron selection cuts [102] on the acoplanarity, lepton polar angle and missing transverse momentum, which are not possible (or only with

$\mu^+e^- + \cancel{E}$ (SM)			
Scenario	500 GeV	800 GeV	Efficiency
B'	9.8	8.1	70%
C'	4.2	8.4	50%
G'	5.1	10.0	60%
I'	5.3	12.3	60%
SPS1a	12.2	11.1	60%

Table 3.1: Cross sections in fb of the SM background in $e^+e^- \rightarrow \mu^+e^- + \cancel{E}$ collisions at $\sqrt{s} = 500$ GeV and 800 GeV including cuts. Also given is the efficiency (signal after cuts)/(uncut signal) of the applied cuts.

great difficulty) to implement in CompHEP. It has been shown that in this way the SM background to slepton pair production can be reduced to about 2-3 fb at $\sqrt{s} = 500$ GeV, while the signal cross section shrinks only by a factor of three.

$\tau^+\mu^- + \cancel{E}$ (SM)			
Scenario	500 GeV	800 GeV	Efficiency
B'	3.6	2.5	50%
C'	1.3	1.6	40%
G'	2.1	2.2	50%
I'	2.4	3.6	60%
SPS1a	4.7	2.9	40%

Table 3.2: Cross sections in fb of the SM background in $e^+e^- \rightarrow \tau^+\mu^- + \cancel{E}$ collisions at $\sqrt{s} = 500$ GeV and 800 GeV including cuts. Also given is the efficiency (signal after cuts)/(uncut signal) of the applied cuts.

In addition to the Standard Model background one also has to take into account lepton flavor conserving MSSM processes. The dominant production channels are:

$$\text{B4) } e^+e^- \rightarrow \tilde{l}_i^+ \tilde{l}_i^-,$$

$$\text{B5) } e^+e^- \rightarrow \tilde{\nu}_i \tilde{\nu}_i,$$

$$\text{B6) } e^+e^- \rightarrow \tilde{\chi}_b^+ \tilde{\chi}_a^-,$$

$$\text{B7) } e^+e^- \rightarrow \tilde{\chi}_b^+ e^- \tilde{\nu}_e,$$

where the particles decay into

- $\tilde{l}_i^+ \rightarrow l_i^+ \tilde{\chi}_1^0, \quad \tilde{\nu}_i \tilde{\chi}_1^+,$
- $\tilde{\nu}_i \rightarrow \nu_i \tilde{\chi}_1^0, \quad l_i^- \tilde{\chi}_1^+,$
- $\tilde{\chi}_1^+ \rightarrow l_i^+ \tilde{\nu}_i, \quad \tilde{l}_i^+ \nu_i.$

Tables 3.3, 3.4 and 3.5 list the MSSM background for the channels μ^+e^- , $\tau^+\mu^-$ and τ^+e^- , respectively. Again, the background was calculated using CompHEP, applying the above cuts, which do not have as large an impact as in the SM case for which they were optimized. The background production channels B4 - B7 were calculated separately and added only incoherently.

$\mu^+e^- + \cancel{E}$ (MSSM)								
$e^+e^- \rightarrow$	B'		C'	G'		I'	SPS1a	
	500	800	800	500	800	800	500	800
$\tilde{l}_i^+\tilde{l}_i^-$	≈ 0	≈ 0	≈ 0	0.02	0.05	0.08	≈ 0	≈ 0
$\tilde{\nu}_i\tilde{\nu}_i$	≈ 0	≈ 0	≈ 0	-	≈ 0	0.25	≈ 0	≈ 0
$\tilde{\chi}_b^+\tilde{\chi}_a^-$	≈ 0	0.03	1.8	-	0.03	≈ 0	≈ 0	0.05
$\tilde{\chi}_b^+e^-\tilde{\nu}_e$	≈ 0	0.01	2.0	-	0.02	≈ 0	≈ 0	0.01
Sum	≈ 0	0.05	3.8	0.02	0.1	0.33	≈ 0	0.06

Table 3.3: Cross sections in fb of the MSSM background in $e^+e^- \rightarrow \mu^+e^- + \cancel{E}$ collisions at $\sqrt{s} = 500$ GeV and 800 GeV. In scenarios C' and I' the cross sections are below 0.01 fb at $\sqrt{s} = 500$ GeV and are therefore omitted. Kinematically forbidden channels are marked by a hyphen. Cross sections smaller than 0.01 fb are denoted by ≈ 0 .

$\tau^+\mu^- + \cancel{E}$ (MSSM)								
$e^+e^- \rightarrow$	B'		C'	G'		I'	SPS1a	
	500	800	800	500	800	800	500	800
$\tilde{l}_i^+\tilde{l}_i^-$	2.7	2.1	≈ 0	≈ 0	0.3	1.5	2.6	2.2
$\tilde{\nu}_i\tilde{\nu}_i$	1.4	1.8	0.06	-	0.1	0.9	1.8	1.9
$\tilde{\chi}_b^+\tilde{\chi}_a^-$	≈ 0	0.6	4.3	-	1.2	0.7	≈ 0	0.3
Sum	4.1	4.5	4.9	≈ 0	1.6	3.1	4.4	4.4

Table 3.4: Cross sections in fb of the MSSM background in $e^+e^- \rightarrow \tau^+\mu^- + \cancel{E}$ collisions at $\sqrt{s} = 500$ GeV and 800 GeV. In scenarios C' and I' the cross sections are below 0.01 fb at $\sqrt{s} = 500$ GeV and are therefore omitted. Kinematically forbidden channels are marked by a hyphen. Cross sections smaller than 0.01 fb are denoted by ≈ 0 .

The direct MSSM background to $\mu^+e^- + \cancel{E}$ is very small, below 0.2 fb in all scenarios except for C' and I', where it amounts to 4 and 0.3 fb, respectively, at $\sqrt{s} = 800$ GeV. With 2-5 fb the $\tau^+\mu^-$ background is considerably larger and comparable to the SM background. In Table 3.5 we now also show the MSSM background to $\tau^+e^- + \cancel{E}$, as it can contribute to the μ^+e^- channel via the decay $\tau^+ \rightarrow \mu^+\nu_\mu\bar{\nu}_\tau$. If $\tilde{\tau}_1$ and $\tilde{\chi}_1^+$ are light enough, as in the scenarios B', I' and SPS1a, this background can be as large as 100 fb. The charginos mainly originate from selectron or $\tilde{\nu}_e$ pair production and decay almost exclusively into staus, $\tilde{\chi}_1^- \rightarrow \tilde{\tau}_1^-\bar{\nu}_\tau$. However, such events typically contain two neutrinos in addition to the two LSPs present also in the signal events. Thus, after the τ decay one has altogether six invisible particles instead

$\tau^+e^- + \cancel{E}$ (MSSM)								
$e^+e^- \rightarrow$	B'		C'	G'		I'	SPS1a	
	500	800	800	500	800	800	500	800
$\tilde{l}_i^+ \tilde{l}_i^-$	29.4	28.1	≈ 0	0.5	1.7	10.0	23.9	24.0
$\tilde{\nu}_i \tilde{\nu}_i$	43.2	65.9	0.06	-	0.1	27.7	35.2	56.1
$\tilde{\chi}_b^+ \tilde{\chi}_a^-$	≈ 0	0.6	4.7	-	1.1	0.4	0.10	1.0
$\tilde{\chi}_i^+ e^- \tilde{\nu}_e$	≈ 0	0.02	1.0	-	0.03	≈ 0	≈ 0	0.05
Sum	72.6	94.6	5.8	0.5	2.9	38.1	59.2	81.1

Table 3.5: Cross sections in fb of the MSSM background in $e^+e^- \rightarrow \tau^+e^- + \cancel{E}$ collisions at $\sqrt{s} = 500$ GeV and 800 GeV. In scenarios C' and I' the cross sections are below 0.01 fb at $\sqrt{s} = 500$ GeV and are therefore omitted. Kinematically forbidden channels are marked by a hyphen. Cross sections smaller than 0.01 fb are denoted by ≈ 0 .

of two, which should allow to discriminate the signal in $\mu^+e^- + \cancel{E}$ from this potentially dangerous MSSM background by cutting on various distributions.

In a recent analysis [103], it was shown that a signal cross section of 1 fb would yield a 5σ effect on the total cross section to $e^+e^- \rightarrow \mu^+e^- + \cancel{E}$ in SPS1a ($\sqrt{s} = 500$ GeV, 500 fb^{-1} luminosity, standard lepton selection criteria). For the $\tau^+\mu^-$ -channel, this is somewhat reduced, with a significance of 5σ for a signal cross section of 2 fb.

Polarized beams At a linear collider one has the possibility to polarize the incoming beams. TESLA aims to reach a maximal electron (positron) polarization of $|P_{e^-}| = 0.8$ ($|P_{e^+}| = 0.6$)². It does not seem immediately apparent that this may help reduce the background. W pair production, a dominant contribution to it, is suppressed by right-handed electron polarization, but so are our LFV signals, as they originate from left-handed slepton mass terms. It is worthwhile, though, to take a closer look. In the μ^+e^- LFV signal, the lepton flavor violation takes place in the positively charged lepton branch. The signal is thus enhanced for right-handed positrons ($P_{e^+} > 0$). To lowest order in the LFV couplings, there is no lepton flavor violation in the negative branch of the t-channel diagram of Figure 3.2. In fact, the contribution to the cross section from incoming right-handed electrons ($P_{e^-} > 0$) is somewhat larger than from left-handed electrons. This can be seen in Figure 3.3, where the signal cross section $\sigma(e^+e^- \rightarrow \mu^+e^- + 2\tilde{\chi}_1)$ is plotted as a function of the incoming electron and positron polarizations in the scenario SPS1a at $\sqrt{s} = 500$ GeV. The cross section can be maximally enhanced from 1 fb (unpolarized) to ≈ 2.3 fb by choosing the polarizations $P_{e^+} = +0.6$ and $P_{e^-} = +0.8$. Unfortunately, we are not able to calculate polarized cross sections with CompHEP. On general grounds, though, one can expect that the W pair background is reduced at this polarization state by roughly one third compared to the unpolarized case. This would result in a signal to background ratio enhancement of almost one order of magnitude.

²For the definition of polarization, see Appendix D.2.

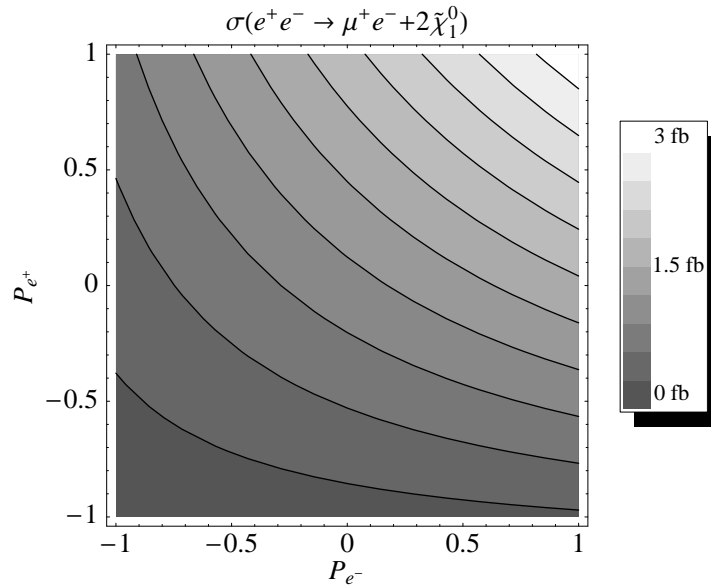


Figure 3.3: Signal cross section for $e^+e^- \rightarrow \mu^+e^- + 2\tilde{\chi}_1^0$ as function of the beam polarizations P_{e^-} and P_{e^+} in scenario SPS1a ($\sqrt{s} = 500$ GeV).

3.2.2 e^-e^- collider

Signal cross section The calculation of the electron-electron collider process $e^-e^- \rightarrow \tilde{l}_j^- \tilde{l}_i^- \rightarrow l_\beta^- l_\alpha^- \tilde{\chi}_1^0 \tilde{\chi}_1^0$ is fully analogous to the electron-positron collider case. The helicity amplitudes, calculated in [104], for the production can be found in Appendix D.3. The main difference is the missing photon and Z boson s-channel and the necessity to include an u-channel exchange, as shown in Figure 3.4. An important consequence of this is that the process $\tau^- \mu^- + 2\tilde{\chi}_1^0$ is only possible with two or more LFV transitions, because there is no s-channel stau or smuon production. As we only consider small LFV mass corrections, we will not discuss this channel. The construction of the total squared amplitude and the cross section works exactly as in (3.16) and (3.20), respectively.

Background analysis The main background processes with the signature $\mu^-e^- + \cancel{E}$ are

$$\text{B1)} \quad e^-e^- \rightarrow W^-e^- \nu_e \rightarrow l_\beta^- \nu_\beta e^- \bar{\nu}_e, \quad \beta \neq 1,$$

$$\text{B2)} \quad e^-e^- \rightarrow \tilde{l}_i^- \tilde{l}_i^- \rightarrow \dots,$$

$$\text{B3)} \quad e^-e^- \rightarrow \tilde{\chi}_b^- e^- \tilde{\nu}_e \rightarrow \dots,$$

i.e. single W^- production, flavor-conserving charged slepton pair production and single chargino production, analogous to the e^+e^- case. The dots refer to different decay channels given in the previous section. The W^- pair production process $e^-e^- \rightarrow W^-W^- \rightarrow l_\beta^- l_\alpha^- \bar{\nu}_\beta \bar{\nu}_\alpha$ ($\alpha, \beta \neq 1$) is in principle allowed in the seesaw model, but is highly suppressed due to the very small admixture of heavy right-handed Majorana neutrinos in the light neutrino mass

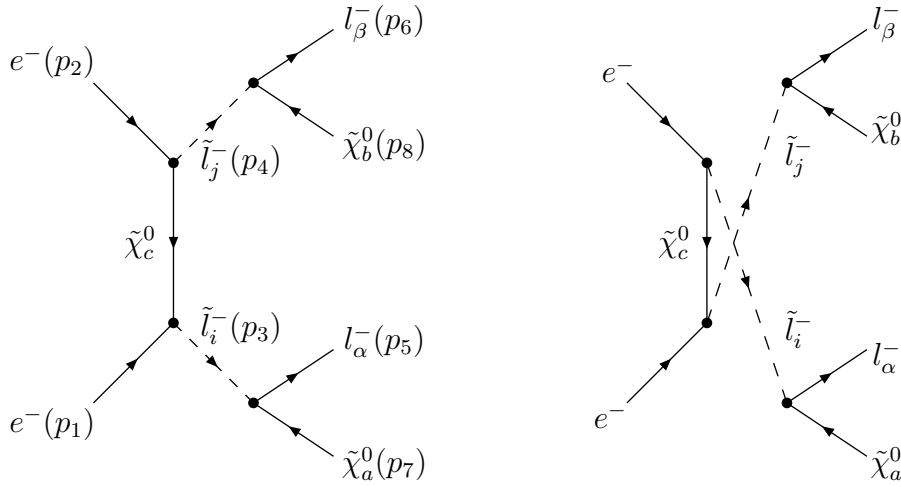


Figure 3.4: Feynman diagrams for $e^-e^- \rightarrow \tilde{l}_j^- \tilde{l}_i^- \rightarrow l_\beta^- l_\alpha^- \tilde{\chi}_b^0 \tilde{\chi}_a^0$. The arrows on scalar lines refer to the lepton number flow.

$\mu^-e^- + \cancel{E}$ (SM)			
Scenario	500 GeV	800 GeV	Efficiency
B'	17.4	39.1	60%
C'	6.8	21.3	50%
G'	9.1	30.1	70%
I'	11.2	34.3	60%
SPS1a	19.2	45.9	50%

Table 3.6: Cross sections in fb of the SM background in $e^-e^- \rightarrow \mu^-e^- + \cancel{E}$ collisions at $\sqrt{s} = 500$ GeV and 800 GeV including cuts. Also given is the efficiency (signal after cuts)/(uncut signal) of the applied cuts.

eigenstates [105]. The analogous argument holds for the SUSY version of this process, i.e. chargino pair production via t -channel sneutrino exchange.

The Standard Model background to $e^-e^- \rightarrow \mu^-e^- + \cancel{E}$, mainly originating from single W^- production, is shown in Table 3.6. The same cuts as in the e^+e^- case are applied. It can be seen that the background tends to be larger than for an e^+e^- collider. Also, there is a strong increase from $\sqrt{s} = 500$ GeV to 800 GeV due to the rise of W^- production with energy.

The total cross sections for the MSSM background processes are summarized in Tables 3.7 and 3.8. In all five scenarios the MSSM background to $\mu^-e^- + \cancel{E}$ is below 1 fb, while the background to $\tau^-e^- + \cancel{E}$ in scenarios B', I' and SPS1a is of the order of 100 fb. This is similar to our findings for e^+e^- collisions.

$\mu^- e^- + \cancel{E}$ (MSSM)								
$e^- e^- \rightarrow$	B'		C'	G'		I'	SPS1a	
	500	800	800	500	800	800	500	800
$\tilde{e}_i^- \tilde{e}_i^-$	0.01	0.01	≈ 0	0.01	0.2	0.4	0.01	0.02
$e^- \tilde{\nu} \tilde{\chi}_1^-$	≈ 0	0.01	0.4	-	0.1	≈ 0	≈ 0	0.01
Sum	0.01	0.02	0.4	0.01	0.3	0.4	0.01	0.03

Table 3.7: Cross sections in fb of the MSSM background in $e^- e^- \rightarrow \mu^- e^- + \cancel{E}$ collisions at $\sqrt{s} = 500$ GeV and 800 GeV. In scenarios C' and I' the cross sections are below 0.01 fb at $\sqrt{s} = 500$ GeV and are therefore omitted. Kinematically forbidden channels are marked by a hyphen. Cross sections smaller than 0.01 fb are denoted by ≈ 0 .

$\tau^- e^- + \cancel{E}$ (MSSM)								
$e^- e^- \rightarrow$	B'		C'	G'		I'	SPS1a	
	500	800	800	500	800	800	500	800
$\tilde{e}_i^- \tilde{e}_i^-$	120.8	102.3	≈ 0	0.2	8.1	60.0	91.3	85.6
$e^- \tilde{\nu} \tilde{\chi}_1^-$	≈ 0	0.01	0.4	-	0.07	≈ 0	≈ 0	0.03
Sum	120.8	102.3	0.4	0.02	8.2	60.0	91.3	85.6

Table 3.8: Cross sections in fb of the MSSM background in $e^- e^- \rightarrow \tau^- e^- + \cancel{E}$ collisions at $\sqrt{s} = 500$ GeV and 800 GeV. In scenarios C' and I' the cross sections are below 0.01 fb at $\sqrt{s} = 500$ GeV and are therefore omitted. Kinematically forbidden channels are marked by a hyphen. Cross sections smaller than 0.01 fb are denoted by ≈ 0 .

3.2.3 Precision mass measurements

Up to now, we only considered processes that are sensitive to off-diagonal slepton mass terms, which is of course the nature of slepton flavor violating processes. It is reasonable to assume that any theoretical extension generating flavor violating terms also produces additional diagonal slepton masses. Such diagonal contributions can carry important information, as will be the case in the supersymmetric seesaw.

The question now is just how such additional diagonal terms can be measured. The off-diagonal terms are small deviations from zero whereas diagonal additions are small deviations from large mSUGRA mass terms. In principle, all three parameters $(\delta m_L^2)_{ii}$ in (3.1) are measurable. This is not impossible as in mSUGRA all sfermion masses are connected to the common mass m_0 , potentially making its determination highly redundant. Nevertheless, it is very unlikely that all three quantities can be constrained or determined with enough precision.

Hence, we have to try to construct quantities that vanish in the flavor-conserving mSUGRA limit. Consider a typical mSUGRA charged slepton mass spectrum (see Table 2.2),

$$m_{\tilde{\tau}_1} < m_{\tilde{e}_R} \approx m_{\tilde{\mu}_R} < m_{\tilde{e}_L} \approx m_{\tilde{\mu}_L} < m_{\tilde{\tau}_2}, \quad (3.27)$$

i.e. selectrons and smuons (both left- and right-handed) are almost degenerate. This imme-

diately motivates the observable

$$m_{\tilde{\mu}_L}^2 - m_{\tilde{e}_L}^2 \equiv m_{\tilde{l}_5}^2 - m_{\tilde{l}_4}^2 \approx 2\langle m_{\tilde{l}} \rangle (m_{\tilde{l}_5} - m_{\tilde{l}_4}), \quad (3.28)$$

where $m_{\tilde{l}_5}^2 - m_{\tilde{l}_4}^2$ is actually more precise, using the proper mass eigenstate indices. The size of this quantity can be easily determined from (3.1) by calculating the appropriate mass eigenvalues. Again, we assume that the mass deviations are small. Then, it suffices to consider only the $\tilde{e}_L - \tilde{\mu}_L$ submatrix,

$$\begin{pmatrix} m_{\tilde{L}}^2 + (\delta m_{\tilde{L}}^2)_{11} & (\delta m_{\tilde{L}}^2)_{12}^* \\ (\delta m_{\tilde{L}}^2)_{12} & m_{\tilde{L}}^2 + (\delta m_{\tilde{L}}^2)_{22} \end{pmatrix}, \quad (3.29)$$

where the two diagonal mSUGRA contributions are equal. This leads to

$$m_{\tilde{l}_5}^2 - m_{\tilde{l}_4}^2 = \sqrt{((\delta m_{\tilde{L}}^2)_{22} - (\delta m_{\tilde{L}}^2)_{11})^2 + 4|(\delta m_{\tilde{L}}^2)_{12}|^2}, \quad (3.30)$$

showing that this observable is sensitive to the hierarchy of the diagonal contributions. For example, in the case of a strong hierarchy and small off-diagonal elements, $(\delta m_{\tilde{L}}^2)_{12}$, $(\delta m_{\tilde{L}}^2)_{11} \ll (\delta m_{\tilde{L}}^2)_{22}$, one simply has $m_{\tilde{l}_5}^2 - m_{\tilde{l}_4}^2 = (\delta m_{\tilde{L}}^2)_{22}$.

Various methods are proposed to precisely measure slepton masses [106, 107]. One possibility [108, 109] is to use the endpoints (3.25) of the lepton energy distributions in slepton pair production, which depend on the slepton mass. The efficiency of this method is affected by the cuts to reduce the background. Alternatively, one can measure the production cross section near the threshold. The characteristic onset of the threshold allows a very precise determination of the slepton masses. The expected experimental accuracy for such mass measurements is $\mathcal{O}(100 \text{ MeV})$. This necessitates the inclusion of beyond leading order effects in the theoretical predictions. With this method, one expects to determine the left-handed selectron and smuon masses at the per mill level in scenario SPS1a [107],

$$m_{\tilde{e}_L, \tilde{\mu}_L} \approx (202 \pm 0.2) \text{ GeV}. \quad (3.31)$$

We assume that a precision of the same order of magnitude may be achieved in the other scenarios also.

It is desirable to arrive at an analogous quantity for the stau mass splitting. This is not straightforward, because the staus are considerably separated from the other sleptons in flavor-conserving mSUGRA, due to

- the large τ Yukawa coupling affecting the running of $(m_{\tilde{L}}^2)_{33}$,
- the strong left-right mixing between the staus (also caused by the dominant τ Yukawa coupling), leading to two mass eigenstates $\tilde{l}_1 \equiv \tilde{\tau}_1 \approx \tilde{\tau}_R$ and $\tilde{l}_6 \equiv \tilde{\tau}_2 \approx \tilde{\tau}_L$.

As can be seen in Table 2.2, this leads to mass differences $m_{\tilde{\tau}_2}^2 - m_{\tilde{e}_L}^2$ of the order of 2-10 GeV. In this work, we take the optimistic viewpoint that a mass measurement of $m_{\tilde{\tau}_2}$ relative to the flavor-conserving mSUGRA value,

$$m_{\tilde{\tau}_2} - m_{\tilde{\tau}_2}^{\text{mSUGRA}}, \quad (3.32)$$

may be possible at some time. This could be achieved by redundantly determining the mSUGRA parameters (2.16) through measurements of several sparticle properties, thus allowing a reconstruction of the expected mSUGRA mass spectrum. The observable (3.32) would be directly sensitive to the slepton mass matrix contribution $(\delta m_{\tilde{L}}^2)_{33}$.

Chapter 4

Supersymmetric seesaw

4.1 Theoretical framework

A very attractive explanation of the apparent smallness of the neutrino masses is provided by the seesaw mechanism [17–19], which introduces heavy right-handed Majorana neutrinos, singlets under the SM gauge groups, to the SM particle content. Without supersymmetry, such massive fermions generate radiative corrections to the Higgs mass proportional to their squared masses, worsening the hierarchy problem. In a softly broken SUSY model, such contributions are cancelled to a high degree by those of their SUSY partners, the right-handed sneutrinos.

The supersymmetric seesaw model is described by additional terms in the superpotential [22],

$$\Delta\mathcal{W} = \hat{\nu}_R^{c\top} \mathbf{Y}_\nu \hat{L} \cdot \hat{H}_u - \frac{1}{2} \hat{\nu}_R^{c\top} \mathbf{M} \hat{\nu}_R^c, \quad (4.1)$$

where $\hat{\nu}_R$ are the right-handed neutrino singlet fields, \hat{L} denotes the left-handed lepton doublets and \hat{H}_u is the Higgs doublet with hypercharge $+1/2$. The 3×3 matrix \mathbf{M} contains Majorana masses, which are allowed for the neutral right-handed singlets $\hat{\nu}_R$, while \mathbf{Y}_ν is the matrix of neutrino Yukawa couplings, leading to the Dirac mass matrix

$$\mathbf{m}_D = \mathbf{Y}_\nu \langle h_u^0 \rangle, \quad (4.2)$$

after electroweak symmetry breaking. The soft SUSY-breaking Lagrangian is modified accordingly,

$$\Delta\mathcal{L}_{\text{soft}} = \tilde{\nu}_R^{c\dagger} \mathbf{m}_{\tilde{\nu}_R}^2 \tilde{\nu}_R^c + (\tilde{\nu}_R^{c\top} \mathbf{A}_\nu \tilde{L} \cdot \tilde{H}_u - \frac{1}{2} \tilde{\nu}_R^{c\top} \mathbf{B}_\nu \tilde{\nu}_R^c + \text{h.c.}), \quad (4.3)$$

with additional SSB terms $\mathbf{m}_{\tilde{\nu}_R}^2$, \mathbf{A}_ν and \mathbf{B}_ν . In principle, these terms modify the sneutrino mass matrix but as they are assumed to be of the order of 1 TeV, they can be neglected (compared to \mathbf{M} , which will be considered to contain masses of the order of 10^{10-15} GeV) in calculating the low energy sneutrino spectrum. See Appendix B.4 for details.

Light neutrinos can be naturally explained if one assumes that the Majorana scale M_R of \mathbf{M} is much larger than the scale of the Dirac mass matrix \mathbf{m}_D , which is of the order

of the electroweak scale. At energies much smaller than M_R one then has an effective superpotential [22]

$$\Delta\mathcal{W}_{\text{eff}} = -\frac{1}{2}(\hat{H}_u \cdot \hat{L}^\top \mathbf{Y}_\nu^\top) \mathbf{M}^{-1} (\mathbf{Y}_\nu \hat{L} \cdot \hat{H}_u), \quad (4.4)$$

with the right-handed neutrinos integrated out. After electroweak symmetry breaking, this superpotential leads to an effective mass matrix \mathbf{m}_ν for the left-handed light neutrinos,

$$\mathbf{m}_\nu = \mathbf{m}_D^\top \mathbf{M}^{-1} \mathbf{m}_D = (v \sin \beta)^2 \mathbf{Y}_\nu^\top \mathbf{M}^{-1} \mathbf{Y}_\nu, \quad (4.5)$$

which is suppressed by the large scale of the right-handed neutrinos as

$$m_\nu = 0.1 \text{ eV} \left(\frac{m_D}{100 \text{ GeV}} \right)^2 \left(\frac{M_R}{10^{14} \text{ GeV}} \right)^{-1}. \quad (4.6)$$

This result can also be obtained by expressing the superpotential (4.1) in matrix form,

$$\frac{1}{2} \begin{pmatrix} 0 & \mathbf{m}_D^\top \\ \mathbf{m}_D & -\mathbf{M} \end{pmatrix}, \quad (4.7)$$

in the $(\hat{L}, \hat{\nu}_R^c)$ basis. The seesaw formulae (4.5) and (4.6) then immediately follow by diagonalizing the seesaw matrix (4.7) in the limit $m_D \ll M_R$. In addition, this procedure shows that the mixing between the left- and right-handed neutrino states is suppressed by mixing angles $\theta_{LR}^\nu \approx \frac{m_D}{M_R}$.

The symmetric light neutrino mass matrix \mathbf{m}_ν can be diagonalized by a unitary matrix \mathbf{U} ,

$$\mathbf{U}^\top \mathbf{m}_\nu \mathbf{U} = \text{diag}(m_1, m_2, m_3), \quad (4.8)$$

that relates the neutrino flavor and mass eigenstates,

$$\begin{pmatrix} \nu_e \\ \nu_\mu \\ \nu_\tau \end{pmatrix} = \mathbf{U} \begin{pmatrix} \nu_1 \\ \nu_2 \\ \nu_3 \end{pmatrix}. \quad (4.9)$$

In general, the Maki-Nakagawa-Sakata (MNS) matrix \mathbf{U}_{MNS} which appears in neutrino oscillation observables is given by

$$\mathbf{U}_{\text{MNS}} = \mathbf{U} \mathbf{U}_e^\dagger, \quad (4.10)$$

with the charged lepton mixing matrix \mathbf{U}_e . In the following we work in the basis where the charged lepton Yukawa coupling matrix \mathbf{Y}_e and the Majorana mass matrix \mathbf{M} of the right-handed neutrinos are diagonal. This can always be achieved by rotating \hat{e}_R , $\hat{\nu}_R$ and \hat{L} appropriately. Consequently, the MNS matrix is identical to the left-handed neutrino mixing matrix \mathbf{U} in this basis. A popular parameterization for \mathbf{U} is

$$\mathbf{U} = \mathbf{V} \cdot \text{diag}(e^{i\phi_1}, e^{i\phi_2}, 1), \quad (4.11)$$

where ϕ_1, ϕ_2 are CP violating Majorana phases and \mathbf{V} can be written in the standard CKM form,

$$\mathbf{V} = \begin{pmatrix} c_{13}c_{12} & c_{13}s_{12} & s_{13}e^{-i\delta} \\ -c_{23}s_{12} - s_{23}s_{13}c_{12}e^{i\delta} & c_{23}c_{12} - s_{23}s_{13}s_{12}e^{i\delta} & s_{23}c_{13} \\ s_{23}s_{12} - c_{23}s_{13}c_{12}e^{i\delta} & -s_{23}c_{12} - c_{23}s_{13}s_{12}e^{i\delta} & c_{23}c_{13} \end{pmatrix}, \quad (4.12)$$

with $c_{ij} = \cos \theta_{ij}$ and $s_{ij} = \sin \theta_{ij}$. θ_{12} , θ_{23} and θ_{13} are the neutrino mixing angles measured in oscillation experiments and δ is the CP violating Dirac phase.

The experimental data on neutrino oscillations determine or at least constrain the mixing matrix \mathbf{V} . Using the results of recent neutrino fits (Section 4.5) and making some further necessary assumptions on the neutrino spectrum one can reconstruct \mathbf{m}_ν from (4.8),

$$\mathbf{m}_\nu = \mathbf{U}^* \cdot \text{diag}(m_1, m_2, m_3) \cdot \mathbf{U}^\dagger. \quad (4.13)$$

A major problem of the seesaw model is that it contains many free parameters. This is already obvious in (4.6), where it can be seen that a given light neutrino mass scale may be achieved by tuning m_D and M_R . In the general three generation case, the seesaw model contains 18 parameters: three Majorana masses $\mathbf{M} = \text{diag}(M_1, M_2, M_3)$ and 15 parameters in the Yukawa coupling matrix \mathbf{Y}_ν (\mathbf{Y}_ν as an arbitrary 3×3 complex matrix contains 18 parameters but 3 phases can be rotated away)¹. On the other hand, the (in principle) observable light neutrino mass matrix \mathbf{m}_ν contains 9 independent parameters (4.13): three mass eigenvalues, three mixing angles and three CP violating phases. Hence, it is not possible to reconstruct the full theory from observable quantities, even if all observables were measured. Nevertheless, one can try to parameterize this ambiguity. Inserting (4.13) into the seesaw formula (4.5) and explicitly using a diagonal Majorana matrix $\mathbf{M} = \text{diag}(M_1, M_2, M_3)$ leads to²

$$\mathbf{U}^* \cdot \text{diag } m_i \cdot \mathbf{U}^\dagger = (v^2 \sin^2 \beta) \mathbf{Y}_\nu^\top \cdot \text{diag } M_i^{-1} \cdot \mathbf{Y}_\nu, \quad (4.14)$$

which is of the form

$$\mathbf{A}^\top \mathbf{A} = \mathbf{B}^\top \mathbf{B}. \quad (4.15)$$

In general, this does not mean that $\mathbf{A} = \mathbf{B}$. Instead, $\mathbf{B} = \mathbf{R}\mathbf{A}$ for any matrix \mathbf{R} satisfying $\mathbf{R}^\top \mathbf{R} = \mathbb{I}$, i.e. a complex orthogonal matrix. Using \mathbf{R} , \mathbf{Y}_ν can be expressed as

$$\mathbf{Y}_\nu = \frac{1}{v \sin \beta} \text{diag } \sqrt{M_i} \cdot \mathbf{R} \cdot \text{diag } \sqrt{m_i} \cdot \mathbf{U}^\dagger. \quad (4.16)$$

This shows that the high energy theory can be fully described by \mathbf{U} , the light neutrino masses m_i , the right-handed Majorana masses M_i and \mathbf{R} . A possible parameterization of \mathbf{R} is given by [22]

$$\mathbf{R} = \begin{pmatrix} c_2c_3 & -c_1s_3 - s_1s_2c_3 & s_1s_3 - c_1s_2c_3 \\ c_2s_3 & c_1c_3 - s_1s_2s_3 & -s_1c_3 - c_1s_2s_3 \\ s_2 & s_1c_2 & c_1c_2 \end{pmatrix}, \quad (4.17)$$

¹In total, the leptonic sector of the seesaw model contains 21 physical parameters; in addition to the 18 parameters mentioned above, there are 3 charged lepton masses (in the basis of diagonal \mathbf{Y}_e).

²Throughout this work, we use the notation $\text{diag } X_i \equiv \text{diag}(X_1, X_2, X_3)$ for diagonal matrices. No summation over the index i is to be performed.

with three complex angles $\theta_j = x_j + ix_j$, $j = 1, 2, 3$ ($c_i = \cos \theta_i$, $s_i = \sin \theta_i$). Hence, there are six real parameters in \mathbf{R} . This can also be inferred by counting the necessary parameters in the theory:

$$18 = 6(\mathbf{U}) + 3(m_i) + 3(M_i) + 6(\mathbf{R}).$$

4.2 Renormalization group evolution

The addition of right-handed neutrinos crucially affects the renormalization group evolution of the theory. The RGEs of the SUSY seesaw model can be found in Appendix C.3. The method to apply them is outlined below.

Neutrino sector In the case of non-degenerate heavy neutrinos it is important to decouple the appropriate degrees of freedom at their respective scales. This is done by matching conditions [110] at the Majorana mass scales M_1 , M_2 and M_3 . We here present the bottom-up integration scheme, successively integrating in the right-handed neutrinos from bottom to top.

Below the mass M_1 of the lightest Majorana neutrino, the right-handed neutrinos are all decoupled and the effective superpotential (4.4) is in use. The only degrees of freedom are the light neutrinos whose effective mass matrix \mathbf{m}_ν is subject to RG running ((C.27) below the SUSY scale and (C.28) above). The input value at the experimental low energy scale is determined (or rather: constrained) by the neutrino observables. The RG evolution then proceeds as follows:

1. At M_1 , the lightest right-handed neutrino is integrated in, and the first row of the Yukawa matrix becomes active,

$$(\mathbf{Y}_\nu)_{ij}|_{M_{1+}} = \delta_{i1} \frac{1}{v \sin \beta} \left(\text{diag } \sqrt{M_i} \cdot \mathbf{R} \cdot \text{diag } \sqrt{m_i} \cdot \mathbf{U}^\dagger \right)_{ij} \Big|_{M_{1-}}, \quad (4.18)$$

where the parameters on the right-hand side are evaluated at M_1 . $|_{M_{1+(-)}}$ denotes a value just above (below) the threshold. Accordingly, the light neutrino matrix also experiences a shift due to tree-level matching:

$$(\mathbf{m}_\nu)_{ij}|_{M_{1+}} = (\mathbf{m}_\nu)_{ij}|_{M_{1-}} - (\mathbf{Y}_\nu^\dagger)_{i1} M_1^{-1} (\mathbf{Y}_\nu)_{j1} \Big|_{M_{1-}}. \quad (4.19)$$

At this point, the RGE for the Majorana matrix \mathbf{M} becomes active, causing M_1 to evolve. Above M_1 , the full set of RGEs for \mathbf{m}_ν , \mathbf{Y}_ν and \mathbf{M} is to be solved.

2. Analogously, at M_2 , the second row of \mathbf{Y}_ν , representing ν_{R2} , is switched on,

$$(\mathbf{Y}_\nu)_{ij}|_{M_{2+}} = (\mathbf{Y}_\nu)_{ij}|_{M_{2-}} + \delta_{i2} \frac{1}{v \sin \beta} \left(\text{diag } \sqrt{M_i} \cdot \mathbf{R} \cdot \text{diag } \sqrt{m_i} \cdot \mathbf{U}^\dagger \right)_{ij} \Big|_{M_{2-}}, \quad (4.20)$$

and accordingly,

$$(\mathbf{m}_\nu)_{ij}|_{M_{2+}} = (\mathbf{m}_\nu)_{ij}|_{M_{2-}} - (\mathbf{Y}_\nu^\dagger)_{i2} M_2^{-1} (\mathbf{Y}_\nu)_{j2} \Big|_{M_{2-}}. \quad (4.21)$$

3. At the third threshold there is a minor complication because \mathbf{M} is no longer diagonal due to the flavor mixing in (C.26). On the other hand, the mass eigenvalues M_i are to be inserted into the matching conditions. This demands a re-diagonalization,

$$\mathbf{U}_M^\dagger \mathbf{M} \mathbf{U}_M = \text{diag } M_i, \quad (4.22)$$

and a re-alignment of \mathbf{Y}_ν ,

$$\mathbf{Y}_\nu \rightarrow \mathbf{U}_M^* \mathbf{Y}_\nu, \quad (4.23)$$

to be applied before the matching condition³:

$$(\mathbf{Y}_\nu)_{ij}|_{M_{3+}} = (\mathbf{Y}_\nu)_{ij}|_{M_{3-}} + \delta_{i3} \frac{1}{v \sin \beta} \left(\text{diag } \sqrt{M_i} \cdot \mathbf{R} \cdot \text{diag } \sqrt{m_i} \cdot \mathbf{U}^\dagger \right)_{ij} \Big|_{M_{3-}}, \quad (4.24)$$

$$(\mathbf{m}_\nu)_{ij}|_{M_{3+}} = 0. \quad (4.25)$$

Above M_3 , \mathbf{m}_ν vanishes; all right-handed neutrinos are now integrated in and the full high energy theory is applied.

4. Finally, \mathbf{Y}_ν and \mathbf{M} are evolved to the GUT scale, ready to be used for generating slepton flavor violation.

Slepton sector The crucial property of the SUSY seesaw model is the transmission of the apparent lepton flavor violation in the neutrino sector (i.e. \mathbf{Y}_ν) to the slepton sector through radiative corrections with $\nu_R/\tilde{\nu}_R$ in loops above the scale of the right-handed neutrinos. We are mostly interested in corrections to the charged slepton and sneutrino mass matrix which are generated by (from Appendix C.3):

$$\begin{aligned} \frac{dm_L^2}{d \log \mu} &= \left. \frac{dm_L^2}{d \log \mu} \right|_{\text{MSSM}} \\ &+ \frac{1}{16\pi^2} \left(m_L^2 \mathbf{Y}_\nu^\dagger \mathbf{Y}_\nu + \mathbf{Y}_\nu^\dagger \mathbf{Y}_\nu m_L^2 + 2 \left(\mathbf{Y}_\nu^\dagger m_{\tilde{\nu}_R}^2 \mathbf{Y}_\nu + m_{h_u}^2 \mathbf{Y}_\nu^\dagger \mathbf{Y}_\nu + \mathbf{A}_\nu^\dagger \mathbf{A}_\nu \right) \right), \end{aligned} \quad (4.26)$$

$$\frac{dm_{\tilde{e}}^2}{d \log \mu} = \left. \frac{dm_{\tilde{e}}^2}{d \log \mu} \right|_{\text{MSSM}}, \quad (4.27)$$

$$\frac{d\mathbf{A}_e}{d \log \mu} = \left. \frac{d\mathbf{A}_e}{d \log \mu} \right|_{\text{MSSM}} + \frac{1}{16\pi^2} \left(2\mathbf{Y}_e \mathbf{Y}_\nu^\dagger \mathbf{A}_\nu + \mathbf{A}_e \mathbf{Y}_\nu^\dagger \mathbf{Y}_\nu \right). \quad (4.28)$$

These have to be solved from the GUT scale downwards to the electroweak scale. It is natural to separate the solution of this running into mSUGRA and right-handed neutrino contribution parts:

$$\mathbf{m}_L^2 = m_0^2 \mathbb{I} + (\delta \mathbf{m}_L^2)_{\text{mSUGRA}} + \delta \mathbf{m}_L^2, \quad (4.29)$$

$$\mathbf{m}_{\tilde{e}}^2 = m_0^2 \mathbb{I} + (\delta \mathbf{m}_{\tilde{e}}^2)_{\text{mSUGRA}} + \delta \mathbf{m}_{\tilde{e}}^2, \quad (4.30)$$

$$\mathbf{A}_e = A_0 \mathbf{Y}_e + (\delta \mathbf{A}_e)_{\text{mSUGRA}} + \delta \mathbf{A}_e, \quad (4.31)$$

³Alternatively, one could continuously diagonalize \mathbf{M} and align \mathbf{Y}_ν during the RG evolution. This is not necessary, as the RGEs are invariant under unitary transformations of $\hat{\nu}_R$ [110].

where $(\delta m_{\tilde{L}}^2)_{\text{mSUGRA}}$, $(\delta m_{\tilde{e}}^2)_{\text{mSUGRA}}$ and $(\delta \mathbf{A}_e)_{\text{mSUGRA}}$ denote the usual flavor-diagonal MSSM renormalization group contributions with mSUGRA conditions at the GUT scale. On the other hand, $\delta m_{\tilde{L}}^2$ is the non-diagonal left-handed slepton mass matrix contribution (3.1) considered in the previous chapter, now calculated in the SUSY seesaw model. As can be seen in (4.27), $m_{\tilde{e}}^2$ remains diagonal, receiving no additional corrections due to right-handed neutrinos at one-loop order, $\delta m_{\tilde{e}}^2 = 0$. The trilinear coupling matrix \mathbf{A}_e is affected in the SUSY seesaw model but the impact on LFV processes is subdominant, of the order of 10% at most. This is because left-right couplings of the sleptons (to which \mathbf{A}_e contributes) are always suppressed by the lepton masses, m_{l_i}/m_Z . The contribution $\delta \mathbf{A}_e$ is included in the numerical results but does not change the qualitative discussion.

An approximate solution to the above RG equations would be extremely helpful for discussion purposes. This can be achieved in the leading-logarithmic approximation, where the RGEs are solved to lowest order in $\Delta(\log \mu)$ from the starting point M_{GUT} . Inserting the mSUGRA conditions for $m_{\tilde{L}}^2$, $m_{\tilde{\nu}_R}^2$, $m_{h_u}^2$, \mathbf{A}_e and \mathbf{A}_ν , leads to [21]

$$\delta m_{\tilde{L}}^2 = -\frac{1}{8\pi^2}(3m_0^2 + A_0^2)(\mathbf{Y}_\nu^\dagger \mathbf{L} \mathbf{Y}_\nu), \quad (4.32)$$

$$\delta \mathbf{A}_e = -\frac{3A_0}{16\pi^2} \mathbf{Y}_e \cdot (\mathbf{Y}_\nu^\dagger \mathbf{L} \mathbf{Y}_\nu), \quad (4.33)$$

where \mathbf{L} is a diagonal matrix,

$$\mathbf{L} = \text{diag} \left(\log \frac{M_{\text{GUT}}}{M_i} \right), \quad (4.34)$$

that describes the logarithmic running from the GUT scale to the Majorana scales, taking into account a possible hierarchy between the right-handed masses M_i . In this approximation, the slepton mass corrections, and thus all low energy observables discussed in Chapter 3, depend on the quantity (see (4.16)),

$$\mathbf{Y}_\nu^\dagger \mathbf{L} \mathbf{Y}_\nu = \frac{1}{v^2 \sin^2 \beta} \mathbf{U} \cdot \text{diag} \sqrt{m_i} \cdot \mathbf{R}^\dagger \cdot \text{diag} \left(M_i \log \frac{M_{\text{GUT}}}{M_i} \right) \cdot \mathbf{R} \cdot \text{diag} \sqrt{m_i} \cdot \mathbf{U}^\dagger. \quad (4.35)$$

For example, the approximation (3.8) for the branching ratio of $l_i \rightarrow l_j \gamma$ now reads

$$Br(l_i \rightarrow l_j \gamma) \approx \frac{1}{8\pi^2} \alpha^3 \tan^2 \beta \frac{m_{l_i}^4}{\tilde{m}^4} \frac{m_{l_i}}{\Gamma_i} \frac{(3m_0^2 + A_0^2)^2}{\tilde{m}^4} |(\mathbf{Y}_\nu^\dagger \mathbf{L} \mathbf{Y}_\nu)_{ij}|^2. \quad (4.36)$$

4.3 Bi-unitary parameterization

As we have seen, the matrix \mathbf{R} and the masses M_i parameterize the ambiguity in mapping the effective low energy model to the full high energy theory: $(\mathbf{m}_\nu, \mathbf{R}, M_i) \rightarrow (\mathbf{Y}_\nu, M_i)$. It is not possible to reconstruct the high energy parameters from the (in principle) observable \mathbf{m}_ν alone.

On the other hand, in the SUSY version of the seesaw model, one can (again, in principle) measure the quantities $(\mathbf{Y}_\nu^\dagger \mathbf{Y}_\nu)_{ij}$ via their impact on the slepton mass matrix⁴. As will be shown, this additional information allows in principle to reconstruct the full high energy theory from observable quantities: $(\mathbf{m}_\nu, \mathbf{Y}_\nu^\dagger \mathbf{Y}_\nu) \rightarrow (\mathbf{Y}_\nu, M_i)$. To this end, we adopt a biunitary diagonalization of \mathbf{Y}_ν [33],

$$\mathbf{Y}_\nu = \mathbf{U}_R^\dagger \cdot \text{diag } Y_i \cdot \mathbf{U}_L, \quad (4.37)$$

with unitary matrices \mathbf{U}_L and \mathbf{U}_R . Such a diagonalization is always possible for an arbitrary matrix \mathbf{Y}_ν [111]. The eigenvalues Y_i can be chosen real and positive by moving any phases into \mathbf{U}_L ,

$$\text{diag } Y_i = \text{diag } |Y_i| \cdot \text{diag } e^{i \arg Y_i} \quad (4.38)$$

$$\Rightarrow \mathbf{Y}_\nu = \mathbf{U}_R^\dagger \cdot \text{diag } |Y_i| \cdot \mathbf{U}'_L, \quad \text{with } \mathbf{U}'_L = \text{diag } e^{i \arg Y_i} \cdot \mathbf{U}_L. \quad (4.39)$$

The diagonalization expressions

$$\mathbf{Y}_\nu^\dagger \mathbf{Y}_\nu = \mathbf{U}_L^\dagger \cdot \text{diag } Y_i^2 \cdot \mathbf{U}_L, \quad (4.40)$$

$$\mathbf{Y}_\nu \mathbf{Y}_\nu^\dagger = \mathbf{U}_R^\dagger \cdot \text{diag } Y_i^2 \cdot \mathbf{U}_R, \quad (4.41)$$

follow immediately from (4.37), which shows that the mixing matrix \mathbf{U}_L and the eigenvalues Y_i can be determined if $\mathbf{Y}_\nu^\dagger \mathbf{Y}_\nu$ is known.

Now, we also take into account \mathbf{m}_ν through the seesaw formula (4.5), inserting (4.37),

$$\frac{1}{v^2 \sin^2 \beta} \mathbf{m}_\nu = \mathbf{U}_L^\dagger \cdot \text{diag } Y_i \cdot \mathbf{U}_R^* \cdot \text{diag } M_i^{-1} \cdot \mathbf{U}_R^\dagger \cdot \text{diag } Y_i \cdot \mathbf{U}_L, \quad (4.42)$$

and separate \mathbf{U}_R, M_i (which are unknown at this point),

$$\frac{1}{v^2 \sin^2 \beta} \text{diag } Y_i^{-1} \cdot \mathbf{U}_L^* \mathbf{m}_\nu \mathbf{U}_L^\dagger \cdot \text{diag } Y_i^{-1} = \mathbf{U}_R^* \cdot \text{diag } M_i^{-1} \cdot \mathbf{U}_R^\dagger. \quad (4.43)$$

\mathbf{U}_R and the right-handed neutrino masses M_i can be determined by diagonalizing the left-hand side of (4.43). As this procedure is not trivial, we will outline it in detail. First, \mathbf{U}_L is determined via (4.40), yielding the Yukawa coupling eigenvalues Y_i . These are inserted into (4.42), which reads

$$\mathbf{X} = \mathbf{U}_R^* \cdot \text{diag } M_i^{-1} \cdot \mathbf{U}_R^\dagger, \quad (4.44)$$

with

$$\mathbf{X} = \frac{1}{v^2 \sin^2 \beta} \text{diag } Y_i^{-1} \cdot \mathbf{U}_L^* \mathbf{m}_\nu \mathbf{U}_L^\dagger \cdot \text{diag } Y_i^{-1}. \quad (4.45)$$

Multiplying (4.44) with its hermitian conjugate leads to

$$\mathbf{X}^\dagger \mathbf{X} = \mathbf{U}_R \cdot \text{diag } |M_i|^{-2} \cdot \mathbf{U}_R^\dagger, \quad (4.46)$$

⁴As can be seen in the leading-log approximations (4.32) and (4.33), the logarithmic running between M_{GUT} and M_i slightly modifies this behavior: $\mathbf{Y}_\nu^\dagger \mathbf{Y}_\nu \rightarrow \mathbf{Y}_\nu^\dagger \mathbf{L} \mathbf{Y}_\nu$. For the moment, we neglect this effect. It will be shown in Chapter 7 that the logarithmic enhancement can be correctly taken care of through iterative RG running.

representing a standard diagonalization of a hermitian matrix $\mathbf{X}^\dagger\mathbf{X}$ with a unitary matrix \mathbf{U}_R . To determine the phases of the eigenvalues M_i^{-1} , we calculate (4.44)

$$\mathbf{U}_R^\dagger\mathbf{X}\mathbf{U}_R = \text{diag } M_i^{-1}. \quad (4.47)$$

Any phases found in this matrix are absorbed into $\mathbf{U}_R \rightarrow \mathbf{U}_R \cdot \text{diag } e^{-i/2\arg M_i^{-1}}$. As the final result, we have two unitary matrices \mathbf{U}_L , \mathbf{U}_R and the real, positive eigenvalues Y_i and M_i which fully describe the seesaw model.

Ultimately, this proves that if $\mathbf{Y}_\nu^\dagger\mathbf{Y}_\nu$ and \mathbf{m}_ν are completely known, \mathbf{Y}_ν and M_i can be fully reconstructed. The number of independent parameters adds up correctly,

$$18 = 9(\mathbf{Y}_\nu^\dagger\mathbf{Y}_\nu) + 9(\mathbf{m}_\nu). \quad (4.48)$$

In summary, we identified in this chapter three different parameterizations of the SUSY seesaw sector, each with its own advantages and drawbacks:

1. *High energy basis* (\mathbf{Y}_ν, M_i). This is the basis in which the high energy SUSY seesaw model is defined. The Yukawa coupling matrix \mathbf{Y}_ν and the right-handed neutrino masses M_i are naturally given at M_{GUT} . Theoretical models and Yukawa textures are most easily applied in this parameterization, but a phenomenologically viable low energy theory in the form of correct neutrino oscillation parameters and allowed lepton flavor violating process rates is not guaranteed.
2. *Seesaw basis* ($\mathbf{m}_\nu, \mathbf{R}, M_i$). This parameterization guarantees a successful light neutrino sector but not viable LFV process rates. Its main advantage is that it allows one to keep the important Majorana masses M_i as input while studying the influence of the light neutrino parameters. A disadvantage is the appearance of the unknown matrix \mathbf{R} , which lacks a clear physical interpretation.
3. *Low energy basis* ($\mathbf{Y}_\nu^\dagger\mathbf{Y}_\nu, \mathbf{m}_\nu$). Expressing the neutrino sector in these quantities, it is possible to guarantee both viable light neutrino parameters and slepton mass contributions through LFV processes. It thus enables one to perform a proper bottom-up analysis with the possibility to reconstruct the high energy theory from the observables.

4.4 Leptogenesis

Another attractive feature of the seesaw model is that it provides a natural mechanism to generate the observed baryon number asymmetry of the universe (BAU), which can be expressed in terms of the baryon to photon number density η_B at the photon recombination time. Observations of the Cosmic Microwave Background radiation combined with observations of the large scale structure provide a precise measurement [112, 113],

$$\eta_B = \frac{n_B - n_{\bar{B}}}{n_\gamma} = (6.3 \pm 0.3) \cdot 10^{-10}. \quad (4.49)$$

There are three conditions that must be fulfilled for successful baryogenesis:

1. baryon number violation,
2. C and CP violation,
3. deviation from thermal equilibrium.

These are the famous Sakharov conditions [65], which can be met in the Standard Model, but the experimental value of η_B is still too large to be explained. Therefore, the observed baryon asymmetry requires new physics.

A detailed discussion of the BAU generation mechanism via leptogenesis in the seesaw model is beyond the scope of this work. We will only give a short review of the relevant facts. For further details, the reader is referred to [48, 114–116].

After the inflationary phase, right-handed neutrinos are produced, the number of which depending on the cosmological scenario. These neutrinos decay, violating CP and lepton number and generating a lepton asymmetry η_L . Finally, the transformation of the lepton asymmetry into a baryon asymmetry is performed by $B + L$ violating sphaleron processes [117], independent of the seesaw mechanism. The observed baryon asymmetry is then given by

$$\eta_B \approx -\frac{3}{4} c_{\text{sph}} f_{\text{dil}} \kappa_f \epsilon_1, \quad (4.50)$$

where

- ϵ_1 is the CP asymmetry generated by the decays of the lightest right-handed neutrino ν_{R1} . Here it is assumed that the masses of the right-handed neutrinos are sufficiently hierarchical so that only the decays of the lightest one contribute to the asymmetry. This is already the case for hierarchies as small as $M_{2,3} \gtrsim 2M_1$. In the seesaw model, ϵ_1 is [118]

$$\epsilon_1 = -\frac{1}{8\pi} \frac{1}{(\mathbf{Y}_\nu \mathbf{Y}_\nu^\dagger)_{11}} \sum_{i \neq 1} \text{Im} [(\mathbf{Y}_\nu \mathbf{Y}_\nu^\dagger)_{1i} (\mathbf{Y}_\nu \mathbf{Y}_\nu^\dagger)_{i1}] f \left(\frac{M_i^2}{M_1^2} \right), \quad (4.51)$$

with

$$f(x) = \sqrt{x} \left(\frac{2}{x-1} + \ln \frac{1+x}{x} \right). \quad (4.52)$$

- κ_f is the efficiency factor of washout processes (decays, inverse decays, $\Delta L = 1$ and $\Delta L = 2$ processes), which dilute the generated asymmetry. κ_f can be expressed as a function of the effective neutrino mass

$$\tilde{m}_1 = v^2 \sin^2 \beta \frac{(\mathbf{Y}_\nu \mathbf{Y}_\nu^\dagger)_{11}}{M_1}, \quad (4.53)$$

that is a measure of the coupling of the right-handed neutrinos to the thermal bath, and which generically lies in the range $m_1 < \tilde{m}_1 \lesssim m_3$. κ_f is determined by solving the Boltzmann equations for the $B - L$ asymmetry density and the density of the lightest

right-handed neutrinos. A reliable numerical fit in the region $\sqrt{\Delta m_{12}^2} < \tilde{m}_1 < \sqrt{\Delta m_{23}^2}$ is [114]

$$\kappa_f(\tilde{m}_1) \approx 0.24 \left(\frac{\tilde{m}_1}{8.3 \cdot 10^{-4} \text{ eV}} \right)^{-1.1}, \quad (4.54)$$

where Δm_{12}^2 and Δm_{23}^2 are the solar and atmospheric mass differences measured in neutrino oscillations. This \tilde{m}_1 -region of a mildly strong washout is preferred because, on the one hand, it is largely independent of the initial conditions after inflation and has minimal theoretical uncertainties. On the other hand, it does not yield an unrecoverable efficiency loss. The above fit for κ_f was obtained in the non-SUSY seesaw model, but is expected to hold true in the SUSY version also.

- f_{dil} is the dilution factor between the currently observed baryon asymmetry and the asymmetry at the time $T \approx M_1$. This dilution is due to standard photon production until the recombination of the photons [119]. Approximately, one has

$$f_{\text{dil}} \approx 0.017. \quad (4.55)$$

- c_{sph} is the factor for the conversion of the $B - L$ asymmetry after leptogenesis into the baryon asymmetry due to sphaleron processes. Sphalerons are non-perturbative transitions between different $SU(2)_L$ vacua that violate $B + L$ and which occur at temperatures above the scale of electroweak symmetry breaking. c_{sph} is in general a number of order $\mathcal{O}(1)$ and is

$$c_{\text{sph}} = 8/23 \quad (4.56)$$

in the MSSM.

In the case of hierarchical right-handed neutrinos $M_i^2 \gg M_1^2$, one has $f\left(\frac{M_i^2}{M_1^2}\right) \approx 3\frac{M_1}{M_i}$ in (4.52) for $i \neq 1$. Equation (4.51) can then be approximated as

$$\epsilon_1 \approx -\frac{3}{8\pi} \frac{M_1}{(\mathbf{Y}_\nu \mathbf{Y}_\nu^\dagger)_{11}} \sum_{i \neq 1} \frac{\text{Im}[(\mathbf{Y}_\nu \mathbf{Y}_\nu^\dagger)_{1i}^2]}{M_i}. \quad (4.57)$$

In terms of the matrix \mathbf{R} , this can be written as [120]

$$\epsilon_1 \approx -\frac{3}{8\pi} \frac{M_1}{v^2 \sin^2 \beta} \frac{\sum_i m_i^2 \text{Im}[(\mathbf{R}_{1i})^2]}{\sum_i m_i |\mathbf{R}_{1i}|^2}. \quad (4.58)$$

Similarly, \tilde{m}_1 is expressed as

$$\tilde{m}_1 = \sum_i m_i |\mathbf{R}_{1i}|^2, \quad (4.59)$$

which happens to be the denominator of (4.58). With the experimental value (4.49), we can turn (4.58) around, and solve for M_1 ,

$$M_1 \approx \eta_B \frac{32\pi v^2 \sin^2 \beta}{9} \frac{\kappa_f(\tilde{m}_1) \tilde{m}_1}{c_{\text{sph}} f_{\text{dil}} \sum_i m_i^2 \text{Im}[(\mathbf{R}_{1i})^2]}. \quad (4.60)$$

This relation can be interpreted as the condition on M_1 for successful baryogenesis via thermal leptogenesis. (4.58) also yields an upper bound on $|\epsilon_1|$. Due to the orthogonality condition $\sum_i (\mathbf{R}_{1i})^2 = 1$, one has [120]

$$|\epsilon_1| \leq \frac{3}{8\pi} \frac{M_1}{v^2 \sin^2 \beta} (m_3 - m_1), \quad (4.61)$$

which goes to zero for degenerate light neutrinos. Analogously, a lower bound on M_1 can be deduced from (4.60) [120],

$$M_1 > 10^{9-10} \text{ GeV}, \quad (4.62)$$

for hierarchical light neutrinos, $m_1 = 0$ eV.

There is a serious problem with leptogenesis in a mSUGRA framework due to a possible overabundance of gravitinos [121, 122]. If heavier than the LSP, which is generally the case in mSUGRA, the gravitino can decay into energetic photons, thereby spoiling big-bang nucleosynthesis. The number of gravitinos is proportional to the reheating temperature T_R of inflation. This results in an upper bound $T_R < 10^7, 10^9, 10^{12}$ GeV for gravitino masses $m_{3/2} = 100, 1000, 3000$ GeV, respectively [123]. If right-handed neutrinos are to be produced thermally after inflation, one then has $M_1 \lesssim T_R$. In order to meet this gravitino bound, M_1 should not be much larger than 10^{11} GeV. Compared with (4.62), it is clear that there is not much room left.

4.5 Neutrino data

The favored interpretation of the experimental results on solar neutrinos suggests $\nu_e \rightarrow \nu_{\mu,\tau}$ oscillations driven by the mass squared difference $\Delta m_{12}^2 = m_2^2 - m_1^2$ in the range of the large mixing angle (LMA) solution, while the results on atmospheric neutrinos are interpreted by $\nu_\mu \rightarrow \nu_\tau$ oscillations driven by $\Delta m_{23}^2 = m_3^2 - m_2^2$ in the case of three active neutrinos. For the present analysis, we use the global fits in a three-neutrino framework performed in [124].

Most likely, at the time when a linear collider will be in operation, more precise measurements of the neutrino parameters will be available than today. To take this into account, we use the central values of the mass squared differences $\Delta m_{ij}^2 = m_j^2 - m_i^2$ and mixing angles θ_{ij} from the current global fit to existing data [124] with errors that indicate the anticipated 2σ confidence level (CL) intervals of running and proposed experiments.

The expected future improvements in the experimental errors of the light neutrino parameters are summarized below:

- Δm_{12}^2 and $\sin^2 2\theta_{12}$: The long-baseline reactor experiment KAMLAND is designed to test the LMA solution of the solar neutrino problem. Data taking was started in 2002 and the solar neutrino parameters will be determined with an accuracy of $\delta(\Delta m_{12}^2)/\Delta m_{12}^2 = 10\%$ and $\delta(\sin^2 2\theta_{12}) = \pm 0.1$ within three years of measurement [125].
- Δm_{23}^2 and $\sin^2 2\theta_{23}$: Several long-baseline experiments based on neutrino beams, superbeams and new reactor experiments are planned or under construction for the next

decade. It is expected that their combined sensitivity can probe the atmospheric oscillation parameters with an accuracy of $\delta(\Delta m_{23}^2)/\Delta m_{23}^2 = 6\%$ and $\delta\theta_{23} = 0.81_{-0.10}^{+0.13}$ [126].

- $\sin^2 2\theta_{13}$: The CHOOZ reactor experiment restricts the angle θ_{13} to $\sin^2 2\theta_{13} < 0.1$ [127]. The long baseline experiment MINOS [128] can probe the range $\sin^2 2\theta_{13} \gtrsim 0.02 - 0.05$. The combined sensitivity of MINOS and other neutrino beam and reactor experiments is expected to be $\delta(\sin^2 2\theta_{13}) < 3 \cdot 10^{-3}$ [126].
- *Neutrino mass spectra*: The inverse hierarchical spectrum with two heavy and a single light state is disfavored according to an analysis [129,130] of the neutrino spectrum from supernova SN1987A, unless the mixing angle θ_{13} is large (compare, however, [131]). We therefore restrict our analysis to the direct (normal) hierarchy.
- *Dirac CP phase δ* : At a neutrino factory, one will be able to distinguish maximal from minimal CP violation. Without an existing fit, we vary δ in the full range $0 < \delta < 2\pi$ [132].
- *Majorana CP phases ϕ_1, ϕ_2* : Some information about one Majorana phase may be obtained by combining results of future double beta and tritium decay experiments and neutrino mass bounds obtained from fits to the large scale structure of the universe [133]. As this is very difficult, we allow a variation of both phases in their full ranges, $0 < \phi_i < 2\pi$, $i = 1, 2$.
- *Neutrino mass scale*: While neutrino oscillation experiments provide information on the neutrino mass squared differences Δm_{ij}^2 , the absolute scale of the neutrino masses is not known so far. Upper bounds can be obtained from the neutrino hot dark matter contribution to the cosmological large scale structure evolution and the Cosmic Microwave Background, tritium beta decay experiments and neutrinoless double beta decay experiments [134]. A next generation double beta decay experiment like GENIUSI will test the quantity $m_{ee} = |\sum_i V_{1i}^2 e^{i2\phi_i} m_i|$ down to 10^{-2} eV. Since $V_{13}^2 = \sin^2 2\theta_{13}/4 < 0.025$, the contribution of m_3 drops out and a bound $m_{ee} < 10^{-2}$ eV will imply $m_1 < 10^{-2}$ eV/ $\cos 2\theta_{12}$. Using the KAMLAND sensitivity $\delta(\sin^2 2\theta_{12}) = \pm 0.1$, one obtains the bound $m_1 < 3 \cdot 10^{-2}$ eV. On the other hand, a large mass m_1 could be tested by future tritium beta decay projects. A positive signal at the final sensitivity of the KATRIN experiment would imply $m_1 = 0.3 \pm 0.1$ eV [135]. Such a value would be compatible with the evidence claim for neutrinoless double beta decay [136].

The current best fit and 2σ CL ranges of the oscillation parameters are specified in Table 4.1, together with the future 2σ uncertainty ranges, which are based on the expected results from future experiments, that we will use in our numerical analysis. For the remaining light neutrino parameters, currently no positive experimental signals exist. As mentioned above, the CP violating phases δ , ϕ_1 and ϕ_2 will be very difficult to determine and thus are allowed to vary in their full ranges,

$$\delta, \phi_i = 0 - 2\pi, \quad i = 1, 2. \quad (4.63)$$

	best fit	present	future
$\sin^2 \theta_{12}$	0.30	$+0.05$ -0.05	$+0.05$ -0.05
$\sin^2 \theta_{23}$	0.52	$+0.14$ -0.16	$+0.10$ -0.10
$\sin^2 \theta_{13}$	0.005	$+0.032$ -0.005	$+0.001$ -0.005
$\Delta m_{12}^2/10^{-5} \text{ eV}^2$	6.90	$+1.50$ -0.80	$+0.36$ -0.36
$\Delta m_{23}^2/10^{-3} \text{ eV}^2$	2.3	$+0.7$ -0.9	$+0.7$ -0.9

Table 4.1: 2σ CL fits of neutrino oscillation parameters characterizing the present and future uncertainties.

With the neutrino mass scale unknown, we use two different neutrino mass spectra, characterized by

$$m_1 = 0 - 0.03 \text{ eV}, \quad (4.64)$$

for a spectrum that includes hierarchical masses. For discussion purposes, this case will be referred to as 'hierarchical'. For a (quasi-)degenerate spectrum, we use

$$m_1 = 0.3_{-0.16}^{+0.11} \text{ eV}. \quad (4.65)$$

Chapter 5

Results for degenerate right-handed neutrinos

The goal of this and the subsequent chapter is to present patterns of observables that are representative of the general outcome. To this end, we study the cases of (quasi-)degenerate and strongly hierarchical right-handed neutrino masses. These two cases are specifically chosen to be highly predictive with regard to the experimental observables. In addition, the impact of the light neutrino and mSUGRA parameters is analyzed in detail. Adapting the results of the previous chapter, the method of calculation is as follows:

1. We choose a specific realization for R and the masses M_i that depends on as few parameters as possible without being trivial.
2. Experimental results are used to constrain the neutrino matrix m_ν . The neutrino oscillation parameters are scattered within their expected future 2σ limits with a gaussian distribution. The unknown phases δ , ϕ_1 and ϕ_2 are varied linearly within their full ranges. The undetermined neutrino mass scale m_1 is taken care of through the two cases of hierarchical and degenerate neutrinos and scattered with a constant distribution, as outlined in Section 4.5.
3. The full one-loop seesaw RGEs are solved from M_Z to M_{GUT} .
4. The full one-loop MSSM+seesaw RGEs are solved from M_{GUT} to M_Z , yielding the low energy slepton mass corrections, which are used to calculate the observables of Chapter 3.

In this chapter, we assume that the right-handed Majorana masses are highly degenerate,

$$M_1 \approx M_2 \approx M_3 \approx M_R, \quad (5.1)$$

where M_R is the common mass scale. The matrix $Y_\nu^\dagger LY_\nu$ (4.35), responsible for generating low energy LFV is then given by

$$Y_\nu^\dagger LY_\nu = \frac{M_R}{v^2 \sin^2 \beta} \log \frac{M_{\text{GUT}}}{M_R} U \cdot \text{diag} \sqrt{m_i} \cdot R^\dagger R \cdot \text{diag} \sqrt{m_i} \cdot U^\dagger. \quad (5.2)$$

Due to \mathbf{R} being complex orthogonal but not hermitian, the expression does still depend on the arbitrary six parameters in \mathbf{R} . Hence, we make the further assumption that \mathbf{R} is real, so that it drops out of (5.2),

$$\mathbf{Y}_\nu^\dagger \mathbf{L} \mathbf{Y}_\nu = \frac{M_R}{v^2 \sin^2 \beta} \log \frac{M_{\text{GUT}}}{M_R} \mathbf{U} \cdot \text{diag } m_i \cdot \mathbf{U}^\dagger. \quad (5.3)$$

An immediate consequence is that the Majorana phases of the light neutrino mixing matrix \mathbf{U} also drop out: \mathbf{U} can be replaced with \mathbf{V} . Also, the matrix $\mathbf{Y}_\nu^\dagger \mathbf{Y}_\nu$ is diagonalized by \mathbf{U} , which in the bi-unitary language of Section 4.3 means that the left-handed mixing matrix \mathbf{U}_L can be identified with the hermitian conjugate of \mathbf{U} , $\mathbf{U}_L = \mathbf{U}^\dagger$, making the left-hand side of (4.43) diagonal. The right-handed mixing matrix \mathbf{U}_R can be chosen to be the unity matrix and \mathbf{Y}_ν is given by

$$\mathbf{Y}_\nu = \text{diag } Y_i \cdot \mathbf{U}^\dagger = \frac{1}{v \sin \beta} \text{diag } \sqrt{M_R m_i} \cdot \mathbf{U}^\dagger, \quad (5.4)$$

which can also be deduced from the \mathbf{R} matrix representation (4.16) by setting $\mathbf{R} = \mathbb{I}$ (it drops out anyway) and $\text{diag } M_i = M_R \mathbb{I}$. Expression (5.3) should be compared to the light neutrino matrix (4.13),

$$\mathbf{m}_\nu = \mathbf{U}^* \cdot \text{diag } m_i \cdot \mathbf{U}^\dagger. \quad (5.5)$$

Neglecting CP violating effects, the pattern of LFV transmitted to the sleptons is the same as the light neutrino mixing. This is an immediate consequence of our assumptions, namely degenerate right-handed neutrinos and a real \mathbf{R} matrix, which exclude any other possible influences. Therefore this class of models is highly predictive, maximally correlating neutral and charged lepton flavor violation. Moreover, one obtains conservative upper bounds on M_R for real \mathbf{R} , because a complex matrix \mathbf{R} generically leads to larger values of $\mathbf{Y}_\nu^\dagger \mathbf{L} \mathbf{Y}_\nu$ and thus to larger branching ratios $Br(l_i \rightarrow l_j \gamma)$ (see (4.36)) [22, 48].

As the scale of the lightest neutrino is unknown (Section 4.5), we will consider the cases of hierarchical and degenerate neutrino masses. Typical mass spectra can be parameterized as follows:

1. hierarchical ν_L :

$$m_1 \approx 0, \quad m_2 \approx \sqrt{\Delta m_{12}^2}, \quad m_3 \approx \sqrt{\Delta m_{23}^2}, \quad (5.6)$$

2. quasi-degenerate ν_L , [41]:

$$m_1, \quad m_2 \approx m_1 + \frac{\Delta m_{12}^2}{2m_1}, \quad m_3 \approx m_1 + \frac{\Delta m_{23}^2}{2m_1}, \quad (5.7)$$

$$\text{with } m_1 \gg \sqrt{\Delta m_{23}^2} \gg \sqrt{\Delta m_{12}^2}.$$

The product (5.3) of Yukawa couplings, can then be approximated by [61]

1. $(\mathbf{Y}_\nu^\dagger \mathbf{L} \mathbf{Y}_\nu)_{ij} \approx \frac{M_R}{v^2 \sin^2 \beta} \log \frac{M_{\text{GUT}}}{M_R} \left(\sqrt{\Delta m_{12}^2} V_{i2} V_{j2}^* + \sqrt{\Delta m_{23}^2} V_{i3} V_{j3}^* \right), \quad (5.8)$

2. $(\mathbf{Y}_\nu^\dagger \mathbf{L} \mathbf{Y}_\nu)_{ij} \approx \frac{M_R}{v^2 \sin^2 \beta} \log \frac{M_{\text{GUT}}}{M_R} \left(m_1 \delta_{ij} + \frac{1}{2m_1} (\Delta m_{12}^2 V_{i2} V_{j2}^* + \Delta m_{23}^2 V_{i3} V_{j3}^*) \right). \quad (5.9)$

In both cases the largest branching ratio, proportional to $|(\mathbf{Y}_\nu^\dagger \mathbf{L} \mathbf{Y}_\nu)_{ij}|^2$, for $l_i \rightarrow l_j \gamma$ is expected in the channel $\tau \rightarrow \mu \gamma$ because of $|V_{33} V_{23}^*| \approx |V_{32} V_{22}^*|$ and $\Delta m_{23}^2 \gg \Delta m_{12}^2$. The decays $\mu \rightarrow e \gamma$ and $\tau \rightarrow e \gamma$ are suppressed by the smallness of Δm_{12}^2 and V_{13} . In case 2), there is an additional suppression by $\sqrt{\Delta m_{23}^2/m_1}$ or $\sqrt{\Delta m_{12}^2/m_1}$ relative to case 1). All this is immediately obvious when inserting the best fit values (Section 4.5) for θ_{12} , θ_{23} , Δm_{12}^2 and Δm_{23}^2 ,

$$\mathbf{Y}_\nu^\dagger \mathbf{L} \mathbf{Y}_\nu \approx \frac{M_R}{10^{12} \text{ GeV}} \left(\frac{174 \text{ GeV}}{v \sin \beta} \right)^2 \log \frac{M_{\text{GUT}}}{M_R} \times \begin{pmatrix} 2.5 & \square^* & \square^* \\ 2.6 + 2.8x_{13}e^{i\delta} & 30 - 0.31x_{13} \cos \delta & \square^* \\ -2.8 + 2.7x_{13}e^{i\delta} & 23 - i0.31x_{13} \sin \delta & 27 + 0.31x_{13} \cos \delta \end{pmatrix}, \quad (5.10)$$

in case 1) of hierarchical neutrinos with $m_1 = 0$ eV, and

$$\mathbf{Y}_\nu^\dagger \mathbf{L} \mathbf{Y}_\nu \approx \frac{M_R}{10^{12} \text{ GeV}} \left(\frac{174 \text{ GeV}}{v \sin \beta} \right)^2 \log \frac{M_{\text{GUT}}}{M_R} \begin{pmatrix} 300 & \square^* & \square^* \\ 0.036 + 0.25x_{13}e^{i\delta} & 302 & \square^* \\ -0.038 + 0.24x_{13}e^{i\delta} & 2.1 & 302 \end{pmatrix}, \quad (5.11)$$

for degenerate neutrinos with $m_1 = 0.3$ eV. The boxes denote the conjugate elements fixed by the hermiticity of $\mathbf{Y}_\nu^\dagger \mathbf{L} \mathbf{Y}_\nu$. In both numerical expressions, only the lowest order in θ_{13} is retained with x_{13} being θ_{13} normalized to the best fit value, $x_{13} = \theta_{13}/0.078$. The expressions (5.10) and (5.11) are only used for discussion purposes. In our numerical calculations, we perform the full RGE running and scatter the neutrino parameters as described in Section 4.5.

Small deviations from degenerate Majorana masses Before analyzing the various LFV observables, we would like to comment briefly on the stability of the numerical results in this scenario. Due to RG running (Section 4.2), even a perfectly degenerate right-handed mass spectrum at M_{GUT} will experience non-degeneracies. This effect is included in our analysis, i.e. even though we use (5.1) as input, the final masses used for calculations are non-degenerate at the 10-20% level. In addition, we also probed the stability of our signals when using a relaxed parameter setup, namely:

- Quasi-degenerate Majoranas with small perturbations $\delta M_{1/3} = \frac{|M_{1/3} - M_2|}{M_2}$,
- full variation of the real mixing angles x_i in R (the imaginary parts y_i are still zero),
- full variation of the Majorana phases ϕ_i .

We found that the variation in any of the LFV observables O (such as $Br(\mu \rightarrow e \gamma)$) with respect to $\delta M_{1/3}$, x_i and ϕ_i is at most of the order

$$\frac{\delta O}{O} \lesssim (\delta M_{1/3})^2, \quad (5.12)$$

which are to be expected due to the quadratic dependence of the signal cross sections and rare decays on the Majorana masses (see discussion below). Such a variation was only performed to check the stability but is not part of the following results.

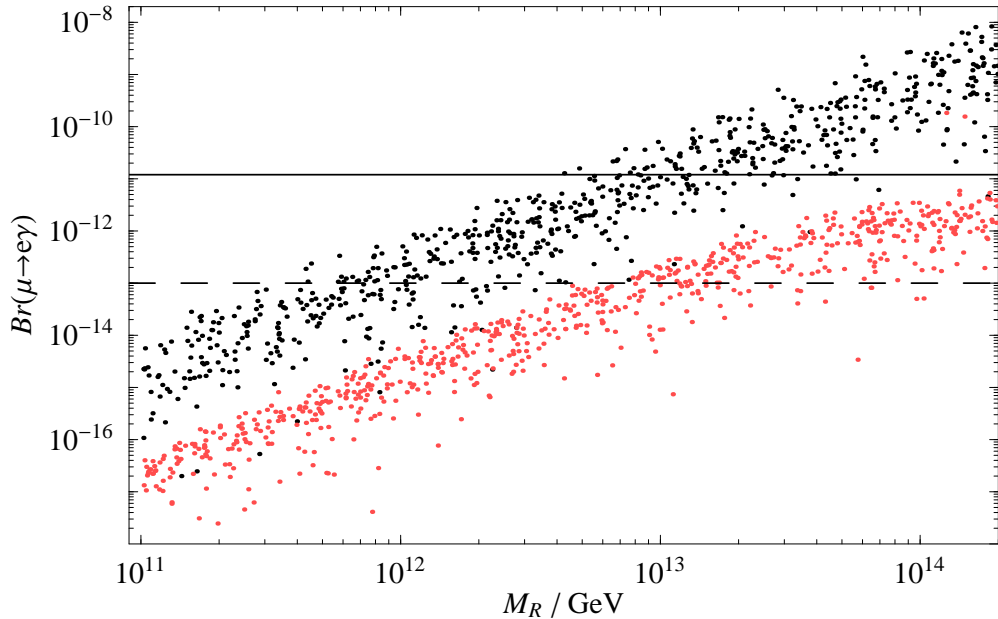


Figure 5.1: $Br(\mu \rightarrow e\gamma)$ as function of M_R for hierarchical (upper) and degenerate (lower) light neutrinos in SPS1a. The solid (dashed) line indicates the current (expected future) experimental sensitivity of $Br(\mu \rightarrow e\gamma)$.

Rare decays The dependence of $Br(\mu \rightarrow e\gamma)$ and $Br(\tau \rightarrow \mu\gamma)$ on the right-handed Majorana mass scale M_R is displayed in Figures 5.1 and 5.2, respectively, for both cases of neutrino mass spectra¹ in the mSUGRA scenario SPS1a. The most salient feature is the typical rise of the branching ratios with $|(Y_\nu^\dagger LY_\nu)_{ij}|^2 \propto M_R^2$. Due to the logarithmic running, this proportionality is actually better approximated with $Br \propto M_R^{1.8}$ in the range $10^{11} \lesssim M_R \lesssim 5 \cdot 10^{13}$. The dependence slightly changes for larger M_R in the case of degenerate light neutrinos. The current and expected future bounds on the branching ratios are denoted by solid and dashed lines in the figures, respectively.

The sensitivity of $Br(\mu \rightarrow e\gamma)$ on M_R for all benchmark mSUGRA scenarios is summarized in Table 5.1. The values should be interpreted as rough estimates, as the statistic uncertainty is rather large (as shown in Figure 5.1), especially for the upper value. The present and future bounds on $Br(\tau \rightarrow e\gamma)$ and $Br(\tau \rightarrow \mu\gamma)$ set no or relatively weak constraints on M_R and are therefore not included in Table 5.1 [87].

Comparing Figures 5.1 and 5.2, one can see that $Br(\mu \rightarrow e\gamma)$ is more strongly affected by the uncertainties in the neutrino parameters than $Br(\tau \rightarrow \mu\gamma)$. This finding may be understood qualitatively from (5.8) and (5.9), where one sees that $Br(\tau \rightarrow \mu\gamma)$ mainly depends on the large angle θ_{23} while $Br(\mu \rightarrow e\gamma)$ involves the small quantities θ_{13} and Δm_{12}^2 . The difference in the scatter range of the predictions for $Br(\tau \rightarrow \mu\gamma)$ and $Br(\mu \rightarrow e\gamma)$ thus reflects the different relative error of the quantities θ_{23}, θ_{13} and Δm_{12}^2 and also the complete lack of knowledge on δ . Furthermore, Figures 5.1 and 5.2 show that the experimental

¹Throughout this chapter, the hierarchical light neutrino case will be shown in dark (black), and the degenerate case in light (red) in the figures.

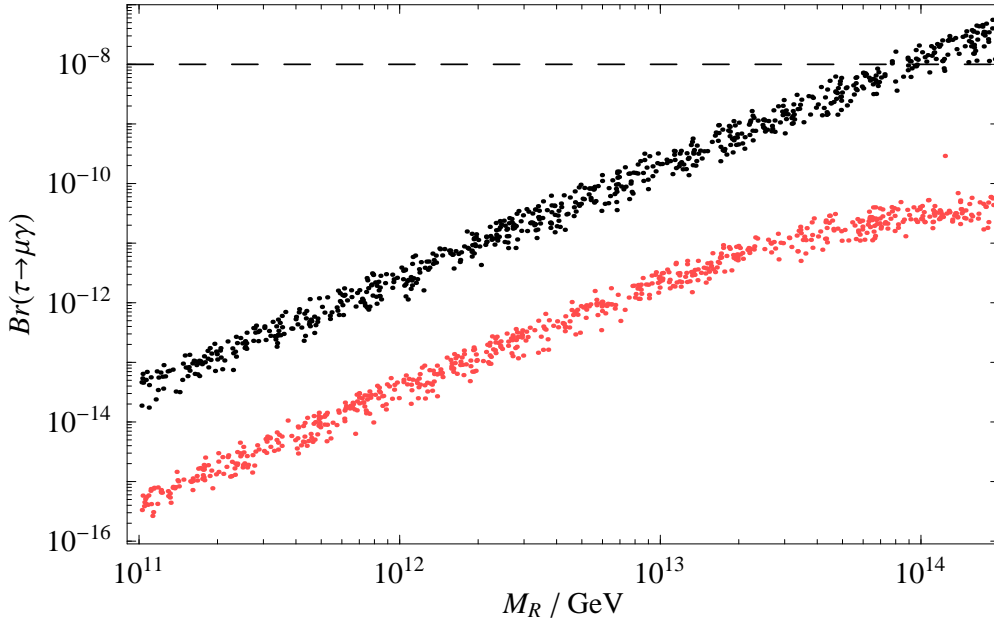


Figure 5.2: $Br(\tau \rightarrow \mu\gamma)$ as function of M_R for hierarchical (upper) and degenerate (lower) light neutrinos in SPS1a. The dashed line indicates the expected future experimental sensitivity of $Br(\tau \rightarrow \mu\gamma)$.

prospects favor the channel $\mu \rightarrow e\gamma$ over $\tau \rightarrow \mu\gamma$ for testing small values of M_R . Larger values of M_R would be probed more accurately in $\tau \rightarrow \mu\gamma$. We find for hierarchical neutrino spectra that a future measurement of $Br(\tau \rightarrow \mu\gamma) \approx 10^{-8}$ would typically determine M_R up to a factor of two given the uncertainties in the neutrino parameters. On the other hand, a measurement of $Br(\mu \rightarrow e\gamma) \approx 10^{-13}$ would determine the right-handed scale only within one or two orders of magnitude, as can be seen in Table 5.1, even if the SUSY parameters are known. Finally, assuming an exactly massless lightest neutrino (as in some previous works, e.g. [20, 22, 44]), the upper bounds on M_R improve by up to one order of magnitude.

The expected suppression for degenerate light neutrinos is clearly visible in both the figures and the table. $Br(l_i \rightarrow l_j\gamma)$ is suppressed by roughly two orders of magnitude as compared to the case of hierarchical neutrino spectra, but exhibits a similar dependence on M_R . At present, no bound can be obtained in any of the scenarios, see Table 5.1. A lightest neutrino with mass $m_1 \approx 0.3$ eV could thus be a natural explanation for the yet unobserved decay $\mu \rightarrow e\gamma$ in the light of the claimed evidence for neutrinoless double beta decay [136].

Contrary to our previous works [61–63], we find a saturation of the branching ratios for large M_R in case of degenerate neutrinos, which is clearly visible in Figures 5.1 and 5.2. This effect only appears in a full one-loop RG evolution of the neutrino sector. We did not see such a saturation in our earlier work as it was based on a simplified solution of the seesaw RGEs.

We also find that for a fixed M_R the branching ratios for $l_i \rightarrow l_j\gamma$ depend strongly on the particular mSUGRA scenario. The most stringent bounds on M_R are obtained in scenario SPS1a due to small sparticle masses and a non-vanishing A_0 , whereas scenario C' with large

$Br(\mu \rightarrow e\gamma)$	$= 1.2 \cdot 10^{-11}$		$= 10^{-13}$	
	hier. ν_L	deg. ν_L	hier. ν_L	deg. ν_L
SPS1a	$4 \cdot 10^{12} - 2 \cdot 10^{14}$	-	$4 \cdot 10^{11} - 3 \cdot 10^{12}$	$8 \cdot 10^{12} - 2 \cdot 10^{14}$
B'	$2 \cdot 10^{13} - 2 \cdot 10^{15}$	-	$1 \cdot 10^{12} - 4 \cdot 10^{13}$	$2 \cdot 10^{13} - 2 \cdot 10^{14}$
C'	$3 \cdot 10^{13} - 1 \cdot 10^{15}$	-	$2 \cdot 10^{12} - 2 \cdot 10^{14}$	$4 \cdot 10^{13} -$
G'	$2 \cdot 10^{13} - 3 \cdot 10^{14}$	-	$8 \cdot 10^{11} - 1 \cdot 10^{13}$	$2 \cdot 10^{13} - 2 \cdot 10^{14}$
I'	$7 \cdot 10^{12} - 2 \cdot 10^{14}$	-	$4 \cdot 10^{11} - 1 \cdot 10^{13}$	$1 \cdot 10^{13} - 1 \cdot 10^{14}$

Table 5.1: Uncertainty in M_R at the present and future sensitivities of $Br(\mu \rightarrow e\gamma)$ due to variation of the neutrino parameters (values in GeV).

gaugino masses yields the weakest bounds.

As mentioned in Section 4.5, inverse hierarchical light neutrino mass spectra are disfavored. Therefore, we concentrated on the (normal) hierarchical and degenerate cases. An analogous analysis of the inverse hierarchical case would be straightforward. It is expected that LFV rates for inverse hierarchical schemes lie in the intermediate range between the cases we discuss, $Br(\text{degenerate}) \ll Br(\text{inverse}) < Br(\text{hierarchical})$ [41].

In Chapter 3, we have seen that not only lepton flavor but also CP violating effects can be encoded into the slepton mass matrix, giving rise to electric dipole moments of the electron or muon. In the case considered here, the only possible source of CP violation is the Dirac phase δ of the light neutrino mixing matrix. It turns out that this does not give rise to measurable electric dipole moments. In scenario SPS1a, the maximally possible value compatible with the current bound on $Br(\mu \rightarrow e\gamma)$ is $d_e \approx 10^{-33}$ ecm, barely approaching the future sensitivity (3.15). The electric dipole moment of the muon is of the order of 10^{-31} ecm, far below the current and even the expected future sensitivity. This observation holds true in all scenarios considered.

Predictions for e^+e^- and e^-e^- collisions Figures 5.3 and 5.4 show the e^+e^- collider cross sections for $\mu^+e^- + 2\tilde{\chi}_1^0$ and $\tau^+\mu^- + 2\tilde{\chi}_1^0$ at $\sqrt{s} = 500$ GeV as a function of the right-handed Majorana mass scale M_R in scenario SPS1a. Just like the branching ratios $Br(l_i \rightarrow l_j\gamma)$, the cross sections exhibit the typical proportionality to $(Y_\nu^\dagger LY_\nu)_{ij}^2 \propto M_R^2$. This behavior indicates that the signal cross sections are dominated by Feynman graphs involving the lepton flavor violating vertices to first order as was assumed in Section 3.2. The latter in turn implies that $e^+e^- \rightarrow \tau^+\mu^- + 2\tilde{\chi}_1^0$ is dominantly a s -channel process and thus suppressed relative to $e^+e^- \rightarrow \mu^+e^- + 2\tilde{\chi}_1^0$ where both s - and t -channel contribute. For a detailed breakdown of the dominant intermediate slepton states, see the following paragraph on the beam energy dependence.

Furthermore, the cross sections saturate for large M_R , which is seen most clearly in the μ^+e^- -channel for hierarchical light neutrinos. This can be understood by realizing that for large M_R the mass differences of the sleptons with a dominant left-handed component become comparable to the corresponding slepton widths. As mentioned in Section 3.2, in this case the cross sections can be approximated by the incoherent sum (3.21). Focussing on the μ^+e^- -channel, the dominant contribution is determined by the \tilde{e}_L - $\tilde{\mu}_L$ mixing angle or,

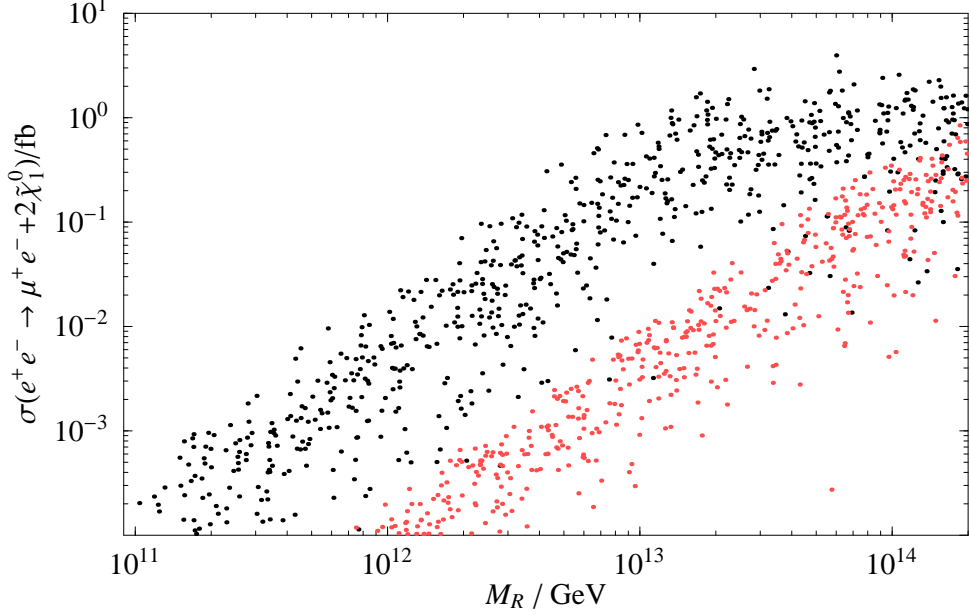


Figure 5.3: $\sigma(\mu^+e^- + 2\tilde{\chi}_1^0)$ as function of M_R for hierarchical (upper) and degenerate (lower) light neutrinos in SPS1a ($\sqrt{s} = 500$ GeV).

more precisely, by

$$\tan 2\theta_{\tilde{e}\tilde{\mu}} \approx \frac{2(m_{l_L}^2)_{12}}{(m_{l_L}^2)_{11} - (m_{l_L}^2)_{22}} \approx \frac{2(\mathbf{Y}_\nu^\dagger \mathbf{L} \mathbf{Y}_\nu)_{12}}{(\mathbf{Y}_\nu^\dagger \mathbf{L} \mathbf{Y}_\nu)_{11} - (\mathbf{Y}_\nu^\dagger \mathbf{L} \mathbf{Y}_\nu)_{22}}, \quad (5.13)$$

where the second equality follows from (4.32) and (B.15), if the lepton masses are neglected. Using (5.8) one then sees that $\tan 2\theta_{\tilde{e}\tilde{\mu}}$ and thus the cross section is independent of M_R . In the $\tau^+\mu^-$ channel the saturation is less pronounced due to effects of the heavier τ mass which dominate the denominator in the expression analogous to (5.13), except for very large values of M_R . The finite τ mass is also responsible for a suppression of all channels with a τ lepton in the final state relative to the μ^+e^- channel, which can be seen comparing Figures 5.3 and 5.4.

Beside these differences, the dependence of the cross sections and the branching ratios on the neutrino parameters and M_R are very similar. Again, the impact of the neutrino uncertainties is weaker in the $\tau^+\mu^-$ than in the μ^+e^- channel. Also, the τ^+e^- channel is unobservably small. Since this channel is unfavorable due to the τ mass suppression pointed out above and the comparably large MSSM background, we will concentrate on the μ^+e^- and $\tau^+\mu^-$ final states. As already noted, the proportionality with $|\mathbf{Y}_\nu^\dagger \mathbf{L} \mathbf{Y}_\nu|^2$ is also dominated by the M_R^2 (actually, $M_R^{1.8}$) dependence, and there is again a suppression for degenerate light neutrinos. Such correlations between collider processes and rare decays could be expected. Already in the context of general, albeit small, lepton flavor violating slepton mass terms, we anticipated the relation $\sigma(e^+e^- \rightarrow l_i^+ l_j^- + 2\tilde{\chi}_1^0) \propto Br(l_i \rightarrow l_j \gamma)$, see (3.23). The correlation between $\sigma(e^+e^- \rightarrow \mu^+e^- + 2\tilde{\chi}_1^0)$ at $\sqrt{s} = 500$ GeV and $Br(\mu \rightarrow e \gamma)$ is illustrated in Figure 5.5. For $Br(\mu \rightarrow e \gamma) \lesssim 10^{-13}$, this correlation is so accurate that

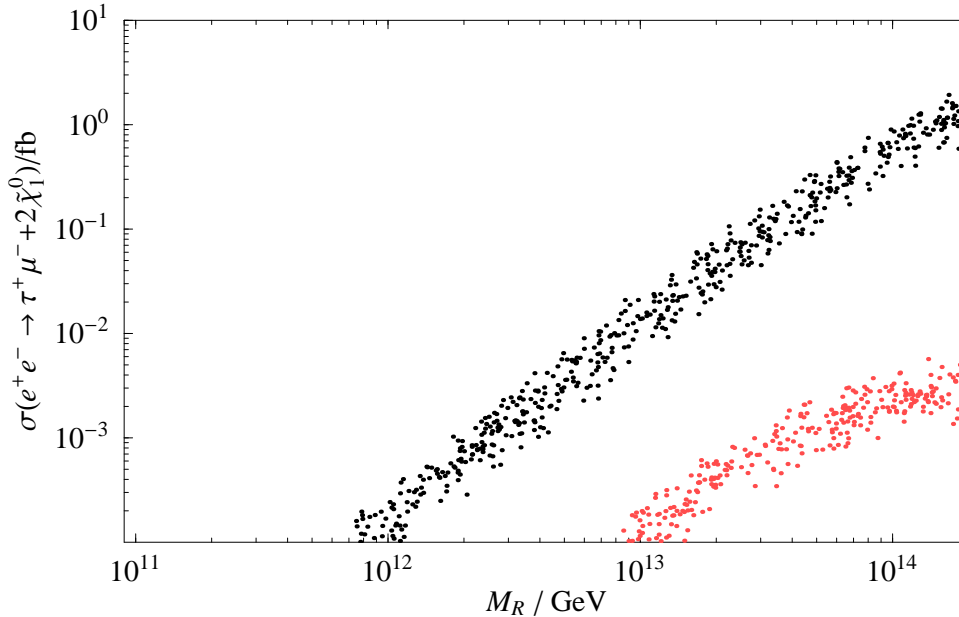


Figure 5.4: $\sigma(\tau^+\mu^- + 2\tilde{\chi}_1^0)$ as function of M_R for hierarchical (upper) and degenerate (lower) light neutrinos in SPS1a ($\sqrt{s} = 500$ GeV).

the neutrino uncertainties drop out almost completely. For hierarchical light neutrinos, the correlation extends to values up to 10^{-11} . Only for larger values of M_R the correlation is washed out because of the saturation of the cross sections explained above which sets in at different values of M_R depending on the precise values of the neutrino parameters. On the other hand, in the case of degenerate neutrinos, the branching ratio in Figure 5.1 exhibits a saturation for large $Br(\mu \rightarrow e\gamma)$, leading to a breaking of the correlation with the collider cross section. In the interesting intermediate range between the experimental sensitivities $10^{-13} < Br(\mu \rightarrow e\gamma) < 10^{-11}$, a collider has a better chance to see a signal for degenerate rather than for hierarchical light neutrinos.

Figure 5.6 shows the analogous correlation between $\sigma(e^+e^- \rightarrow \tau^+\mu^- + 2\tilde{\chi}_1^0)$ and $Br(\tau \rightarrow \mu\gamma)$, which is even stronger. It is accurate throughout the whole range of M_R , allowing all scenarios to be plotted. The degenerate case is also shown but yields vanishingly small $\tau^+\mu^-$ signal cross sections that are always smaller than 0.01 fb as in Figure 5.4.

These correlations between low energy and collider processes can be used to estimate the LC cross sections that are allowed by bounds on or measurements of the radiative decays. Taking scenario SPS1a as an example, one can read off from Figure 5.5 that the present bound $Br(\mu \rightarrow e\gamma) < 1.2 \cdot 10^{-11}$ implies $\sigma(e^+e^- \rightarrow \mu^+e^- + 2\tilde{\chi}_1^0) < 0.3$ fb (0.9 fb for degenerate neutrinos), while a measurement of $Br(\mu \rightarrow e\gamma) \approx 10^{-13}$ by the upcoming experiment at PSI would predict $\sigma(e^+e^- \rightarrow \mu^+e^- + 2\tilde{\chi}_1^0) \approx 3 \cdot 10^{-3}$ fb. In other words, if $\mu \rightarrow e\gamma$ will not be detected at PSI, one does not expect an observable μ^+e^- signal at a 500 GeV LC either. On the other hand, taking into account the background discussion of Section 3.2, the presently allowed cross section is in the observable range. The reach of an e^+e^- collider at $\sqrt{s} = 500$ GeV in the different scenarios is shown in Table 5.2, confirming the findings on

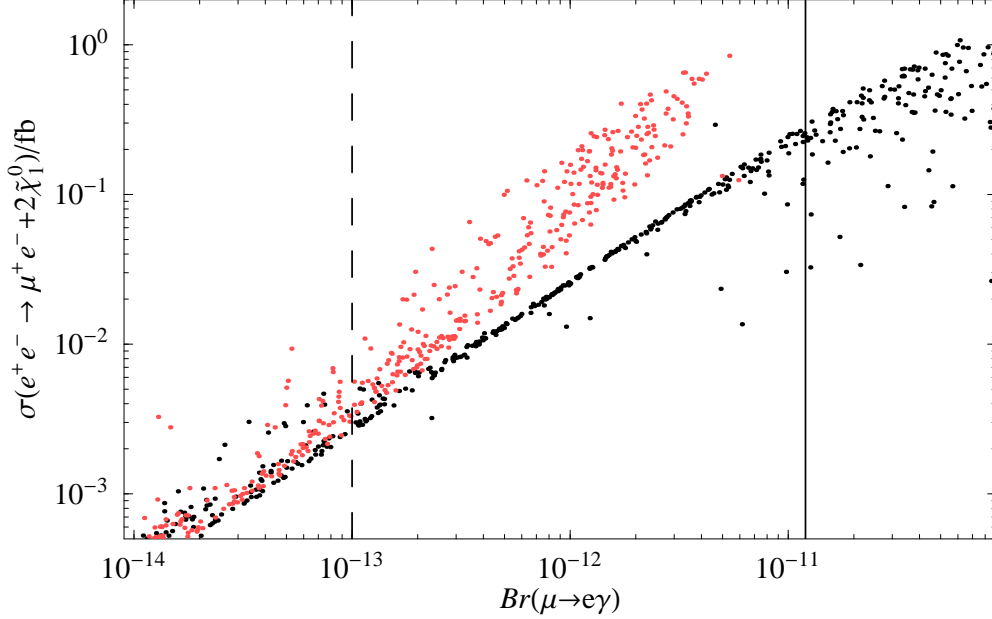


Figure 5.5: $\sigma(\mu^+e^- + 2\tilde{\chi}_1^0)$ as function of $Br(\mu \rightarrow e\gamma)$ for hierarchical (lower) and degenerate (upper) light neutrinos in SPS1a ($\sqrt{s} = 500$ GeV). The solid (dashed) line indicates the current (expected future) experimental sensitivity of $Br(\mu \rightarrow e\gamma)$.

SPS1a for the other scenarios.

$Br(\mu \rightarrow e\gamma)$	$< 1.2 \cdot 10^{-11}$		$< 10^{-13}$	
	hier. ν_L	deg. ν_L	hier. ν_L	deg. ν_L
SPS1a	0.3	0.8	0.005	0.01
B'	1.3	0.6	0.02	0.03
C'	1.2	0.2	0.07	0.03
G'	0.8	0.4	0.01	0.01
I'	< 0.01	< 0.01	< 0.01	< 0.01

Table 5.2: Maximal expectation at an e^+e^- collider for the signal $\sigma(\mu^+e^- + 2\tilde{\chi}_1^0)$ at $\sqrt{s} = 500$ GeV, depending on the maximally allowed branching ratio (values in fb).

Analogously, from Figure 5.6 one concludes that the present bound $Br(\tau \rightarrow \mu\gamma) < 3.1 \cdot 10^{-7}$ provides no constraints on M_R . More importantly, the sensitivity goal $Br(\tau \rightarrow \mu\gamma) \approx 10^{-8}$ of future searches will not rule out sizable LC cross sections, namely $\sigma(e^+e^- \rightarrow \tau^+\mu^- + 2\tilde{\chi}_1^0) \approx 1$ fb in scenarios SPS1 and B'. The other scenarios are heavily suppressed by kinematics, making it necessary to go to higher beam energies (see next paragraph). In fact, in the $\tau^+\mu^-$ -channel LC experiments may reach farther than the $\tau \rightarrow \mu\gamma$ experiments planned in the future. At any rate, here we have a good example for the complementarity of low and high energy searches.

In principle, one has correlations also in channels which differ in flavor. This is exemplified in Figure 5.7 for $\sigma(e^+e^- \rightarrow \tau^+\mu^- + 2\tilde{\chi}_1^0)$ and $Br(\mu \rightarrow e\gamma)$. However, because of the different

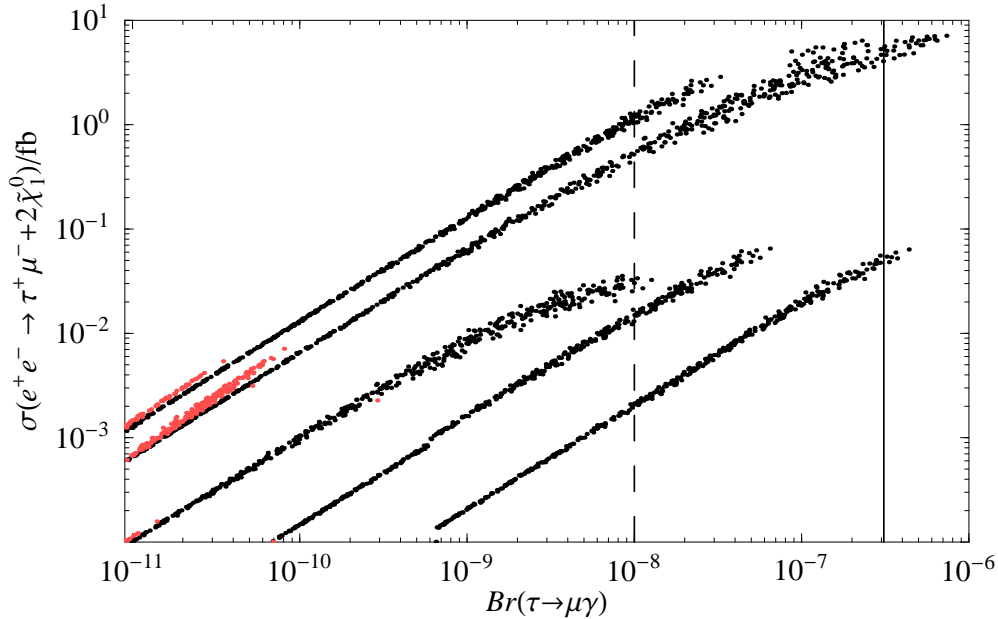


Figure 5.6: $\sigma(\tau^+\mu^- + 2\tilde{\chi}_1^0)$ as function of $Br(\tau \rightarrow \mu\gamma)$ for hierarchical (dark points) and degenerate (light points, lower left) neutrinos in scenarios B', SPS1a, C', G', I' (left to right) ($\sqrt{s} = 500$ GeV). The solid (dashed) line indicates the current (expected future) experimental sensitivity of $Br(\tau \rightarrow \mu\gamma)$.

flavor violating couplings involved, this correlation suffers considerably from uncertainties in the neutrino sector. Nevertheless, the experimental bound $Br(\mu \rightarrow e\gamma) < 1.2 \cdot 10^{-11}$ yields a stronger constraint on scenario SPS1a than the one obtained from Fig. 5.6, excluding $\sigma(\tau^+\mu^- + 2\tilde{\chi}_1^0)$ of the order of 0.1 fb at $\sqrt{s} = 500$ GeV already today. It must be emphasized that such a flavor cross-correlation crucially depends on the seesaw parameters used. The given bound here only applies in the case of degenerate Majoranas and a real R matrix.

We have also studied the prospects for e^-e^- collisions. Figure 5.8 shows $\sigma(e^-e^- \rightarrow \mu^-e^- + 2\tilde{\chi}_1^0)$ in scenario SPS1a at $\sqrt{s} = 500$ GeV. As has been mentioned in Section 3.2.2, the $\tau^-\mu^-$ final state is strongly suppressed because at least two flavor violating couplings are required due to the absence of the s -channel (see Figure 3.4). The τ^-e^- final state is disfavored for the same reasons as the τ^+e^- channel in e^+e^- collisions. Thus, μ^-e^- remains as the only promising channel.

The correlation between $\sigma(e^-e^- \rightarrow \mu^-e^- + 2\tilde{\chi}_1^0)$ and $Br(\mu \rightarrow e\gamma)$ is plotted in Figure 5.9. The reach of an e^-e^- collider at $\sqrt{s} = 500$ GeV in the different scenarios is given in Table 5.3. We see that the cross section permitted by the present bound on $\mu \rightarrow e\gamma$ lies in the range of 1-10 fb for scenarios SPS1a and B', which would make the detection comparatively easy, especially in the case of degenerate neutrinos.

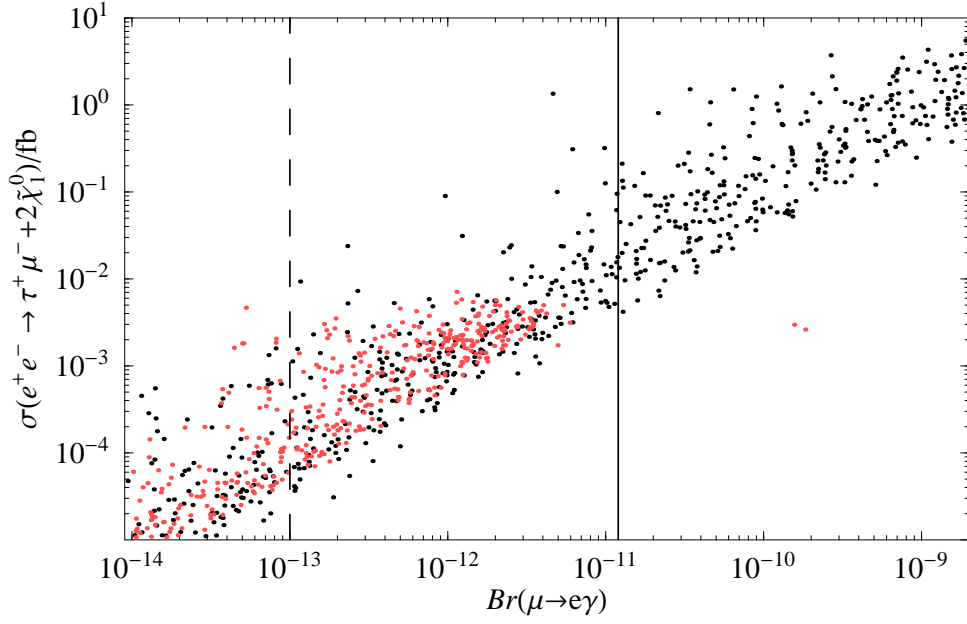


Figure 5.7: $\sigma(\tau^+\mu^- + 2\tilde{\chi}_1^0)$ as function of $Br(\mu \rightarrow e\gamma)$ for hierarchical (dark points) and degenerate (light points) neutrinos in scenario SPS1a ($\sqrt{s} = 500$ GeV). The solid (dashed) line indicates the current (expected future) experimental sensitivity of $Br(\mu \rightarrow e\gamma)$.

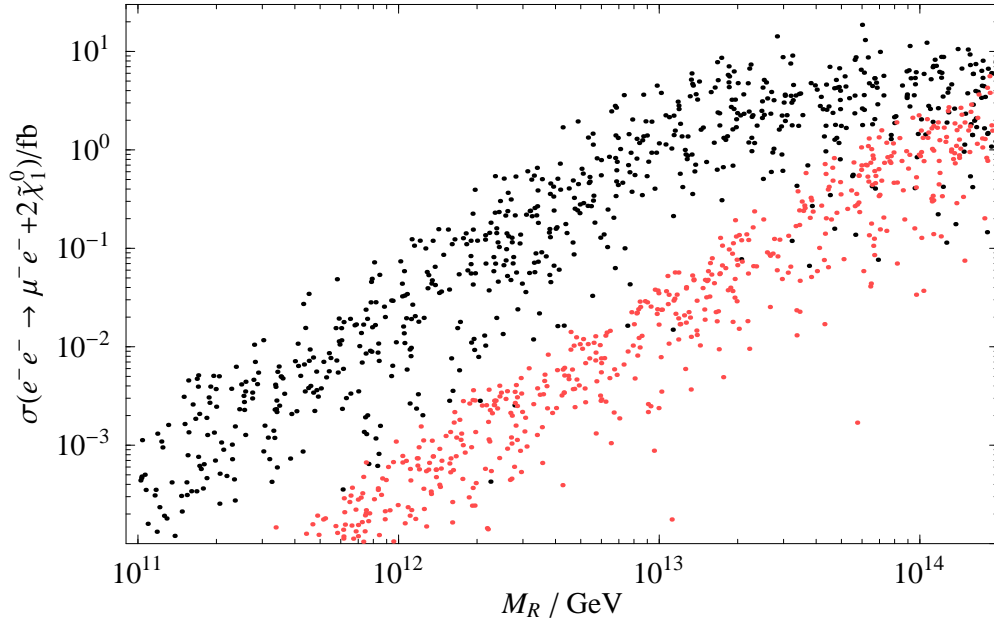


Figure 5.8: $\sigma(\mu^-e^- + 2\tilde{\chi}_1^0)$ as function of M_R in scenario SPS1a for hierarchical (upper) and degenerate (lower curve) neutrinos ($\sqrt{s} = 500$ GeV).

$Br(\mu \rightarrow e\gamma)$	$< 1.2 \cdot 10^{-11}$		$< 10^{-13}$	
	hier. ν_L	deg. ν_L	hier. ν_L	deg. ν_L
SPS1a	1.5	5.6	0.01	0.06
B'	7.9	4.3	0.1	0.2
C'	0.4	0.08	0.02	0.01
G'	0.2	0.2	0.003	0.004
I'	< 0.01	< 0.01	< 0.01	< 0.01

Table 5.3: Maximal expectation at an e^-e^- collider for the signal $\sigma(\mu^-e^- + 2\tilde{\chi}_1^0)$ at $\sqrt{s} = 500$ GeV, depending on the maximally allowed branching ratio (values in fb).

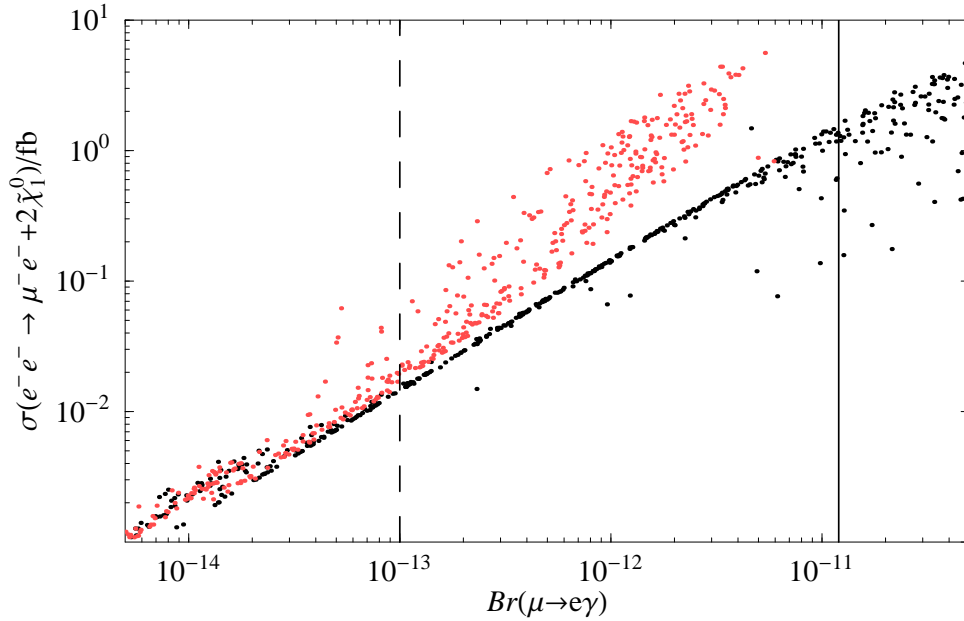


Figure 5.9: $\sigma(\mu^-e^- + 2\tilde{\chi}_1^0)$ as function of $Br(\mu \rightarrow e\gamma)$ for hierarchical (lower) and degenerate (upper) neutrino masses in scenario SPS1a ($\sqrt{s} = 500$ GeV). The solid (dashed) line indicates the current (expected future) experimental sensitivity of $Br(\mu \rightarrow e\gamma)$.

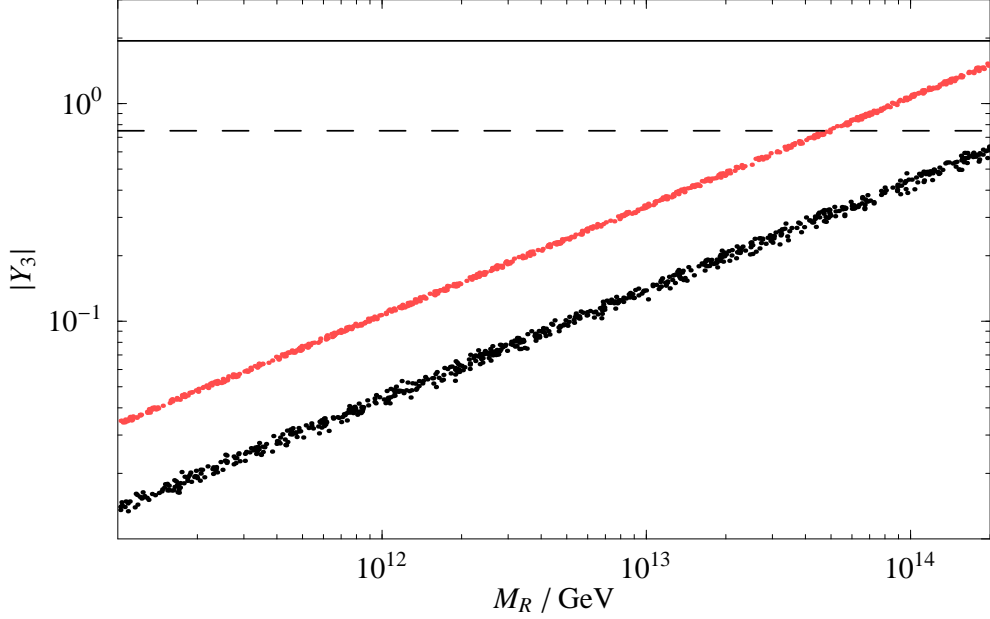


Figure 5.10: Largest Yukawa coupling eigenvalue $|Y_3|$ at M_{GUT} as function of the right-handed Majorana mass scale M_R in the hierarchical (lower) and degenerate (upper) neutrino case. The solid line denotes the upper limit due to perturbativity, $|Y_3| < \sqrt{0.3 \cdot 4\pi}$. The dashed line shows the top Yukawa coupling at M_{GUT} .

Perturbativity For theoretical reasons, it is important that the seesaw model remains perturbative, i.e. the largest neutrino Yukawa coupling eigenvalue should approximately fulfill

$$\frac{|Y_3|^2}{4\pi} \lesssim 0.3. \quad (5.14)$$

Otherwise, any calculations performed in perturbation theory will be useless. The practical test for perturbativity is the stability of the RG running routines. Above $|Y_3| \gtrsim \sqrt{0.3 \cdot 4\pi}$, the neutrino RGEs quickly explode and no consistent renormalization group development is possible. Figure 5.10 shows the largest Yukawa coupling at M_{GUT} as a function of M_R . The solid line gives the upper limit due to the perturbativity constraint (5.14). As can be seen, the scattering was performed such that the theory remains perturbative in all cases. This holds true in all scenarios considered. In addition, the dashed line in Figure 5.10 denotes the top Yukawa coupling strength at M_{GUT} . Third generation Yukawa coupling unification $|Y_3| = Y_t$ at M_{GUT} , as favored in certain GUT unification models, would be achieved for a right-handed mass scale of $M_R \approx 3 \cdot 10^{14}$ GeV for hierarchical and $M_R \approx 5 \cdot 10^{13}$ GeV for degenerate neutrinos. With the upper bounds of Table 5.1 on M_R , this excludes the possibility of Yukawa coupling unification for hierarchical neutrinos in SPS1a. On the other hand, it is still possible for degenerate left- and right-handed neutrinos. Table 5.4 summarizes the values of M_R for successful top Yukawa unification together with their compatibility with the current bound $Br(\mu \rightarrow e\gamma) < 1.2 \cdot 10^{-11}$ in all scenarios. The small variation in the values is only due to different $\tan\beta$ in the scenarios.

	hier. ν_L	deg. ν_L
SPS1a	$3 \cdot 10^{14}$	$5 \cdot 10^{13} \checkmark$
B'	$1 \cdot 10^{14} \checkmark$	$6 \cdot 10^{13} \checkmark$
C'	$2 \cdot 10^{14} \checkmark$	$3 \cdot 10^{13} \checkmark$
G'	$2 \cdot 10^{14}$	$4 \cdot 10^{13} \checkmark$
I'	$2 \cdot 10^{14}$	$5 \cdot 10^{13} \checkmark$

Table 5.4: Values of M_R (in GeV) for successful third generation Yukawa coupling unification $Y_t = |Y_3|$ at M_{GUT} in the case of hierarchical and degenerate neutrinos. The checkmark denotes compatibility with the current bound on M_R from $Br(\mu \rightarrow e\gamma) < 1.2 \cdot 10^{-11}$ (Table 5.1).

Beam energy dependence Up to now, we always considered a beam energy of 500 GeV for the LFV collider signals. Generically, a different beam energy will not change the lepton flavor violating signals qualitatively. Its only effect is to change the size of the total cross section. A caveat to this description is the possibility to traverse certain slepton mass thresholds so that some sleptons are not produced at tree level at certain energies, which could affect the flavor transitions. In order to test the dependence of the collider processes on the beam energy, we fix the seesaw parameters. The neutrino oscillation parameters are at their current best fit values, $m_1 = 0$ eV, the CP violating phase is chosen to be zero, and for M_R a generic value of 10^{13} GeV is used. The resulting signal cross sections for $\mu^+e^- + 2\tilde{\chi}_1^0$, $\tau^+\mu^- + 2\tilde{\chi}_1^0$ and $\mu^-e^- + 2\tilde{\chi}_1^0$ are plotted in Figure 5.11 as a function of \sqrt{s} .

The threshold of the process $\mu^+e^- + 2\tilde{\chi}_1^0$ in SPS1a is at a beam energy of $\sqrt{s} = 345$ GeV, corresponding to the intermediate slepton states² $\tilde{\mu}_L^+\tilde{e}_R^-$ and $\tilde{e}_L^+\tilde{e}_R^-$ (Table 2.2). In the first case, the flavor transition $e^+ \rightarrow \tilde{\mu}_L^+$ occurs in the slepton production, whereas in the second case, the produced right-handed selectron will decay into a muon, $\tilde{e}_L^+ \rightarrow \mu^+$.

As has been noted, $\tau^+\mu^- + 2\tilde{\chi}_1^0$ is almost exclusively a s -channel process. Its threshold in SPS1a is at $\sqrt{s} = 339$ GeV, i.e. the onset of producing two staus, $\tilde{\tau}_2^+\tilde{\tau}_1^-$. Nevertheless, this channel is suppressed by the left-right mixing of the staus (which, in addition, is only possible in Z boson exchange). The dominant contribution is from the production of two smuons, $\tilde{\mu}_L^+\tilde{\mu}_L^-$, starting at $\sqrt{s} = 404$ GeV, of which one decays into a tau. This behavior is clearly visible in Figure 5.11 as a pronounced knee just above a beam energy of 400 GeV.

In the case of $e^-e^- \rightarrow \mu^-e^- + 2\tilde{\chi}_1^0$, the threshold in SPS1a is at $\sqrt{s} = 345$ GeV, as needed for the production of $\tilde{\mu}_L^-\tilde{e}_R^-$ and $\tilde{e}_L^-\tilde{e}_R^-$ pairs. The main contribution, on the other hand, is from $\tilde{\mu}_L^-\tilde{e}_L^-$ and $\tilde{e}_L^-\tilde{e}_L^-$ pairs, due to dominant couplings, again causing a visible bend at $\sqrt{s} \approx 400$ GeV. These observations for the threshold behavior apply analogously to the other scenarios.

Because of the larger sparticle masses, the scenarios C' and G' would benefit from a higher beam energy. At $\sqrt{s} = 500$ GeV the beam energy is just above the production thresholds for the relevant sleptons in these two scenarios. This is especially true for an e^-e^- collider, where using 800 GeV would immensely enhance the signal rates in C' and G'. Unfortunately, it would also enhance the single W production background (Section 3.2). On the other hand,

² \tilde{e}_L^+ ($\tilde{\mu}_L^+$) is the antiparticle to the left-handed slepton \tilde{e}_L^- ($\tilde{\mu}_L^-$).

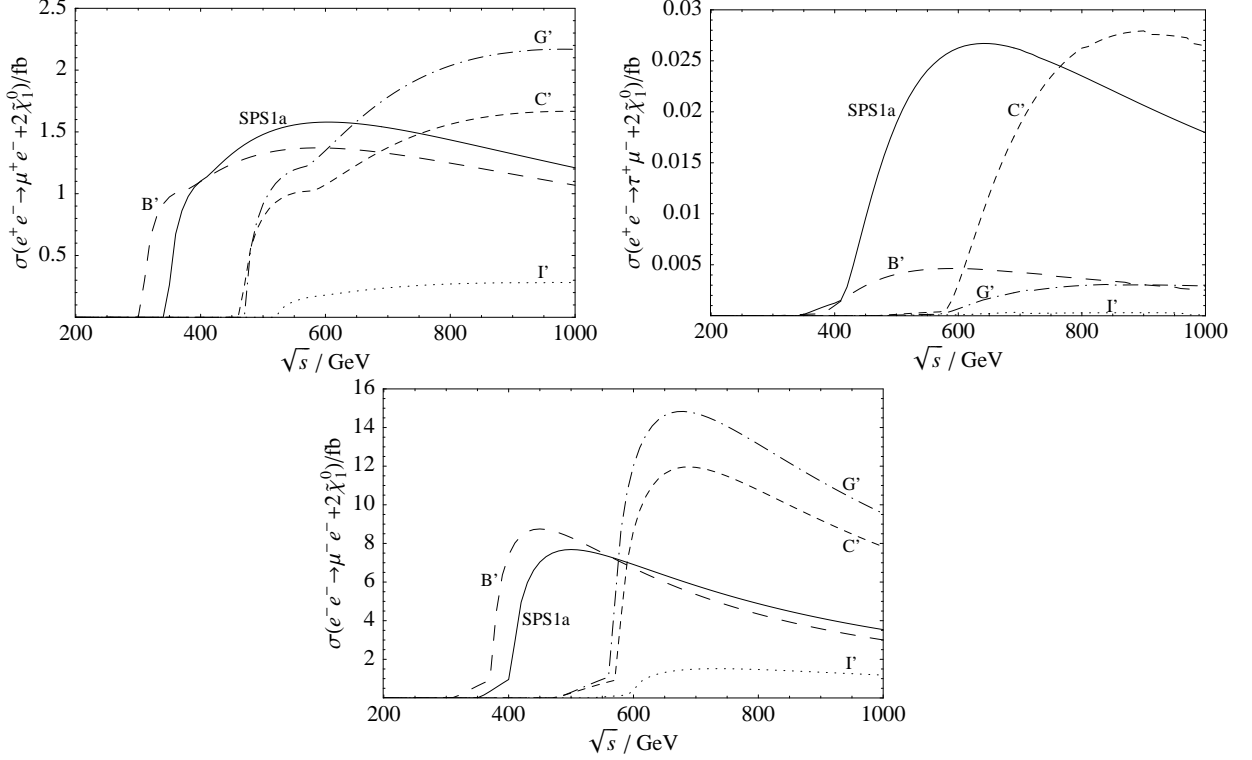


Figure 5.11: $\sigma(\mu^+e^- + 2\tilde{\chi}_1^0)$, $\sigma(\tau^+\mu^- + 2\tilde{\chi}_1^0)$ and $\sigma(\mu^-e^- + 2\tilde{\chi}_1^0)$ as function of \sqrt{s} in all scenarios considered. The neutrino sector is fixed: oscillation parameters at their best fit values, $m_1 = 0$ eV, vanishing CP phases, $M_R = 10^{13}$ GeV.

for the signals $\mu^\pm e^-$, a beam energy of 500 GeV is almost ideal for the scenarios SPS1a and B' with regard to the total signal cross section. The cross section $\sigma(\tau^+\mu^- + 2\tilde{\chi}_1^0)$ is negligible in absolute size just because of the relatively small $M_R = 10^{13}$ GeV used. As noted above, the sensitivity in this channel starts around $M_R = 10^{14}$ GeV.

Slepton mass measurements As the last class of observables, we will discuss precision measurements of slepton mass differences. As shown in Section 3.2.3, slepton masses can give valuable information that is complementary to LFV signals in that they are sensitive to the diagonal elements in $Y_\nu^\dagger LY_\nu$. Figure 5.12 shows the mass difference between the fifth (predominantly a left-handed selectron) and the fourth (left-handed smuon) slepton correlated with the $Br(\mu \rightarrow e\gamma)$ in SPS1a. In the hierarchical neutrino case, mass differences of up to 1 GeV are still allowed by the current bound $Br(\mu \rightarrow e\gamma) < 1.2 \cdot 10^{-11}$. On the other hand, for degenerate neutrinos there is an upper limit on the mass difference of approximately 0.1 GeV, irrespective of the branching ratio bound. This can be understood by rewriting (3.30), using (4.32),

$$m_{\tilde{l}_5}^2 - m_{\tilde{l}_4}^2 \propto \sqrt{((Y_\nu^\dagger LY_\nu)_{22} - (Y_\nu^\dagger LY_\nu)_{11})^2 + 4|(Y_\nu^\dagger LY_\nu)_{12}|^2}, \quad (5.15)$$

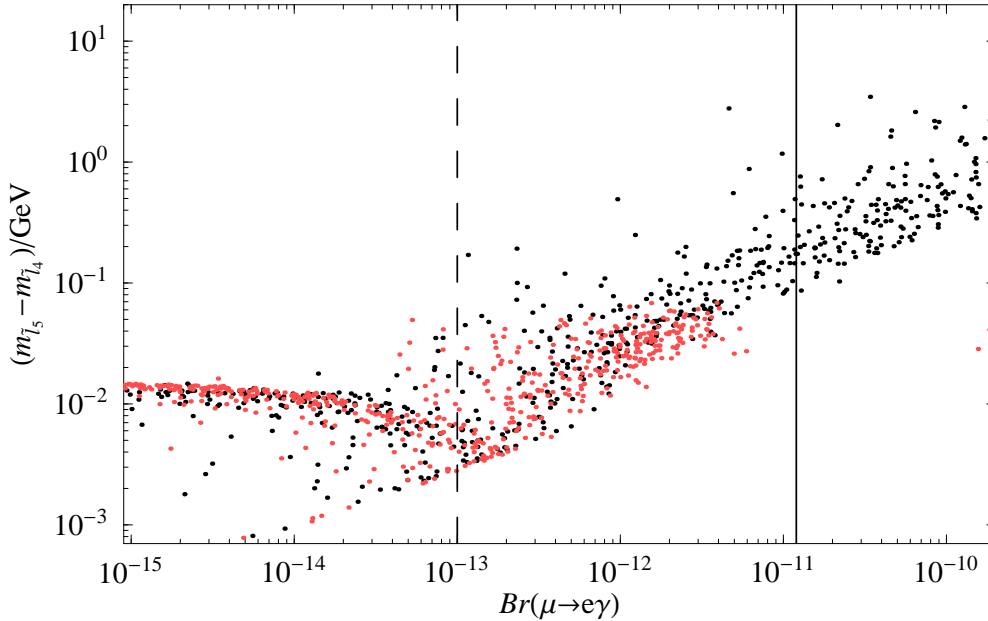


Figure 5.12: $m_{\tilde{l}_5} - m_{\tilde{l}_4}$ as function of $Br(\mu \rightarrow e\gamma)$ in scenario SPS1a for hierarchical (dark) and degenerate (light) neutrinos. The solid (dashed) line indicates the current (expected future) experimental sensitivity of $Br(\mu \rightarrow e\gamma)$.

and inserting (5.10) or (5.11), respectively. In the degenerate neutrino case, the diagonal elements of $Y_\nu^\dagger LY_\nu$ are also highly degenerate (a natural consequence), whereas the off-diagonal elements are suppressed. The mass difference (5.15), being sensitive to the hierarchy of the diagonal elements is thus severely limited. In (5.10) for hierarchical neutrinos, though, there is a strong hierarchy between $(Y_\nu^\dagger LY_\nu)_{22}$ and $(Y_\nu^\dagger LY_\nu)_{11}$ leading to a sizeable $\tilde{e}_L - \tilde{\mu}_L$ mass difference. The approximate upper bounds on $m_{\tilde{l}_5} - m_{\tilde{l}_4}$ are summarized in Table 5.5 for all scenarios, although the values are actually quite insensitive to the scenario. With the precision estimate (3.31) of $\delta m_{\tilde{l}_i} \approx 0.2$ GeV, the currently allowed mass differences are well within the experimental possibilities in the case of hierarchical light neutrinos.

$Br(\mu \rightarrow e\gamma)$	$< 1.2 \cdot 10^{-11}$	$< 10^{-13}$
SPS1a	2	0.2
B'	1	0.1
C'	2	0.1
G'	1	0.1
I'	1	0.1

Table 5.5: Maximal expectation for the mass difference $m_{\tilde{l}_5} - m_{\tilde{l}_4}$ (in GeV) compatible with the present and future bounds on $Br(\mu \rightarrow e\gamma)$ in the case of hierarchical neutrinos. For degenerate neutrinos, the mass difference is always smaller than 0.1 GeV.

In order to get a measurable observable in the degenerate case also, we have to resort to absolute mass determination, or more exactly speaking, to mass deviations from the flavor-

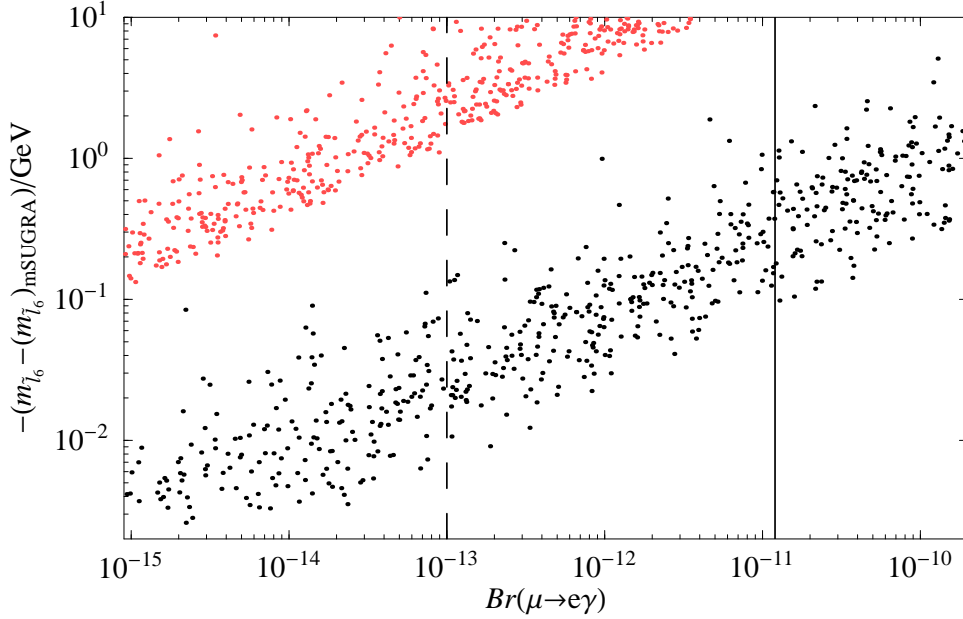


Figure 5.13: $m_{\tilde{l}_6} - m_{\tilde{l}_6}^{\text{mSUGRA}}$ as function of $Br(\mu \rightarrow e\gamma)$ in scenario SPS1a for hierarchical (lower) and degenerate (upper) neutrinos. The solid (dashed) line indicates the current (expected future) experimental sensitivity of $Br(\mu \rightarrow e\gamma)$.

conserving mSUGRA limit. As noted in Section 3.2.3, we take the optimistic stance that these might be measurable in the future. Figure 5.13 displays the quantity $m_{\tilde{l}_6} - m_{\tilde{l}_6}^{\text{mSUGRA}}$, i.e. the shift of the heavy stau mass from its mSUGRA value, as a function of $Br(\mu \rightarrow e\gamma)$ in SPS1a. The left-handed slepton mass matrix corrections are mostly negative (4.32) and insert the numerical matrix (5.10) or (5.11)). Hence the above mass difference turns out to be negative also, i.e. the addition of right-handed neutrinos generically drives the slepton masses to lower values, which could make the sleptons to be detected more easily.

Due to the large diagonal term $(Y_\nu^\dagger L Y_\nu)_{33}$ for degenerate neutrinos, the mass difference is much larger than for hierarchical neutrinos, about one to two orders of magnitude. Differences as much as 10 GeV are currently possible, compared to around 1 GeV in the hierarchical case. We summarize the allowed mass differences in Table 5.6. The upper bounds are currently in the region of 2 GeV and 10 GeV for hierarchical and degenerate neutrinos, respectively, almost independent of the mSUGRA scenario. This is because the mass differences are mostly limited due to our perturbativity limit (5.14), rather than the bound on $Br(\mu \rightarrow e\gamma)$.

mSUGRA parameter dependence In our discussion, we took care of the variety in the mSUGRA parameters only through using five different benchmark scenarios. This is useful to get a quick overview of the possible variations, but is insufficient to test the sensitivities of our signals, especially the relative sensitivity between rare decays and LFV collider processes, with regard to the mSUGRA parameters. We now fix the seesaw parameters (best fit, $m_1 = 0$, no CP violation, $M_R = 10^{13}$ GeV), as we did for analyzing different beam energies,

$Br(\mu \rightarrow e\gamma)$	$< 1.2 \cdot 10^{-11}$		$< 10^{-13}$	
	hier. ν_L	deg. ν_L	hier. ν_L	deg. ν_L
SPS1a	2	10	0.3	10
B'	2	6	0.4	5
C'	3	9	0.7	9
G'	3	11	0.2	11
I'	2	11	0.2	9

Table 5.6: Maximal expectation for the mass difference $m_{\tilde{l}_6} - m_{\tilde{l}_6}^{\text{mSUGRA}}$ compatible with the present and future bounds on $Br(\mu \rightarrow e\gamma)$. The values are in GeV.

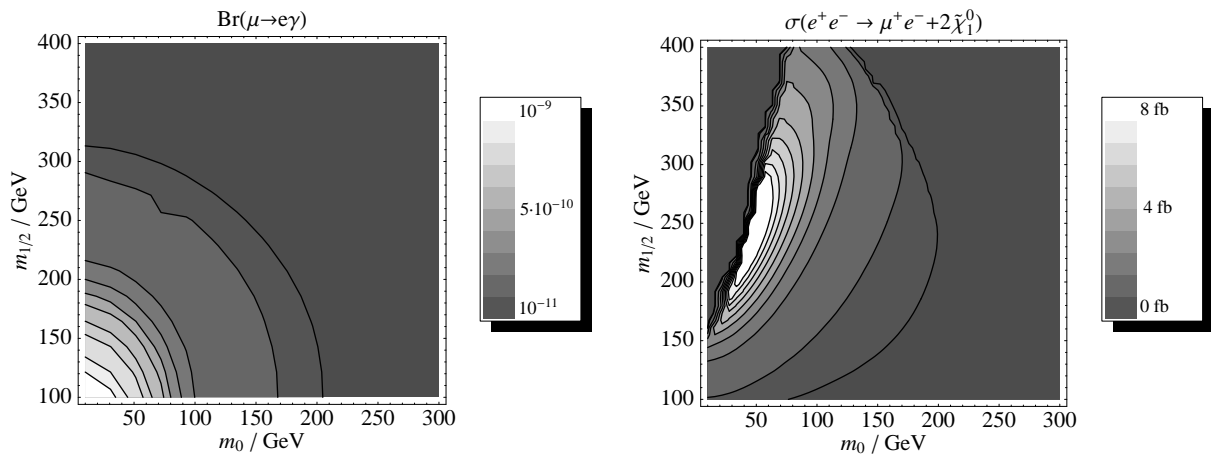


Figure 5.14: $Br(\mu \rightarrow e\gamma)$ (left panel) and $\sigma(\mu^+e^- + 2\tilde{\chi}_1^0)$ at $\sqrt{s} = 500$ GeV (right panel) as function of m_0 and $m_{1/2}$. Their values vary linearly in the ranges indicated in the legends. The seesaw parameters are fixed (best fit, $m_1 = 0$, no CP violation, $M_R = 10^{13}$ GeV), and the other mSUGRA parameters are as in scenario SPS1a ($A_0 = -100$ GeV, $\text{sign } \mu = +$, $\tan \beta = 10$).

and study the dependence of our signals on m_0 , $m_{1/2}$ and A_0 .

Figure 5.14 shows the branching ratio of $\mu \rightarrow e\gamma$ and the cross section for $\mu^+e^- + 2\tilde{\chi}_1^0$ ($\sqrt{s} = 500$ GeV) as contours in the m_0 - $m_{1/2}$ plane. The other mSUGRA parameters are at their SPS1a values, $A_0 = -100$ GeV, $\text{sign } \mu = +$, $\tan \beta = 10$. The branching ratio falls off uniformly towards larger m_0 and $m_{1/2}$, which can be expected due to the masses of sleptons and gauginos in the loop (Figure 3.1) that correlate with m_0 and $m_{1/2}$, respectively. The cross section, on the other hand, has a more extensive reach into the $m_{1/2}$ direction but rapidly falls off for large m_0 , as this quickly drives the slepton masses beyond the production threshold of 500 GeV. A certain correlation between m_0 and $m_{1/2}$, as displayed in the right panel of Figure 5.14, is to be expected in order to get a sizeable cross section, because the produced sleptons have to be heavy enough to decay into the lightest neutralinos. The area on the left-handed side is excluded by the lightest neutralino not being the LSP. In this region, the cross section is automatically zero, which is not the case for the branching ratio.

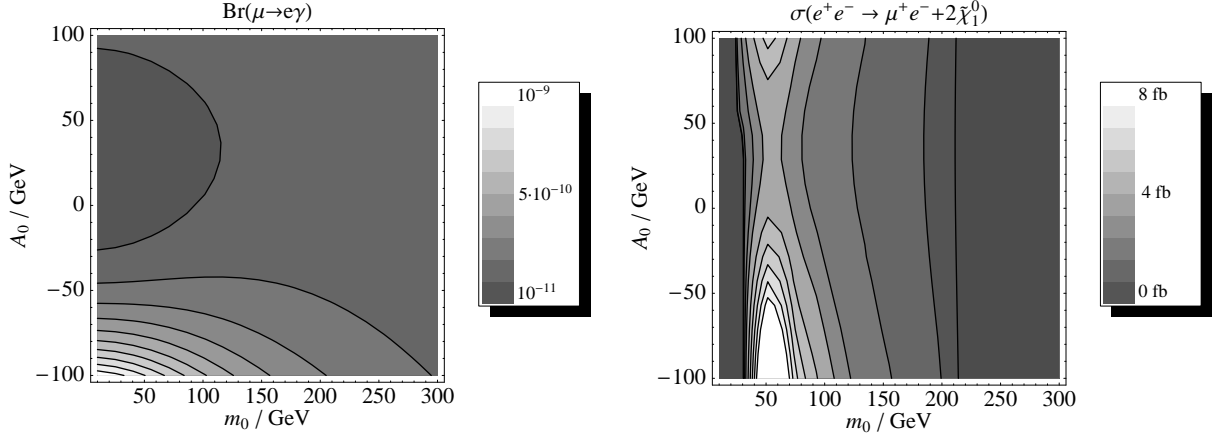


Figure 5.15: $Br(\mu \rightarrow e\gamma)$ (left panel) and $\sigma(\mu^+e^- + 2\tilde{\chi}_1^0)$ at $\sqrt{s} = 500$ GeV (right panel) as function of m_0 and A_0 . Their values vary linearly in the ranges indicated in the legends. The seesaw parameters are fixed (best fit, $m_1 = 0$, no CP violation, $M_R = 10^{13}$ GeV), and the other mSUGRA parameters are as in scenario SPS1a ($m_{1/2} = 250$ GeV, $\text{sign } \mu = +$, $\tan \beta = 10$).

The role of A_0 has often been neglected in the available mSUGRA benchmark scenarios. Four of our five scenarios use a zero value for this quantity which can be quite important in LFV processes. This is most easily seen in (4.32), where A_0 directly contributes to the SUSY seesaw slepton mass corrections,

$$\delta m_{\tilde{L}}^2 \propto (3m_0^2 + A_0^2). \quad (5.16)$$

Although the contribution of an equal size m_0 will be three times larger, it will also quickly drive the slepton masses to higher values suppressing our LFV signals. On the other hand, the main non-LFV effect of A_0 is the strengthening of the stau left-right mixing, which can shift the heavy and dominantly left-handed stau to larger masses, but not as effectively as m_0 . In Figure 5.15, $Br(\mu \rightarrow e\gamma)$ and $\sigma(\mu^+e^- + 2\tilde{\chi}_1^0)$ ($\sqrt{s} = 500$ GeV) are plotted as contours in the m_0 - A_0 plane. The remaining mSUGRA parameters are fixed at their SPS1a values, $m_{1/2} = 250$ GeV, $\text{sign } \mu = +$, $\tan \beta = 10$. As expected, the cross section strongly rises with $|A_0|$. The dependence is not perfectly symmetric around $A_0 = 0$, an effect of the role of A_0 in the slepton left-right mixing (B.17): If $A_e \propto A_0$ is positive, it partially cancel with the negative μ term. The quick fall off with large values of m_0 is the same as in Figure 5.14. The increase of the branching ratio with $|A_0|$ is not as dramatic, especially in the positive A_0 direction. A strong positive trilinear coupling $A_0 \gtrsim 100$ GeV would hence be favorable for a collider.

Chapter 6

Results for hierarchical right-handed neutrinos

We now adopt the other extreme, assuming that the right-handed Majorana masses are strongly hierarchical, at least with respect to the heaviest right-handed neutrino,

$$M_1, M_2 \ll M_3. \quad (6.1)$$

In this case, it is natural to consider only hierarchical light neutrinos also, since the combination of degenerate light neutrinos and hierarchical heavy neutrinos would necessitate a considerable fine-tuning between Y_ν and M in the high energy theory.

To zero order in $\frac{M_1}{M_3}$, $\frac{M_2}{M_3}$ and $\frac{m_1}{m_2}$, Y_ν can be written as (4.16)

$$Y_\nu = \frac{\sqrt{M_3 m_3}}{v \sin \beta} \text{diag}(0, 0, 1) \cdot R \cdot \text{diag} \left(0, \sqrt{\frac{m_2}{m_3}} e^{-i\phi_2}, 1 \right) \cdot V^\dagger, \quad (6.2)$$

with $m_2 \approx \sqrt{\Delta m_{12}^2}$ and $m_3 \approx \sqrt{\Delta m_{23}^2}$. Also, we extracted the Majorana phases from U (4.11), showing that ϕ_1 drops out and the effect of ϕ_2 is suppressed by $\sqrt{m_2/m_3}$. The parameterization (4.17) of the matrix $R(\theta_1, \theta_2, \theta_3)$ is now very useful, because the angle θ_3 does not enter (6.2). Finally, one arrives at

$$Y_\nu = \frac{\sqrt{M_3 m_3}}{v \sin \beta} \cos \theta_2 \times \begin{pmatrix} 0 & 0 & 0 \\ 0 & 0 & 0 \\ s_1 \kappa e^{-i\phi_2} V_{12}^* + c_1 V_{13}^* & s_1 \kappa e^{-i\phi_2} V_{22}^* + c_1 V_{23}^* & s_1 \kappa e^{-i\phi_2} V_{32}^* + c_1 V_{33}^* \end{pmatrix}, \quad (6.3)$$

with $\kappa = \sqrt{m_2/m_3}$ and $c_1 = \cos \theta_1$, etc. By inserting the oscillation parameter best fit values (Section 4.5) for θ_{12} , θ_{23} , Δm_{12}^2 and Δm_{23}^2 , we get the numerical result

$$Y_\nu \approx \cos \theta_2 \sqrt{\frac{M_3}{10^{12} \text{ GeV}} \frac{174 \text{ GeV}}{v \sin \beta}} \times \begin{pmatrix} 0 & 0 & 0 \\ 0 & 0 & 0 \\ 1.6 s_1 e^{-i\phi_2} + 0.57 x_{13} c_1 e^{-i\delta} & 5.2 c_1 + 1.7 s_1 e^{-i\phi_2} & 4.9 c_1 - 1.7 s_1 e^{-i\phi_2} \end{pmatrix}. \quad (6.4)$$

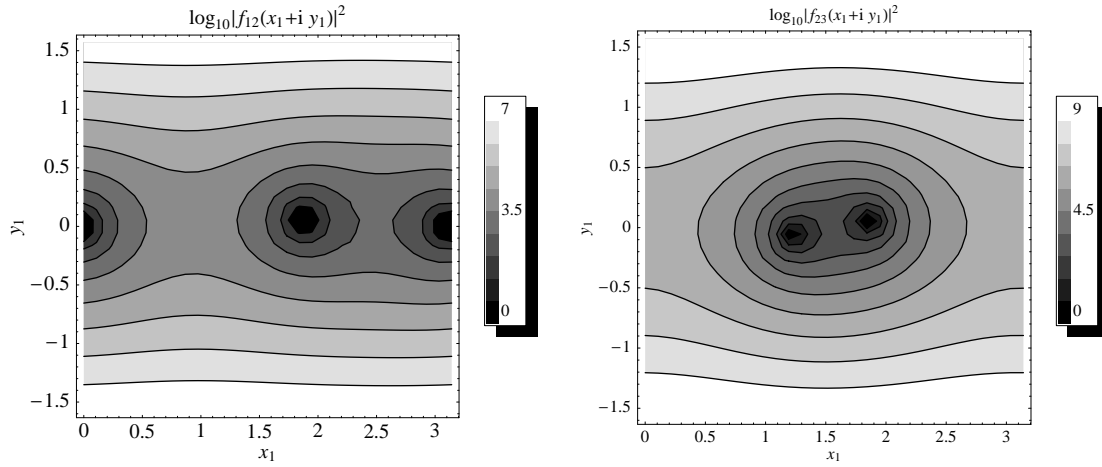


Figure 6.1: $\log_{10} |f_{12}(x_1 + iy_1)|^2$ (left panel) and $\log_{10} |f_{23}(x_1 + iy_1)|^2$ (right panel). Their values vary linearly in the ranges indicated in the legends. The other seesaw parameters are fixed (best fit oscillation, $m_1 = 0$ eV, $\delta = \pi/16$, $\phi_2 = \pi/8$).

As in the previous chapter, $x_{13} = \theta_{13}/0.078$, and only the lowest order in θ_{13} is retained in (6.4). The analogous analytic expression for $Y_\nu^\dagger LY_\nu$ has a complicated structure and is too unwieldy to gain much insight from. Some important conclusions can be drawn from the general dependence on the five relevant, unknown seesaw parameters M_3 , x_1 , x_2 , y_1 , y_2 ,

$$(Y_\nu^\dagger LY_\nu)_{ij} \propto M_3 |\cos(x_2 + iy_2)|^2 \log \frac{M_{\text{GUT}}}{M_3} f_{ij}(x_1 + iy_1), \quad (6.5)$$

where $x_{1/2}$ and $y_{1/2}$ are the real and imaginary parts of the R matrix angles $\theta_{1/2}$, respectively. f_{ij} are functions of $\theta_1 = x_1 + iy_1$, also depending on the light neutrino parameters.

First, we see that x_2 , y_2 and M_3 only enter through the combination¹ $M_3 |\cos(x_2 + iy_2)|^2$. These three parameters are impossible to separate by measuring low energy observables, reducing the number of effective parameters by two. Also, $M_3 |\cos(x_2 + iy_2)|^2$ is a priori not bounded from below (for $x_2 = \pi/2$ and $y_2 = 0$, it is zero), which can be a problem, because if $M_3 |\cos \theta_2|^2$ is of the order of M_2 or smaller, the approximation (6.2) would make no sense, as the neglected contributions proportional to M_2 or M_1 would have to be taken into account. The assumption

$$M_3 |\cos \theta_2|^2 \gg M_2 \quad (6.6)$$

is thus more apt than $M_3 \gg M_2$ (6.1). As can be guessed from (6.3), the functions f_{ij} are rather complicated. Figure 6.1 shows $|f_{12}(x_1 + iy_1)|^2$ and $|f_{23}(x_1 + iy_1)|^2$ (to which $Br(\mu \rightarrow e\gamma)$ and $Br(\tau \rightarrow \mu\gamma)$ are proportional, respectively) for a given set of neutrino parameters (best fit, $m_1 = 0$, $\delta = \pi/16$, $\phi_2 = \pi/8$). The odd values for the CP phases have only been chosen to give a generic result instead of a special case like $\delta = 0$. Both plots reveal a large variation of $|f_{ij}|^2$ within about eight orders of magnitude. Beyond the

¹Actually, there is again the additional $\log \frac{M_{\text{GUT}}}{M_3}$ dependence, which we neglect in the current discussion.

depicted range, the functions are cyclic with respect to x_1 and rise exponentially with y_1 . This behavior is easy to understand with

$$\cos(x + iy) = \cos x \cosh y - i \sin x \sinh y, \quad (6.7)$$

$$\sin(x + iy) = \sin x \cosh y + i \cos x \sinh y. \quad (6.8)$$

The pronounced minima in Figure 6.1, responsible for the large variation, are very narrow (the plots are logarithmic in $|f_{ij}|^2$), their positions being dependent on the the light neutrino parameters. They are always located on or close to the x_1 axis. It is thus expected that the branching ratios and other LFV observables strongly depend on x_1 . In [48], analytic expressions for the positions of these minima can be found for certain special cases.

This scenario of hierarchical right-handed neutrinos is a natural environment to include leptogenesis by enforcing the condition (4.60) on M_1 to get a baryon asymmetry of $\eta_B \approx 6.3 \cdot 10^{-10}$. In order to satisfy the gravitino bound we use only those scatter points for which $M_1 < 10^{11}$ GeV. In summary, the parameter space is explored as follows:

- The light neutrino parameters are scattered as usually for the hierarchical case as outlined in Section 4.5.
- The R matrix parameters x_1 , x_2 and x_3 are linearly varied in their full range, $0, \dots, 2\pi$, whereas the imaginary parts y_1 , y_2 and y_3 are linearly scattered within $10^{-3}, \dots, 1$ on a logarithmic scale. Beyond this y_i range, the perturbativity of Y_ν is quickly lost [22, 48]. On the other hand, all three y_i have to be non-zero to make leptogenesis possible [48].
- With the x_i and y_i thus given, M_1 is fixed by the leptogenesis condition (4.60). We only use those scatter points that generate a value of $M_1 < 10^{11}$ GeV to approximately fulfill the gravitino bound. In addition, we demand \tilde{m}_1 to lie between $\sqrt{\Delta m_{12}^2}$ and $\sqrt{\Delta m_{23}^2}$, so that the fit (4.54) for the washout factor κ_f is appropriate.
- M_3 is scattered logarithmically between $10M_1$ and 10^4M_1 .
- M_2 is varied between M_1 and $0.1M_3$. The lower value potentially violates the desired hierarchy for leptogenesis, but it is rarely generated stochastically.

It is important to keep this procedure in mind as scatter plots can be easily plagued by non-physical artifacts.

Determination of M_3 Figure 6.2 displays the branching ratio of $\mu \rightarrow e\gamma$ as a function of the effective heaviest right-handed neutrino mass $M_3|\cos\theta_2|^2$ in SPS1a. The typical rise with $|Y_\nu^\dagger LY_\nu|^2 \propto M_3^2|\cos\theta_2|^4$ is the dominant feature. With the current limit $Br(\mu \rightarrow e\gamma) < 1.2 \cdot 10^{-11}$, an upper bound of roughly $M_3|\cos\theta_2|^2 \lesssim 10^{14}$ GeV can be read of from the figure, although there is a considerable amount of uncertainty. A measurement of $Br(\mu \rightarrow e\gamma) \approx 10^{-13}$ would determine $M_3|\cos\theta_2|^2$ within two orders of magnitude, $M_3|\cos\theta_2|^2 \approx 10^{11-13}$ GeV, analogous to M_R in the previous chapter.

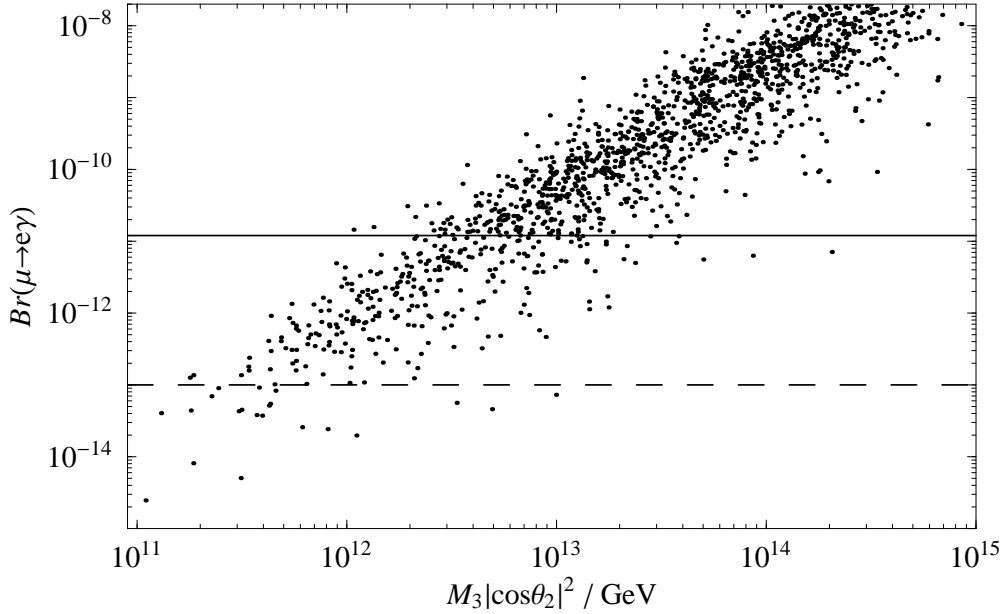


Figure 6.2: $Br(\mu \rightarrow e\gamma)$ as function of $M_3 |\cos \theta_2|^2$ in SPS1a. See text for a description of the scatter procedure. The solid (dashed) line indicates the current (expected future) experimental sensitivity of $Br(\mu \rightarrow e\gamma)$.

The thinning of the points towards lower values of $M_3 |\cos \theta_2|^2$ is in part an artifact of the scattering procedure². It also signifies the simple fact that the viable parameter space compatible with successful leptogenesis is strongly limited for small M_1 . With a minimal M_1 of about $5 \cdot 10^9$ GeV (4.62), M_3 must be larger than $5 \cdot 10^{10}$ GeV, which is close to the reach of the future sensitivity of $\mu \rightarrow e\gamma$.

Table 6.1 summarizes the uncertainty in determining $M_3 |\cos \theta_2|^2$ for all scenarios. As discussed above, a true bound on M_3 can not be made in general. Nevertheless, as will be shown below, $|\cos \theta_2|^2$ is of order unity in case of successful leptogenesis. Hence, the bounds will roughly apply to M_3 also.

$Br(\mu \rightarrow e\gamma)$	$= 1.2 \cdot 10^{-11}$	$= 10^{-13}$
SPS1a	$1 \cdot 10^{12} - 2 \cdot 10^{14}$	$2 \cdot 10^{11} - 1 \cdot 10^{13}$
B'	$9 \cdot 10^{12} - 5 \cdot 10^{14}$	$1 \cdot 10^{12} - 9 \cdot 10^{13}$
C'	$3 \cdot 10^{13} - 9 \cdot 10^{14}$	$2 \cdot 10^{12} - 2 \cdot 10^{14}$
G'	$8 \cdot 10^{12} - 4 \cdot 10^{14}$	$9 \cdot 10^{11} - 2 \cdot 10^{13}$
I'	$2 \cdot 10^{12} - 2 \cdot 10^{14}$	$5 \cdot 10^{11} - 2 \cdot 10^{13}$

Table 6.1: Uncertainty in $M_3 |\cos \theta_2|^2$ at the present and future sensitivities of $Br(\mu \rightarrow e\gamma)$ due to variation of the remaining seesaw parameters (values in GeV). See text for a detailed description of the scatter procedure.

²The distribution of M_1 is not linear on a logarithmic scale, but is more pronounced for larger $M_1 \approx 10^{11}$ GeV. This affects the distribution of M_3 accordingly.

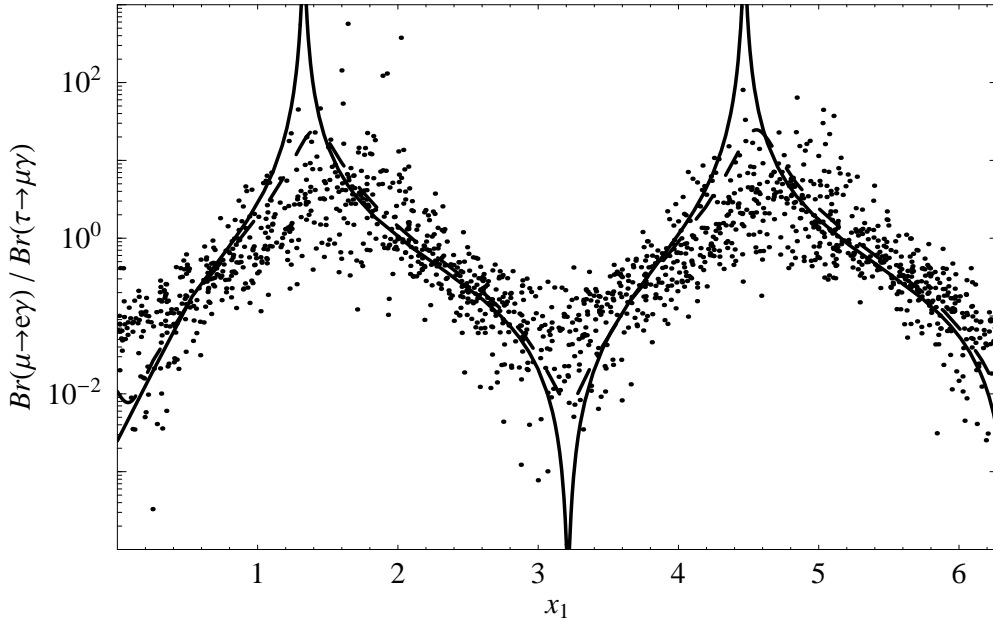


Figure 6.3: $Br(\mu \rightarrow e\gamma)/Br(\tau \rightarrow \mu\gamma)$ as function of the R matrix parameter x_1 in SPS1a. See text for a description of the scatter procedure. Superimposed are two curves for which all seesaw parameters but x_1 are fixed (best fit oscillation values, $m_1 = 0$ eV and no CP violating phases). The solid (dashed) curve is for $y_1 = 0.01$ ($y_1 = 0.1$).

Determination of x_1 A lot of the residual variation in Figure 6.2 is generated by the dependence on x_1 , as exemplified in Figure 6.1, if y_1 is not too large. In order to extract x_1 , we need an observable that does not scale with $M_3|\cos\theta_2|^2$. A natural choice is a ratio of branching ratios, from which $M_3|\cos\theta_2|^2$ drops out. Figure 6.3 displays $Br(\mu \rightarrow e\gamma)/Br(\tau \rightarrow \mu\gamma)$ as a function of x_1 in SPS1a. With only upper bounds on $Br(\mu \rightarrow e\gamma)$ and $Br(\tau \rightarrow \mu\gamma)$, no information on x_1 can be gained at the moment. Nevertheless, the figure shows that measuring both branching ratios would provide a means to determine or constrain the angle x_1 . In addition, it may give us a possibility to distinguish between hierarchical and degenerate right-handed neutrinos. In the previous section, we did not discuss the ratio $Br(\mu \rightarrow e\gamma)/Br(\tau \rightarrow \mu\gamma)$, which is generically situated between 0.005 and 0.1 (for both hierarchical and degenerate light neutrinos), as it does not provide much useful information on its own. Comparing these numbers with Figure 6.3, it can be seen that there is a significant difference to the presently discussed case. For values of $x_1 \approx \pi/2, 3\pi/2$, there is a huge enhancement of $Br(\mu \rightarrow e\gamma)$ over $Br(\tau \rightarrow \mu\gamma)$ of up to 2-3 orders of magnitude as compared to degenerate right-handed neutrinos.

Figure 6.3 also includes two curves for fixed values $y_1 = 0.01$ and $y_1 = 0.1$ (the other neutrino parameters are also fixed: best fit oscillation, $m_1 = 0$ eV and no light CP phases). They demonstrate that there is a potential variation of over seven orders of magnitude in $Br(\mu \rightarrow e\gamma)/Br(\tau \rightarrow \mu\gamma)$ if y_1 is small. This variation is caused by the minima of $|f_{12}|^2$ and $|f_{23}|^2$ (Figure 6.1), $Br_{\mu e}/Br_{\tau\mu} \propto |f_{12}/f_{23}|^2$. Due to their narrowness, it is rather improbable to fall into these minima when scattering the seesaw parameters, hence there are only a few

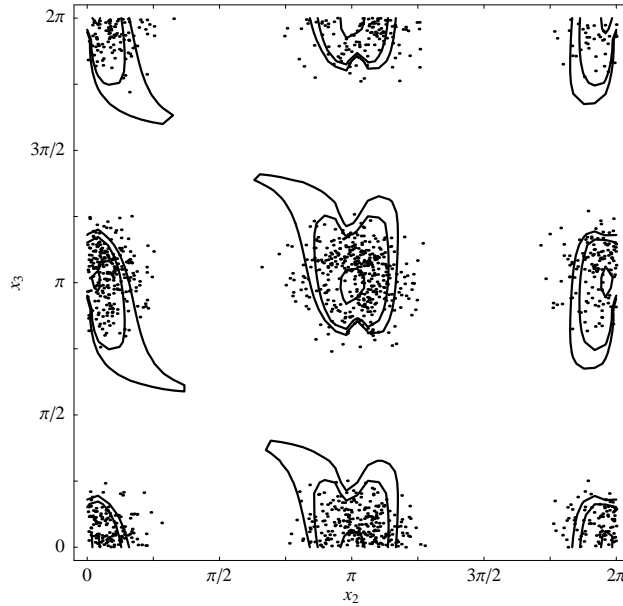


Figure 6.4: Scatter points compatible with successful baryogenesis (4.60) and the gravitino bound $M_1 < 10^{11}$ GeV in the $x_2 - x_3$ plane for the mSUGRA scenario SPS1a. See text for a description of the scatter procedure. Also shown are the contours for a constant $M_1(x_2, x_3) = 10^{10,11,12}$ GeV (inner to outer contours) with all other seesaw parameters fixed (best fit oscillation, $m_1 = 0$, no CP phases, $y_i = 0.1$).

points in Figure 6.3 that exhibit the potential variation.

Leptogenesis The constraint to produce successful leptogenesis has no direct impact on the low energy observables. It only gives us a range for M_1 between $5 \cdot 10^9$ GeV and 10^{11} GeV, acting as a lower base to build the hierarchy of the right-handed neutrinos. As we have seen in (6.5), the low energy observables depend only on x_1 , y_1 and $|\cos(x_2 + iy_2)|^2$ through the R matrix elements R_{32} and R_{33} , in the limit of hierarchical right-handed neutrinos. On the other hand, the CP asymmetry ϵ_1 which drives the leptogenesis is dominated by the R matrix elements R_{1i} , $i = 1, \dots, 3$ for hierarchical light neutrinos (4.58). This makes a correlation in the case of arbitrary values for the x_i and y_i as considered here very difficult.

Quite interestingly, we found that the upper bound on M_1 , forced on us to cope with the gravitino problem, can be a blessing in disguise. Figure 6.4 displays the viable scatter points compatible with leptogenesis and the gravitino bound in the $x_2 - x_3$ plane in SPS1a. It is apparent that both x_2 and x_3 are constrained around values of $x_2, x_3 = 0, \pi, 2\pi$. The contours of constant $M_1(x_2, x_3) = 10^{10,11,12}$ GeV, which are also displayed in the figure, give the answer to that puzzle. The gravitino constraint $M_1 < 10^{11}$ GeV pushes the parameter space into regions around the absolute minimum of M_1 for successful leptogenesis (4.62). These regions are located around $x_2, x_3 = n \cdot \pi$ for small $y_i = 0.001 - 0.1$. The exact locations of these minima also depend on the other neutrino parameters, which is why many scatter points are actually outside the $M_1 = 10^{11}$ GeV contour. We thus see that our scenario of hierarchical

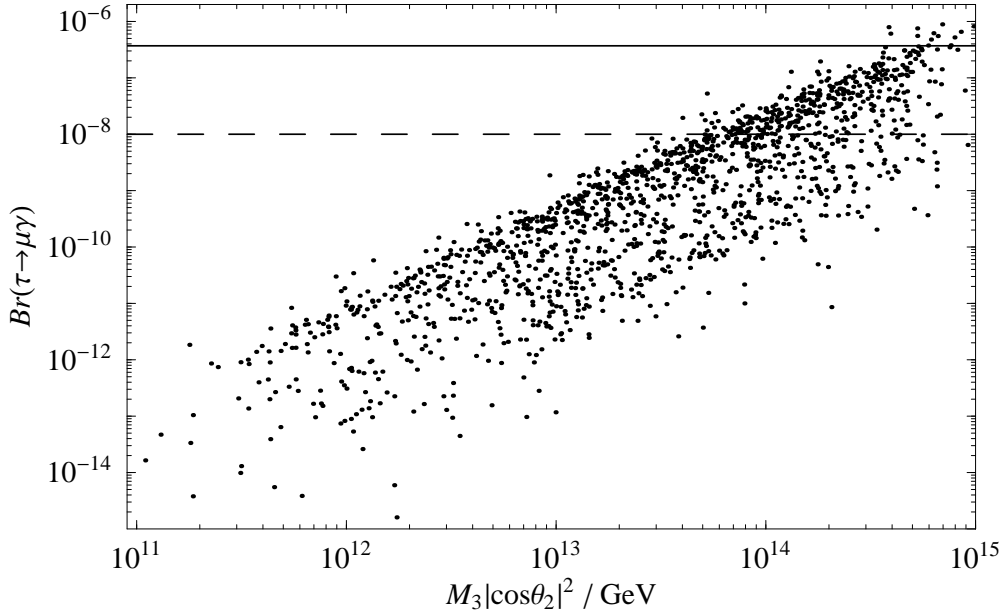


Figure 6.5: $Br(\tau \rightarrow \mu\gamma)$ as function of $M_3|\cos\theta_2|^2$ in SPS1a. See text for a description of the scatter procedure. The solid (dashed) line indicates the current (expected future) experimental sensitivity of $Br(\tau \rightarrow \mu\gamma)$.

left- and right-handed neutrinos exhibits an intriguing complementarity between low energy observables and successful baryogenesis in mSUGRA. Using low energy observables, one might be able to determine the angle x_1 , whereas viable leptogenesis constrains x_2 and x_3 . Indirectly, this also helps to determine M_3 more exactly. As discussed above, low energy observables do not depend directly on M_3 , but rather on $M_3|\cos(x_2 + iy_2)|^2$. With x_2 constrained by the gravitino bound, and for $y_2 = 0.001 - 1$, it turns out that $|\cos(x_2 + iy_2)|^2$ lies between 0.6 and 1.3, thus affecting $M_3|\cos(x_2 + iy_2)|^2$ only moderately.

Apart from these specialties, most correlations among observables and seesaw parameters are at least qualitatively similar to the case of degenerate right-handed neutrinos discussed in the previous chapter. In order to not repeat most of the discussion, we will shortly summarize the various observables:

- In contrast to the degenerate right-handed neutrino case, there is a large uncertainty in the correlation between $Br(\tau \rightarrow \mu\gamma)$ and $M_3|\cos\theta_2|^2$ (Figure 6.5) due to the strong variation in x_1 . This uncertainty is even larger than in the analogous Figure 6.2 for $Br(\mu \rightarrow e\gamma)$.
- There is again a strong correlation between the rare decays $Br(l_i \rightarrow l_j\gamma)$ and the slepton pair production collider processes $\sigma(e^\pm e^-) \rightarrow l_j^+ l_i^- + 2\tilde{\chi}_1^0$. These are shown Figure 6.6 for the $\mu^+ e^-$ - and $\tau^+ \mu^-$ -channel in SPS1a for a beam energy of $\sqrt{s} = 500$ GeV. The correlation is the same as for degenerate right-handed neutrinos and the reach of all collider signals is in the same range as in the previous chapter.

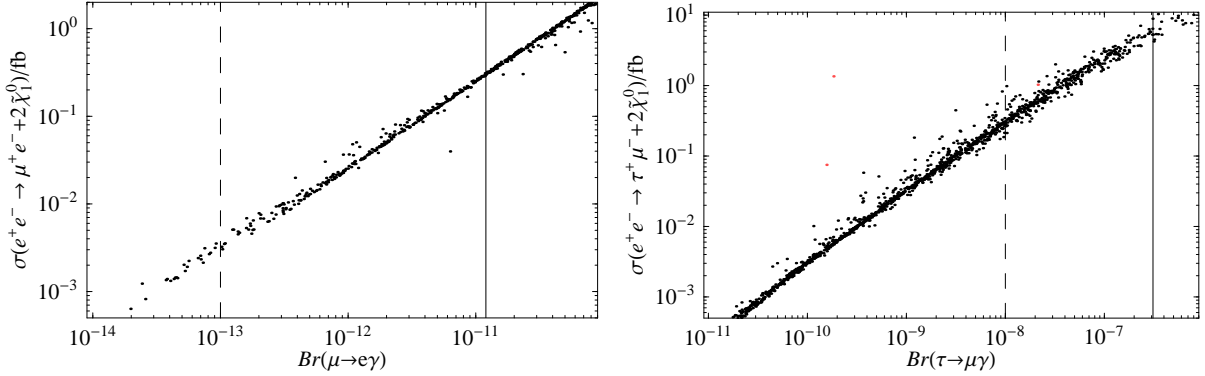


Figure 6.6: $\sigma(\mu^+e^- + 2\tilde{\chi}_1^0)$ as function of $Br(\mu \rightarrow e\gamma)$ (left panel) and $\sigma(\tau^+\mu^- + 2\tilde{\chi}_1^0)$ as function of $Br(\tau \rightarrow \mu\gamma)$ (right panel) in SPS1a ($\sqrt{s} = 500$ GeV). The solid (dashed) lines indicates the current (expected future) experimental sensitivity of $Br(\mu \rightarrow e\gamma)$ and $Br(\tau \rightarrow \mu\gamma)$, respectively.

- No large mass difference between the sleptons \tilde{l}_5 and \tilde{l}_4 can be measured. Intuitively, this can be understood, because the hierarchy does not originate from $Y_\nu^\dagger LY_\nu$ (which generates the slepton mass differences) as in (5.10) but from the right-handed neutrinos. A typical value for all scenarios is $m_{\tilde{l}_5} - m_{\tilde{l}_4} \lesssim 0.1$ GeV as an upper limit compatible with $Br(\mu \rightarrow e\gamma)$.
- The left-handed stau mass shift $m_{\tilde{l}_6} - m_{\tilde{l}_6}^{\text{mSUGRA}}$ is generally of the same order as in the hierarchical ν_L /degenerate ν_R case (Figure 5.13), i.e. about 1 GeV at the current $\mu \rightarrow e\gamma$ bound.
- Despite the non-vanishing y_i which give rise to CP violating effects (e.g. leptogenesis), there is no large enhancement of the electric dipole moments compared to the case considered in the previous chapter. In scenario SPS1a we find a maximal viable value of $d_e \approx 5 \cdot 10^{-33}$ ecm, which might be measurable in the future, see (3.15).
- Mostly due to the strong variation with x_1 , the correlation between the largest Yukawa coupling eigenvalue and M_3 (Figure 6.7) is not as clear as in the case of degenerate right-handed neutrinos. Third generation Yukawa coupling unification $|Y_3| = Y_t$ at M_{GUT} would be possible for $M_3 \gtrsim 3 \cdot 10^{14}$ GeV. With the upper bounds in Table 6.1, Yukawa coupling unification is disfavored for the scenarios SPS1a, G' and I'. The other two scenarios are also on the brink of being excluded.

The mSUGRA bias At this point, a short comment on the theoretical bias adopted by using the mSUGRA framework of soft SUSY-breaking is in order. Especially with its diagonal and universal soft SUSY masses at the GUT scale, mSUGRA is very constraining and could lead to predictions that are based on oversimplified assumptions. The interpretation of our LFV signals crucially depends on a clear correlation between the seesaw parameters

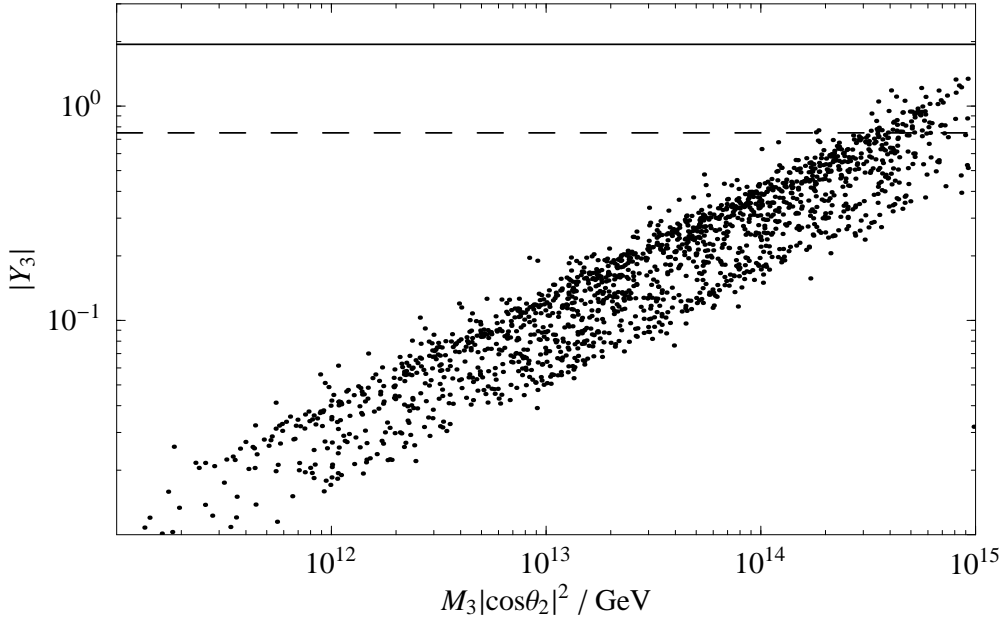


Figure 6.7: Largest Yukawa coupling eigenvalue $|Y_3|$ at M_{GUT} as function of the effective heaviest neutrino mass $M_3 |\cos \theta_2|^2$. The solid line denotes the upper limit due to perturbativity, $|Y_3| < \sqrt{0.3 \cdot 4\pi}$. The dashed line shows the top Yukawa coupling at M_{GUT} . See text for a description of the scatter procedure.

and the off-diagonal slepton mass elements δm_L^2 . There are a couple of modifications with varying degrees of generalization that could be adopted:

Non-universal soft SUSY masses. Instead of identifying all scalar masses with one m_0 at the GUT scale, this common scalar mass could be made specific to each species, e.g.

$$m_L^2 = m_0^L \mathbb{I}, \quad m_e^2 = m_0^e \mathbb{I}, \quad m_Q^2 = m_0^Q \mathbb{I}, \quad \text{etc.}$$

Qualitatively, this will change nothing in our discussion, as we mainly consider only the contributions to m_L^2 ; m_0 would simply be replaced by m_0^L . Quantitatively, it will of course affect our results by modifying the SUSY particle spectrum at low energies, with its impact on decay rates and signal and background cross sections. Also, it would reduce the redundancy in determining m_0^L . Assuming perfect mSUGRA, m_0 could be determined by many slepton and squark mass measurements, making its determination more accurate.

Non-degenerate soft SUSY masses. On a step further, the soft SUSY masses could be flavor dependent at M_{GUT} , e.g.,

$$m_L^2 = \text{diag}((m_0^L)_1^2, (m_0^L)_2^2, (m_0^L)_3^2),$$

keeping the off-diagonal elements zero, and accordingly for the trilinear coupling A_e ,

$$A_e = \text{diag}((A_0^L)_1, (A_0^L)_2, (A_0^L)_3).$$

Such a generalization could already seriously worsen our results, e.g. the leading-log mass correction (4.32) would be modified to

$$\delta m_L^2 = -\frac{1}{8\pi^2}(\mathbf{Y}_\nu^\dagger \mathbf{L} \mathbf{Y}_\nu),$$

with \mathbf{L} now also containing the hierarchy of the different soft masses and trilinear couplings,

$$\mathbf{L} = \text{diag} \left((3(m_0^L)^2 + (A_0^L)^2) \log \frac{M_{\text{GUT}}}{M_i} \right).$$

It would therefore be impossible to separate the effect of the hierarchy in the right-handed neutrino masses M_i from the SUSY parameter hierarchy $(m_0^L)^2$ and $(A_0^L)_i$.

Non-diagonal soft SUSY masses. Allowing an arbitrary, non-diagonal (but compatible with bounds on LFV) scalar mass matrix at the GUT scale would finally destroy any correlation between the LFV signals discussed so far and the seesaw parameters.

Chapter 7

Bottom-up approach

The previous two chapters demonstrated that it is possible to arrive at predictions on low energy LFV observables by making sensible assumptions to reduce the number of unknown parameters. It seems obvious that the R matrix description (4.16) with its nine arbitrary parameters $M_i, x_i, y_i, i = 1, 2, 3$, is not able to provide a suitable means to probe the whole viable parameter space of the SUSY seesaw mechanism. A scattering over all nine parameters (plus the partially constrained light neutrino sector) might be possible but is of course highly inefficient. It is not possible to enforce a certain value of, say, $Br(\mu \rightarrow e\gamma)$, to simulate its measurement. This had to be expected, as the R matrix description is specifically constructed to ensure a viable light neutrino sector, but not necessarily experimentally viable charged LFV process rates.

Parameter	Observables
$ (\delta m_{\tilde{L}}^2)_{12} $	$Br(\mu \rightarrow e\gamma), \sigma(e^\pm e^- \rightarrow \mu^\pm e^- + 2\tilde{\chi}_1^0)$
$ (\delta m_{\tilde{L}}^2)_{13} $	$Br(\tau \rightarrow e\gamma), \sigma(e^\pm e^- \rightarrow \tau^\pm e^- + 2\tilde{\chi}_1^0)$
$ (\delta m_{\tilde{L}}^2)_{23} $	$Br(\tau \rightarrow \mu\gamma), \sigma(e^\pm e^- \rightarrow \tau^\pm \mu^- + 2\tilde{\chi}_1^0)$
$(\delta m_{\tilde{L}}^2)_{11}$??
$(\delta m_{\tilde{L}}^2)_{22} - (\delta m_{\tilde{L}}^2)_{11}$	$m_{\tilde{l}_5} - m_{\tilde{l}_4}$
$(\delta m_{\tilde{L}}^2)_{33}$	$m_{\tilde{l}_6} - m_{\tilde{l}_6}^{\text{mSUGRA}}$
$\text{Im}(\delta m_{\tilde{L}}^2)_{ij}, i \neq j$	d_e, d_μ

Table 7.1: Parameters of the left-handed slepton correction matrix $\delta m_{\tilde{L}}^2$ and the most important observables which are potentially sensitive to them.

Chapter 3 provided an alternative in the form of the bi-unitary parameterization (4.37). In this description, the in principle measurable quantities $Y_\nu^\dagger Y_\nu$ and \mathbf{m}_ν are treated as input from which the full high energy seesaw sector (Y_ν, M_i) can be reconstructed, allowing the simulation of any experimental situation, in order to determine its theoretical consequences. With the current experimental situation unfortunately still being too vague, there are many scenarios that could be discussed. We will focus on a few such situations to give a proof of concept for a bottom-up reconstruction of the seesaw model, which, in general, works as follows:

1. Information on the neutrino sector is used to determine or constrain the light neutrino mixing matrix m_ν , as outlined in Section 4.5.
2. Measurements (present or future) of LFV observables are used to determine or constrain the corrections $\delta m_{\tilde{L}}^2$ to the left-handed slepton matrix $m_{\tilde{L}}^2$ as departures from its flavor-conserving mSUGRA value. Table 7.1 lists the parameters of $\delta m_{\tilde{L}}^2$, together with the most important observables discussed in this work. See Chapter 3 for a detailed discussion. Even this first step is not trivial. Apart from the ever present fact that there are not enough observables to fully reconstruct $\delta m_{\tilde{L}}^2$, there is the problem that the mapping of observables to $\delta m_{\tilde{L}}^2$ is not always perfectly unique. For example, the present bounds on $Br(\tau \rightarrow e\gamma)$ and $Br(\tau \rightarrow \mu\gamma)$ are so weak compared to $Br(\mu \rightarrow e\gamma)$, that they in general allow a significant (about 20-30%) spilling over of the $\tilde{\tau}\tilde{e}$ and $\tilde{\tau}\tilde{\mu}$ mixing into $\tilde{\mu}\tilde{e}$. In other words, the mass-insertion approximation assuming small off-diagonal elements is not always applicable. In our opinion, the best way to deal with this is to first apply the weakest bound and then successively move on to the stronger bounds, at each step taking into account the possible spilling over from weaker bounds. This could also be performed iteratively, until convergence to a consistent pattern for $\delta m_{\tilde{L}}^2$ that satisfies all experimental limits is achieved.
3. The MSSM+seesaw RGEs are then solved from the experimental low energy scale to M_{GUT} . The bi-unitary procedure of Section 4.3 is used to calculate the masses M_i of the right-handed neutrinos and the neutrino Yukawa coupling matrix Y_ν , allowing the proper integration of the right-handed neutrinos at their respective mass scales. The only problem is that the slepton mass corrections are not directly proportional to $Y_\nu^\dagger Y_\nu$ but also include the accumulated running from M_{GUT} to the different M_i . In the leading-logarithmic approximations, this is expressed as

$$\delta m_{\tilde{L}}^2 \propto Y_\nu^\dagger \cdot \text{diag} \left(\log \frac{M_{\text{GUT}}}{M_i} \right) \cdot Y_\nu. \quad (7.1)$$

In order to separate this logarithmic enhancement, the RGE development can be performed iteratively until the result converges with a small error. In the first run, we use some intermediate value for the right-handed masses, e.g. $M_i = 10^{13}$ GeV, and solve the RGEs from bottom to top. This results in a new set of M_i^{eff} via (4.43), which in general are too large as they effectively include a logarithmic running enhancement,

$$M_i^{\text{eff}} = M_i \log \frac{M_{\text{GUT}}}{M_i}. \quad (7.2)$$

Nevertheless, the RGEs are solved top-down with these new values to compare the resulting $(m_{\tilde{L}}^2)_{\text{RGE}}$ with the desired input $(m_{\tilde{L}}^2)_{\text{exp}}$ from experiment. As long as the difference between the two is too large, this procedure is repeated, at each step using the M_i calculated in the previous step. Once the error is acceptable, we perform a final bottom-up running to produce a high energy seesaw parameter setup (Y_ν, M_i) that is consistent with all experimental constraints or measurements.

A numerical example

In order to show the ability of the above procedure to reconstruct the high energy seesaw parameters, we give a very specific example in the mSUGRA scenario SPS1a. We assume that the branching ratios are measured with values

$$Br(\mu \rightarrow e\gamma) = 10^{-13}, \quad (7.3)$$

$$Br(\tau \rightarrow \mu\gamma) = 10^{-9}, \quad (7.4)$$

$$Br(\tau \rightarrow e\gamma) = 10^{-9}, \quad (7.5)$$

roughly corresponding to the expected future sensitivities of these observables (although the value for $Br(\tau \rightarrow e\gamma)$ is rather wishful thinking at this moment). These branching ratios can be translated into corrections to the left-handed slepton mass matrix $\mathbf{m}_{\tilde{L}}^2$. Schematically, this is done by inverting the mass-insertion approximation (3.8), yielding $(|\delta\mathbf{m}_{\tilde{L}}^2|)_{ij}$. For our numerical results, we use the full branching ratio formula, numerically inverting $Br(l_i \rightarrow l_j\gamma)(|\delta\mathbf{m}_{\tilde{L}}^2|)_{ij}$.

In addition, we choose a fixed but arbitrary quasi-degenerate spectrum of diagonal entries in $\delta\mathbf{m}_{\tilde{L}}^2$,

$$(\delta\mathbf{m}_{\tilde{L}}^2)_{ii} = -(180, 181, 182) \text{ GeV}^2. \quad (7.6)$$

These assumptions lead to a low energy left-handed slepton mass matrix,

$$\delta\mathbf{m}_{\tilde{L}}^2 = - \begin{pmatrix} 180 & 0.6 & 136 \\ 0.6 & 181 & 136 \\ 136 & 136 & 182 \end{pmatrix} \text{ GeV}^2, \quad (7.7)$$

where we additionally assumed that the phases of the off-diagonal elements vanish (the branching ratios are only sensitive on the absolute values $|\delta\mathbf{m}_{\tilde{L}}^2|_{ij}$). For the light neutrinos, a degenerate mass spectrum with $m_1 = 0.3 \text{ eV}$ is used, where the oscillation parameters are at their best fit values (Section 4.5), and the CP violating phases are put to zero. The light neutrino mass matrix is then given by

$$\mathbf{m}_\nu = \begin{pmatrix} 3.0 & 0.003 & 0.002 \\ 0.003 & 3.02 & 0.02 \\ 0.002 & 0.02 & 3.02 \end{pmatrix} 10^{-10} \text{ GeV}. \quad (7.8)$$

$\delta\mathbf{m}_{\tilde{L}}^2$ and \mathbf{m}_ν are inserted into the above iterative RG running procedure as a starting point. After just two iterations, $(\mathbf{m}_{\tilde{L}}^2)_{\text{RGE}}$ converges to within 5% of the input (7.7), producing a fully reconstructed seesaw model parameterized as

$$\text{diag } M_i = (8 \cdot 10^{12}, 2 \cdot 10^{13}, 4 \cdot 10^{13}) \text{ GeV}, \quad (7.9)$$

$$\text{diag } Y_i = (0.22, 0.45, 0.53), \quad (7.10)$$

$$\mathbf{U}_L = \begin{pmatrix} 0.95 & -0.30 & -0.0013 \\ 0.21 & 0.68 & -0.71 \\ 0.21 & 0.67 & 0.71 \end{pmatrix}, \quad (7.11)$$

$$\mathbf{U}_R = \begin{pmatrix} 0.99 & -5 \cdot 10^{-5} & 1 \cdot 10^{-4} \\ 5 \cdot 10^{-5} & 0.99 & -3 \cdot 10^{-3} \\ -1 \cdot 10^{-4} & 3 \cdot 10^{-3} & 0.99 \end{pmatrix}. \quad (7.12)$$

As can be seen, the right-handed neutrino masses are quasi-degenerate with a mass scale $M_R \approx 10^{13}$ GeV, and the flavor mixing is sizeable only in the left-handed mixing matrix U_L , whereas U_R is almost diagonal. This example thus roughly belongs to the class of quasi-degenerate left- and right-handed neutrinos presented in Chapter 5, which is not surprising as it was intentionally constructed that way. Accordingly, the R matrix is close to the unity matrix.

To lend more substance to this example, we now allow a variation of the diagonal entries in δm_L^2 in the range $(-4000 \dots 0 \text{ GeV}^2)^1$ and include arbitrary phases for the off-diagonal elements. This corresponds to the most general matrix δm_L^2 which satisfies (7.3-7.5). Also, the light neutrino parameters are varied in their expected future intervals for a quasi-degenerate mass spectrum. Due to these uncertainties in the low energy input, the right-handed neutrino masses are no longer fixed but are situated in the intervals

$$6.5 \cdot 10^9 < M_1 < 1.5 \cdot 10^{14}, \quad (7.13)$$

$$1.2 \cdot 10^{12} < M_2 < 1.6 \cdot 10^{14}, \quad (7.14)$$

$$6.3 \cdot 10^{12} < M_3 < 3.1 \cdot 10^{14}, \quad (7.15)$$

and the hierarchy between the Majorana masses is constrained by

$$1.0 < \frac{M_2}{M_1} < 5.9 \cdot 10^3, \quad (7.16)$$

$$1.0 < \frac{M_3}{M_2} < 4.3 \cdot 10^1, \quad (7.17)$$

$$1.2 < \frac{M_3}{M_1} < 1.2 \cdot 10^4. \quad (7.18)$$

Consequently, both M_2 and M_3 are determined within two orders of magnitude around 10^{13} GeV, whereas M_1 can be as small as 10^{10} GeV. A quasi-degenerate mass spectrum is a viable solution, as realized in the specific numerical example above. In fact, the hierarchy between M_3 and M_2 is constrained to be rather small. On the other hand, M_1 can be detached from the other two masses by a considerable amount, $\frac{M_2}{M_1} \approx \mathcal{O}(10^3)$. This can also be seen in Figure 7.1, where $\frac{M_3}{M_1}$ is plotted against M_1 . At $M_1 \approx 10^{14}$ GeV, the Majorana mass spectrum approaches degeneracy. It should be stressed that these results have been derived without making any assumptions on the high energy model, like a real R matrix or a specific right-handed neutrino spectrum. We only assume a specific pattern of branching ratio measurements (7.3-7.5) and a quasi-degenerate light neutrino mass spectrum. This example also shows that full knowledge of the low energy input is not necessary in order to draw important conclusions.

No Slepton flavor violation Much has been said in this work about the connection between neutrino and slepton flavor violation. There is one texture for the neutrino Yukawa coupling matrix Y_ν , where this correlation can be spoiled. No slepton flavor violation will

¹The diagonal elements of $Y_\nu^\dagger Y_\nu$ are always positive, $(Y_\nu^\dagger Y_\nu)_{ii} = \sum_k |Y_{ki}|^2$. Hence, the elements $(\delta m_L^2)_{ii}$, $i = 1, 2, 3$, are negative (4.32).

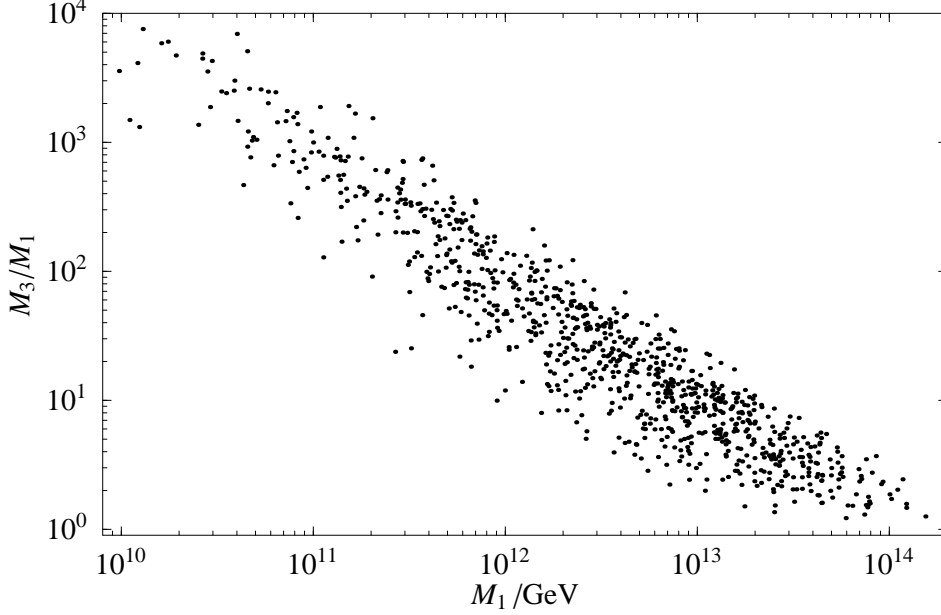


Figure 7.1: $\frac{M_3}{M_1}$ as function of M_1 in SPS1a. See text for a description of the scatter procedure.

be observed if $Y_\nu^\dagger Y_\nu$ is diagonal² (in a basis where Y_e and M are also diagonal),

$$Y_\nu^\dagger Y_\nu = \text{diag } |Y_i|^2, \quad (7.19)$$

with the absolute squares of the Yukawa coupling eigenvalues Y_i as diagonal entries. No off-diagonal slepton mass matrix elements will be generated in this case to one-loop order. In the language of the bi-unitary parametrization, this means that U_L can be identified with the identity matrix (4.40),

$$U_L = \mathbb{I}. \quad (7.20)$$

From (4.43), the right-handed masses M_i and the right-handed mixing matrix U_R can be calculated via the diagonalization

$$\frac{1}{v^2 \sin^2 \beta} \text{diag } Y_i^{-1} \cdot m_\nu \cdot \text{diag } Y_i^{-1} = U_R^* \cdot \text{diag } M_i^{-1} \cdot U_R^\dagger, \quad (7.21)$$

where the only unknown parameters are the neutrino Yukawa coupling eigenvalues. This scenario is the most striking example of how precision measurements of the slepton masses are necessary to unambiguously determine the seesaw parameters, because they are the only observables known to us which are sensitive to the diagonal elements $(Y_\nu^\dagger Y_\nu)_{ii}$.

The simplest realization of (7.19) is given by choosing the Yukawa coupling eigenvalues to be degenerate,

$$\text{diag } Y_i = Y \mathbb{I}. \quad (7.22)$$

²We are neglecting the logarithmic running, $Y_\nu^\dagger Y_\nu \rightarrow Y_\nu^\dagger L Y_\nu$, for discussion purposes. This does not change the qualitative results. If $Y_\nu^\dagger Y_\nu$ is diagonal, so is $Y_\nu^\dagger L Y_\nu$, and vice versa.

Although highly unlikely in the light of the strongly hierarchical Yukawa couplings of the other fermions, it is a possibility. Equation (7.21) is then simply given by

$$\mathbf{U}_R^\top \mathbf{m}_\nu \mathbf{U}_R = \text{diag} \frac{(Y v \sin \beta)^2}{M_i} = \text{diag} m_i, \quad (7.23)$$

which is nothing but the diagonalization (4.8) of the effective light neutrino matrix \mathbf{m}_ν , yielding the neutrino masses m_i . Thus, \mathbf{U}_R can be identified with the neutrino mixing matrix \mathbf{U} , and \mathbf{Y}_ν is simply

$$\mathbf{Y}_\nu = Y \mathbf{U}^\dagger. \quad (7.24)$$

In true seesaw spirit, the light neutrino masses are suppressed as $m_i = \frac{(Y v \sin \beta)^2}{M_i}$, i.e. the hierarchy of the light neutrino masses is exactly the inverse of the right-handed neutrino mass hierarchy³. This scenario is thus not compatible with a vanishing mass scale m_1 , as the largest right-handed neutrino mass would have to approach infinity. Also note that (7.24) is intriguingly similar to (5.4),

$$\mathbf{Y}_\nu = \text{diag} Y_i \cdot \mathbf{U}^\dagger = \frac{1}{v \sin \beta} \text{diag} \sqrt{M_R m_i} \cdot \mathbf{U}^\dagger, \quad (7.25)$$

which applies in the case of degenerate M_i with a real \mathbf{R} matrix. Here, the hierarchy of the light neutrino masses is correlated quadratically with the Yukawa coupling hierarchy,

$$m_i = \frac{(Y_i v \sin \beta)^2}{M_R}. \quad (7.26)$$

Both cases coincide trivially if the light masses would be perfectly degenerate, which is of course ruled out.

³The numbering of the mass eigenvalues will change if sorted in the usual fashion: $m_1 < m_2 < m_3$.

Chapter 8

Conclusions

We studied in great detail how the unknown parameters of the SUSY seesaw model can be determined from measurements of observables at or below collider energies, namely rare LFV decays $l_\alpha \rightarrow l_\beta \gamma$, slepton pair production processes $e^\pm e^- \rightarrow \sum_{i,j} \tilde{l}_j^\pm \tilde{l}_i^- \rightarrow l_\beta^\pm l_\alpha^- + 2\tilde{\chi}_1^0$ at linear colliders and slepton mass differences. This is a challenging task as there is an intricate dependence of the observables on the unknown seesaw, light neutrino and mSUGRA parameters. In order to separate these different influences, we first considered two classes of seesaw models, namely quasi-degenerate and strongly hierarchical right-handed neutrinos.

In the case of degenerate right-handed neutrinos, and assuming a close correlation between lepton flavor violation in the neutrino sector and charged LFV, the common mass scale M_R of the right-handed neutrinos is the only unknown high energy seesaw parameter on which the observables are sensitive. For hierarchical light neutrinos, a measurement of $Br(\mu \rightarrow e\gamma) \approx 10^{-13}$ would probe M_R in the range $5 \cdot 10^{11}$ GeV to 10^{14} GeV, depending on the mSUGRA scenario, with an uncertainty of about two orders of magnitude in M_R . As all lepton flavor violating observables are suppressed by two orders of magnitude for a neutrino mass scale of $m_1 = 0.3$ eV, compared to a hierarchical light neutrino spectrum, the sensitivity on M_R decreases accordingly by about one order of magnitude.

There are strong correlations between the cross sections for slepton pair production at linear colliders and the branching ratios for the corresponding rare radiative decays. These are largely unaffected by the uncertainties in the light neutrino parameters. We have therefore investigated these correlations very thoroughly and find that they are the stronger, the smaller the branching ratios for the radiative decays are, i.e. the lower M_R . The correlations are somewhat weakened for highly degenerate light neutrinos, in which case the collider process cross sections are favored compared to the rare decay rates. The present bounds on $Br(\mu \rightarrow e\gamma)$ and $Br(\tau \rightarrow \mu\gamma)$ still allow sizable signals at a linear collider of the order of 1 fb at $\sqrt{s} = 500$ GeV in the SUSY scenarios well accessible at that energy. If $\mu \rightarrow e\gamma$ will not be observed at the new PSI experiment, the cross section for $e^+ e^- \rightarrow \sum_{i,j} \tilde{l}_j^+ \tilde{l}_i^- \rightarrow \mu^+ e^- + 2\tilde{\chi}_1^0$ is predicted not to exceed 0.1 fb.

In order to estimate the sensitivity of the collider processes, we have calculated the dominant Standard Model and MSSM background. With appropriate cuts, which were optimized for each scenario, anticipating the future knowledge on the sparticle mass spectra,

the Standard Model and MSSM background to the μ^+e^- -channel amounts to 4-14 fb. At a beam energy of 800 GeV, there can be a strong increase in the signal cross section for scenarios with larger slepton masses. The overall discovery potential for lepton flavor violation at a linear collider is slightly increased by performing searches in e^-e^- collisions in addition to e^+e^- collisions.

We also determined the general dependence of rare decay rates and collider processes on the mSUGRA parameters m_0 , $m_{1/2}$ and A_0 , going beyond the handful of benchmark scenarios used. As loop processes, rare decays have a higher reach to larger sparticle masses and thus to m_0 and $m_{1/2}$. Nevertheless, collider processes have a better sensitivity for $m_0 \approx 100$ GeV and $m_{1/2} \approx 200 - 400$ GeV at $\sqrt{s} = 500$ GeV. Their sensitivity is also significantly improved compared to rare decays for positive values of $A_0 \gtrsim 100$ GeV, a possibility not covered in any of the benchmark scenarios available.

In case of hierarchical light neutrinos there can still be a measurable mass difference between the left-handed smuon and selectron of the order of 0.1-1 GeV. The determination of such mass patterns incompatible with flavor-conserving mSUGRA predictions would provide very useful information, as the mass differences are directly sensitive to the diagonal elements of $Y_\nu^\dagger Y_\nu$, which is not the case for any of the LFV signals.

For hierarchical left- and right-handed neutrinos, many of the aforementioned properties, like the strong correlation between rare decays and collider processes, remain qualitatively true. On the other hand, the now possible mixing between the right-handed neutrinos, which can be expressed by a complex orthogonal matrix R , does play a significant role, making this scenario less predictive. As a remedy, we apply an additional constraint by requiring that our model successfully incorporates the generation of the observed baryon number asymmetry of the universe via leptogenesis. In this way we constructed a realization of the seesaw model that is compatible with current bounds on LFV branching ratios as well as the measurement of the baryon asymmetry. With the future sensitivity $Br(\mu \rightarrow e\gamma) \approx 10^{-13}$, it is possible to probe the heaviest right-handed Majorana mass M_3 in the range 10^{11} GeV - 10^{14} GeV (depending on the SUSY scenario), with an uncertainty of about two orders of magnitude in M_3 . Consistency with successful leptogenesis restricts the lightest right-handed neutrino mass M_1 to be larger than $\approx 5 \cdot 10^9$ GeV. In order to avoid an overproduction of gravitinos in mSUGRA, the reheating temperature of inflation should be smaller than about 10^{11} GeV, setting an approximate upper limit on M_1 of the same scale. This condition also considerably constrains the real angles x_2 and x_3 of the R matrix. The remaining angle x_1 can be determined or constrained by measuring the ratio $Br(\mu \rightarrow e\gamma)/Br(\tau \rightarrow \mu\gamma)$, which might also be utilized to roughly discriminate between the cases of degenerate and hierarchical right-handed neutrinos.

Finally, we presented a general method that can be used to reconstruct the high energy seesaw parameters, among them the heavy right-handed neutrino masses, from low energy observables alone. With a representative example for possible branching ratio measurements, we demonstrated that right-handed neutrino masses can be determined with an uncertainty of two orders of magnitude if only the LFV branching ratios (or alternatively, LFV processes at linear colliders) are measured, without making any further assumptions on the high energy theory. This confirms and generalizes the above results for the determination of M_R for

degenerate, and M_3 for hierarchical right-handed neutrinos. The procedure, for which a proof of applicability was given, is expected to come into its own in the future if there will be actual signals of charged lepton flavor violation. Every new experimental piece of information on the light neutrino sector and the slepton flavor violation processes can be easily implemented and its impact on the unknown high energy physics analyzed. It is hoped that this will allow a glimpse (or maybe more than that) on the physics around the GUT scale.

Zusammenfassung

Das eleganteste Modell zur Erzeugung von Neutrinomassen ist der Seesaw-Mechanismus, in dem sehr schwere rechtshändige Neutrinos zum Teilcheninhalt des Standardmodells hinzugefügt werden. Der Seesaw-Mechanismus kann auf natürliche Weise die kleinen Massen der linkshändigen Neutrinos erklären, welche durch die schweren rechtshändigen Neutrinomassen unterdrückt sind, $m_\nu = (100 \text{ GeV})^2/M_R$. Mit Neutrinomassen von etwa $m_\nu \approx 0,1 \text{ eV}$ sollte die Massenskala M_R der rechtshändigen Neutrinos um die 10^{14} GeV liegen.

Ein großer Nachteil des Seesaw-Modells ist die Tatsache, dass es viele freie Parameter enthält, die nicht durch Messungen im beobachtbaren leichten Neutrinosektor bestimmbar sind. Obwohl prinzipiell möglich, sind Prozesse mit geladener Lepton-Flavor-Verletzung im Seesaw-Modell stark unterdrückt, und können nicht zur Eingrenzung des Parameterraums benutzt werden. Dies ändert sich drastisch, wenn das Modell supersymmetrisiert wird. Die Lepton-Flavor-Verletzung im Neutrinosektor wird in diesem Fall auf den Sleptonsektor übertragen, welcher Strahlungskorrekturen durch die rechtshändigen Neutrinos erfährt. Dadurch sind Zerfallsraten seltener Zerfälle wie $\mu \rightarrow e\gamma$ und $\tau \rightarrow \mu\gamma$ möglich, die nahe der jetzigen experimentellen Grenzen liegen. Neben solchen radiativen Zerfällen sind auch Lepton-Flavor verletzende Prozesse an Teilchenbeschleunigern erlaubt, wobei wir uns hier auf Slepton-Paar-Produktion an $e^\pm e^-$ -Beschleunigern konzentrieren.

In dieser Arbeit wurde detailliert untersucht wie die unbekannt Parameter des supersymmetrischen Seesaw-Modells durch Messung von niederenergetischen Observablen (Lepton-Flavor verletzende seltene Zerfälle $l_\alpha \rightarrow l_\beta\gamma$, Slepton-Paar-Produktion $e^\pm e^- \rightarrow \sum_{i,j} \tilde{l}_j^\pm \tilde{l}_i^\mp \rightarrow l_\beta^\pm l_\alpha^\mp + 2\tilde{\chi}_1^0$ an Linearbeschleunigern und Sleptonmassen-Differenzen) bestimmt werden können. Wegen des komplizierten Zusammenhangs zwischen diesen Messgrößen und den Seesaw-, Neutrino-, und SUSY-Parametern stellt dies eine große Herausforderung dar. Um die verschiedenen Einflüsse zu trennen, wurden zuerst zwei Klassen von Seesaw-Modellen betrachtet, nämlich solche die durch (quasi-)entartete und stark hierarchische rechtshändige Neutrinomassen charakterisiert sind.

Im Falle entarteter rechtshändiger Neutrinos wird zusätzlich eine enge Korrelation zwischen der Lepton-Verletzung im Slepton- und im Neutrino-Sektor angenommen. Unter diesen Annahmen ist die gemeinsame Massenskala M_R der rechtshändigen Neutrinos der einzige unbekannt Parameter der zugrundeliegenden Theorie, auf den die oben genannten Observablen sensitiv sind. Für hierarchische leichte Neutrinos würde M_R durch eine Messung von $Br(\mu \rightarrow e\gamma) \approx 10^{-13}$ im Bereich von $5 \cdot 10^{11} \text{ GeV}$ bis 10^{14} GeV mit einer Unsicherheit von etwa zwei Größenordnungen getestet werden, abhängig vom gewählten SUSY Szenario. Bei

einem entarteten Massenspektrum der leichten Neutrinos mit $m_1 = 0.3$ eV sind alle Lepton-Flavor verletzenden Observablen um zwei Größenordnungen gegenüber dem hierarchischen Fall unterdrückt, wodurch die Sensitivität auf M_R um etwa eine Größenordnung sinkt.

Zwischen den Wirkungsquerschnitten von Slepton-Paar-Produktionsprozessen an Linearbeschleunigern und den Verzweigungsverhältnissen der entsprechenden seltenen Zerfälle besteht eine enge Korrelation, welche nur schwach von den Unsicherheiten in den Neutrinoparametern beeinflusst wird. Die Korrelation ist um so stärker, je kleiner die Verzweigungsverhältnisse der seltenen Zerfälle sind. Für stark entartete leichte Neutrinomassen wird die Korrelation geschwächt, wobei die Beschleunigerprozesse etwas im Vorteil gegenüber den Zerfällen sind. Die jetzigen Grenzen an $Br(\mu \rightarrow e\gamma)$ und $Br(\tau \rightarrow \mu\gamma)$ erlauben messbare Signale für Lepton-Flavor verletzende Slepton-Paar-Produktion an Linearbeschleunigern in der Größenordnung von 1 fb bei einer Strahlenergie von 500 GeV. Falls der Zerfall $\mu \rightarrow e\gamma$ nicht im MEG Experiment am PSI gemessen werden wird, sollte der Wirkungsquerschnitt für $e^+e^- \rightarrow \sum_{i,j} \tilde{l}_j^+ \tilde{l}_i^- \rightarrow \mu^+e^- + 2\tilde{\chi}_1^0$ nicht 0,1 fb übersteigen. Mittels geeigneter Schnitte, die auf jedes SUSY Szenario angepasst sind, kann der Standardmodell- und Lepton-Flavor erhaltende SUSY-Hintergrund zum Beschleunigersignal $\mu^+e^- + 2\tilde{\chi}_1^0$ auf etwa 4-14 fb gedrückt werden.

Für hierarchische leichte Neutrinos ist eine messbare Massendifferenz zwischen dem links-händigen Smüon und Seletron im Bereich 0,1-1 GeV möglich. Die Messung solcher Massendifferenzen, die in Lepton-Flavor erhaltender SUSY nicht erwartet werden, wäre sehr interessant, da die Massendifferenzen direkt auf die Diagonalelemente von $Y_\nu^\dagger Y_\nu$ sensitiv sind, was für keine der anderen betrachteten Observablen gilt.

Im Falle hierarchischer links- und rechtshändiger Neutrinos bleiben viele der oben genannten Ergebnisse, wie etwa die Korrelation zwischen Beschleunigerprozessen und seltenen Zerfällen, weiterhin bestehen. Andererseits spielt die Mischung der rechtshändigen Neutrinos, welche mittels einer komplex orthogonalen Matrix R beschrieben werden kann, nun eine große Rolle. Dadurch nimmt die Vorhersagekraft dieses Szenarios etwas ab. Um dies auszugleichen, fordern wir zusätzlich dass das Modell erfolgreich die Bildung der Baryonzahl-Asymmetrie des Universums mittels Leptogenese beschreibt. Damit wurde ein Seesaw-Modell realisiert, das mit den jetzigen Grenzen an den Lepton-Flavor verletzenden Verzweigungsverhältnissen und der Messung der Baryonzahl-Asymmetrie verträglich ist. Mittels der zukünftigen Sensitivität $Br(\mu \rightarrow e\gamma) \approx 10^{-13}$ wäre es möglich, die Masse M_3 des schwersten rechtshändigen Neutrinos im Bereich 10^{11} GeV - 10^{14} GeV (abhängig vom SUSY Szenario) mit einer Unsicherheit von etwa zwei Größenordnungen zu bestimmen. Für erfolgreiche Leptogenese muss die leichteste Masse M_1 grösser als $\approx 5 \cdot 10^9$ GeV sein, und um eine Überproduktion von Gravitinos in mSUGRA zu vermeiden, sollte M_1 zudem unter 10^{11} GeV liegen. Diese Tatsache sorgt auch dafür, dass die reellen Winkel x_2 und x_3 der R -Matrix stark eingeschränkt sind. Der verbleibende Winkel x_1 kann durch eine Messung von $Br(\mu \rightarrow e\gamma)/Br(\tau \rightarrow \mu\gamma)$ bestimmt oder eingeschränkt werden. Diese Observable könnte auch dazu benutzt werden, um zwischen entarteten und hierarchischen rechtshändigen Neutrinos zu unterscheiden.

Zur Verallgemeinerung der obigen Ergebnisse wurde zum Abschluss eine allgemeine Methode präsentiert, mittels der die zugrunde liegenden Hochenergie-Parameter des Seesaw-

Modells allein durch niederenergetische Observable rekonstruiert werden können. Mit Hilfe eines repräsentativen Beispiels wurde gezeigt, dass rechtshändige Neutrinomassen mit einer Unsicherheit von zwei Größenordnungen bestimmbar sind, falls nur die Verzweigungsverhältnisse $Br(l_\alpha \rightarrow l_\beta \gamma)$ (oder die entsprechenden Beschleuniger-Wirkungsquerschnitte) bekannt sind. Dies bestätigt und verallgemeinert die oben genannten, in Grenzfällen ermittelten, Ergebnisse. Das Verfahren sollte in der Zukunft voll zur Geltung kommen, wenn Signale für geladene Lepton-Flavor-Verletzung tatsächlich gemessen werden. Jede neue experimentelle Information zum Neutrinosektor oder zu geladener Lepton-Flavor-Verletzung kann auf einfache Weise berücksichtigt werden, um seinen Einfluss auf die unbekannte Hochenergie-Physik des Seesaw-Modells zu bestimmen. Vielleicht gestattet dies einen kurzen Blick auf die Physik am Rande der GUT-Skala.

Acknowledgments

I would like to express my deepest gratitude to the following people who contributed to the completion of this work:

- Prof. Dr. Reinhold Rückl, for providing excellent working conditions, as well as giving many helpful comments. Without his strong commitment, this work would not have been possible.
- My collaborators at Würzburg, Dr. Heinrich Päs and Dr. Andreas Redelbach, for countless illuminating and inspiring conversations and discussions, and for their help in accomplishing this work. Also I would like to thank them for a critical reading of the manuscript.
- The members of the particle physics group in Würzburg, for a friendly and helpful atmosphere.
- The secretary, Brigitte Wehner, and computer expert Alexander Wagner, for their kind assistance and help in 'worldly' matters.
- Prof. Dr. José Valle, Dr. Martin Hirsch and the other members of the Instituto de Física Corpuscular, for their kind hospitality during my visits in Valencia. A special thanks goes to Prof. Valle for his strong collaborative commitment.

Würzburg, August 2004

Frank Deppisch

Reality is that which, when you stop believing it, does not go away [137].

Appendix A

Numerical parameters

The following numerical parameters, taken from [81, 138], were used throughout our numerical calculations. Unless otherwise noted, all values are at the electroweak scale $m_Z = 91.19$ GeV.

α	=	1/137.036	fine-structure constant
$\alpha(m_Z)$	=	1/127.880	fine-structure constant at m_Z
$\sin^2 \theta_W$	=	0.2311	weak mixing angle
m_Z	=	91.188	Z boson mass
m_W	=	80.423	W boson mass
v	=	174.19	Higgs VEV
α_s	=	0.117	strong coupling constant
$m_e^{(\text{pole})}$	=	$5.01(5.11) \cdot 10^{-4}$	electron (pole) mass
$m_\mu^{(\text{pole})}$	=	$1.04(1.06) \cdot 10^{-1}$	muon (pole) mass
$m_\tau^{(\text{pole})}$	=	1.75(1.78)	tau (pole) mass
Γ_μ	=	$3.00 \cdot 10^{-19}$	muon decay width
Γ_τ	=	$2.26 \cdot 10^{-12}$	tau decay width
m_u	=	$1.72 \cdot 10^{-3}$	u -quark mass
m_d	=	$3.89 \cdot 10^{-3}$	d -quark mass
m_s	=	$0.68 \cdot 10^{-2}$	s -quark mass
m_c	=	0.58	c -quark mass
m_b	=	2.91	b -quark mass
m_t	=	174.3	t -quark mass
M_{GUT}	=	$1.5 \cdot 10^{16}$	GUT scale

Table A.1: Numerical input parameters. Masses and widths are in GeV.

Appendix B

MSSM notation and conventions

B.1 Neutralinos

The higgsinos and electroweak gauginos of the MSSM mix with each other due to electroweak symmetry breaking. The neutral higgsinos ($\tilde{h}_d^0, \tilde{h}_u^0$) and the neutral gauginos (\tilde{B}, \tilde{W}^0) combine to form four neutral mass eigenstates called neutralinos.

In the gauge-eigenstate basis $\psi^0 = (\tilde{B}, \tilde{W}^0, \tilde{h}_d^0, \tilde{h}_u^0)^\top$, the neutralino mass term has the form

$$\mathcal{L} = -\frac{1}{2}\psi^{0\top}\mathbf{Z}\psi^0 + \text{h.c.}, \quad (\text{B.1})$$

where the neutralino mass matrix is given by [139]

$$\mathbf{Z} = \begin{pmatrix} \tilde{M}_1 & 0 & -m_Z s_W c_\beta & m_Z s_W s_\beta \\ 0 & \tilde{M}_2 & m_Z c_W c_\beta & -m_Z c_W s_\beta \\ -m_Z s_W c_\beta & m_Z c_W c_\beta & 0 & -\mu \\ m_Z s_W s_\beta & -m_Z c_W s_\beta & -\mu & 0 \end{pmatrix}, \quad (\text{B.2})$$

with the soft-SUSY breaking gaugino masses \tilde{M}_1, \tilde{M}_2 and the Higgs mixing parameter μ . Diagonalization leads to the mass eigenstates

$$\chi_i^0 = \mathbf{N}_{ij}\psi_j^0, \quad i, j = 1, \dots, 4, \quad (\text{B.3})$$

where \mathbf{N} is a unitary matrix satisfying:

$$\mathbf{N}^*\mathbf{Z}\mathbf{N}^\dagger = \text{diag} \left(m_{\tilde{\chi}_1^0}, m_{\tilde{\chi}_2^0}, m_{\tilde{\chi}_3^0}, m_{\tilde{\chi}_4^0} \right). \quad (\text{B.4})$$

\mathbf{N} can be chosen such that the eigenvalues are real and positive [140]. By convention, they are labelled with ascending mass value, $m_{\tilde{\chi}_1^0} < m_{\tilde{\chi}_2^0} < m_{\tilde{\chi}_3^0} < m_{\tilde{\chi}_4^0}$. The easiest way to determine \mathbf{N} is to take the absolute square of (B.4),

$$\mathbf{N}(\mathbf{Z}^\dagger\mathbf{Z})\mathbf{N}^\dagger = \text{diag} m_{\tilde{\chi}_i^0}^2, \quad (\text{B.5})$$

which is a straightforward unitary diagonalization of $Z^\dagger Z$. The proper Majorana spinors for the neutralinos are

$$\tilde{\chi}_i^0 = \begin{pmatrix} \chi_i^0 \\ \bar{\chi}_i^0 \end{pmatrix}. \quad (\text{B.6})$$

B.2 Charginos

Just like the neutral higgsinos and gauginos, the charged higgsinos ($\tilde{h}_u^+, \tilde{h}_d^-$) and winos (\tilde{W}^+, \tilde{W}^-) mix to form two mass eigenstates with charge ± 1 called charginos. In the gauge eigenstate basis $\psi = (\tilde{W}^+, \tilde{h}_u^+, \tilde{W}^-, \tilde{h}_d^-)^\top$ the chargino mass term has the form

$$\mathcal{L} = -\frac{1}{2}\psi^\top \mathbf{C} \psi + \text{h.c.}, \quad (\text{B.7})$$

with the mass matrix \mathbf{C} in 2×2 block form [140]

$$\mathbf{C} = \begin{pmatrix} 0 & \mathbf{X}^\top \\ \mathbf{X} & 0 \end{pmatrix}, \quad \mathbf{X} = \begin{pmatrix} \tilde{M}_2 & \sqrt{2}m_W s_\beta \\ \sqrt{2}m_W c_\beta & \mu \end{pmatrix}. \quad (\text{B.8})$$

The mass eigenstates are related to the gauge eigenstates by two different, unitary 2×2 matrices \mathbf{O}_1 and \mathbf{O}_2 :

$$\begin{pmatrix} \chi_1^- \\ \chi_2^- \end{pmatrix} = \mathbf{O}_1 \begin{pmatrix} \tilde{W}^- \\ \tilde{H}_1^- \end{pmatrix}, \quad \begin{pmatrix} \chi_1^+ \\ \chi_2^+ \end{pmatrix} = \mathbf{O}_2 \begin{pmatrix} \tilde{W}^+ \\ \tilde{H}_2^+ \end{pmatrix}, \quad (\text{B.9})$$

which can be chosen such that

$$\mathbf{O}_1^* \mathbf{X} \mathbf{O}_2^\dagger = \text{diag} \left(m_{\tilde{\chi}_1^\pm}, m_{\tilde{\chi}_2^\pm} \right), \quad m_{\tilde{\chi}_1^\pm} < m_{\tilde{\chi}_2^\pm}, \quad (\text{B.10})$$

with real positive mass eigenvalues in ascending order. For the practical calculation of $\mathbf{O}_{1/2}$, it is useful to take the absolute squares of (B.10), yielding:

$$\mathbf{O}_1 \mathbf{X} \mathbf{X}^\dagger \mathbf{O}_1^\dagger = \text{diag} m_{\tilde{\chi}_1^\pm}^2, \quad (\text{B.11})$$

$$\mathbf{O}_2 \mathbf{X}^\dagger \mathbf{X} \mathbf{O}_2^\dagger = \text{diag} m_{\tilde{\chi}_1^\pm}^2. \quad (\text{B.12})$$

The Dirac spinors of the charginos are built from the particle-antiparticle two-component spinors as

$$\tilde{\chi}_i^\pm = \begin{pmatrix} \chi_i^\pm \\ \bar{\chi}_i^\mp \end{pmatrix}. \quad (\text{B.13})$$

B.3 Charged Sleptons

In principle, any scalars with the same electric charge, R -parity and color quantum numbers can mix with each other. This means that the mass eigenstates of the sleptons should be obtained by diagonalizing a 6×6 matrix for the charged sleptons $(\tilde{l}_{L\alpha}, \tilde{l}_{R\alpha}) = (\tilde{e}_L, \tilde{\mu}_L, \tilde{\tau}_L, \tilde{e}_R, \tilde{\mu}_R, \tilde{\tau}_R)$ and a 3×3 matrix for the sneutrinos $\tilde{\nu}_\alpha = (\tilde{\nu}_e, \tilde{\nu}_\mu, \tilde{\nu}_\tau)_L$.

The charged slepton (mass)² matrix has the following form (in the above flavor eigenstate basis) [55]

$$\mathbf{m}_{\tilde{l}}^2 = \begin{pmatrix} \mathbf{m}_{\tilde{l}_L}^2 & (\mathbf{m}_{\tilde{l}_{LR}}^2)^\dagger \\ \mathbf{m}_{\tilde{l}_{LR}}^2 & \mathbf{m}_{\tilde{l}_R}^2 \end{pmatrix}, \quad (\text{B.14})$$

where $\mathbf{m}_{\tilde{l}_L}^2$, $\mathbf{m}_{\tilde{l}_R}^2$ and $\mathbf{m}_{\tilde{l}_{LR}}^2$ are 3×3 matrices, $\mathbf{m}_{\tilde{l}_L}^2$, $\mathbf{m}_{\tilde{l}_R}^2$ also being hermitian:

$$\mathbf{m}_{\tilde{l}_L}^2 = \mathbf{m}_L^2 + \text{diag}(m_{l_i}^2) + \mathbb{I}m_Z^2 \cos(2\beta)(-1/2 + \sin^2 \theta_W) \quad (\text{B.15})$$

$$\mathbf{m}_{\tilde{l}_R}^2 = \mathbf{m}_e^2 + \text{diag}(m_{l_i}^2) - \mathbb{I}m_Z^2 \cos(2\beta) \sin^2 \theta_W \quad (\text{B.16})$$

$$\mathbf{m}_{\tilde{l}_{LR}}^2 = \mathbf{A}_e v \cos \beta - \text{diag}(m_{l_i}) \mu \tan \beta. \quad (\text{B.17})$$

The contributions \mathbf{m}_L^2 , \mathbf{m}_e^2 are soft SUSY-breaking mass terms from the SSB Lagrangian (2.7), while the lepton masses m_{l_i} reflect the SUSY prediction, $m_{\tilde{l}_i} = m_{l_i}$. The terms proportional to m_Z^2 originate from so called D-terms generally given by

$$\Delta_\Phi = m_Z^2 (T_{3\Phi} - Q_{\text{EM}\Phi} \sin^2 \theta_W) \cos(2\beta), \quad (\text{B.18})$$

with $T_{3\Phi}$ and $Q_{\text{EM}\Phi}$ the third component of the weak isospin and the electric charge of the supermultiplet to which the relevant particle belongs (for the right-handed sector this is the anti-supermultiplet, $Q_{\text{EM}\tilde{l}} = +1$). They arise from (slepton)²(Higgs)² quartic interactions once the Higgses acquire vacuum expectation values.

In general the mass matrix (B.14) is not diagonal. It is diagonalized by a 6×6 unitary matrix $\mathbf{U}_{\tilde{l}}$,

$$\mathbf{U}_{\tilde{l}}^\dagger \mathbf{m}_{\tilde{l}}^2 \mathbf{U}_{\tilde{l}} = \text{diag}(m_{\tilde{l}_1}^2, \dots, m_{\tilde{l}_6}^2), \quad (\text{B.19})$$

with the charged slepton mass eigenvalues $m_{\tilde{l}_i}^2$, $i = 1, \dots, 6$. The slepton mass eigenstates are expressed in terms of the gauge eigenstates by

$$\tilde{l}_i = (\mathbf{U}_{\tilde{l}})_{\alpha i}^* \tilde{l}_{L\alpha} + (\mathbf{U}_{\tilde{l}})_{(\alpha+3)i}^* \tilde{l}_{R\alpha}, \quad \alpha = 1, 2, 3. \quad (\text{B.20})$$

B.4 Sneutrinos

The sneutrino (mass)² matrix in the flavor eigenstate basis $\tilde{\nu}_\alpha = (\tilde{\nu}_e, \tilde{\nu}_\mu, \tilde{\nu}_\tau)_L$ is given by

$$\mathbf{m}_{\tilde{\nu}}^2 = \mathbf{m}_L^2 + 1/2 m_Z^2 \cos(2\beta) \mathbb{I}, \quad (\text{B.21})$$

where the tiny masses of the light neutrinos are neglected. The mass matrix is diagonalized by a unitary 3×3 matrix $\mathbf{U}_{\tilde{\nu}}$:

$$\mathbf{U}_{\tilde{\nu}}^\dagger \mathbf{m}_{\tilde{\nu}}^2 \mathbf{U}_{\tilde{\nu}} = \text{diag}(m_{\tilde{\nu}_1}^2, m_{\tilde{\nu}_2}^2, m_{\tilde{\nu}_3}^2). \quad (\text{B.22})$$

The mass eigenstates $\tilde{\nu}_i$ are related to the gauge eigenstates by

$$\begin{pmatrix} \tilde{\nu}_1 \\ \tilde{\nu}_2 \\ \tilde{\nu}_3 \end{pmatrix} = \mathbf{U}_{\tilde{\nu}} \begin{pmatrix} \tilde{\nu}_e \\ \tilde{\nu}_\mu \\ \tilde{\nu}_\tau \end{pmatrix}. \quad (\text{B.23})$$

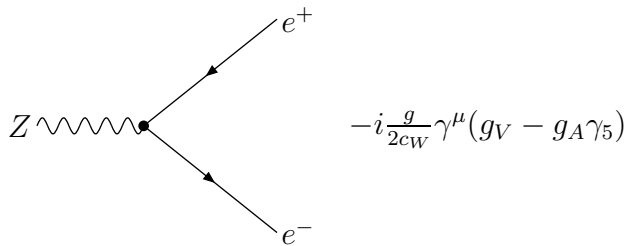
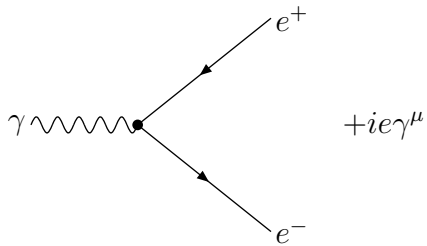
In principle, the addition of right-handed sneutrinos as part of the SUSY seesaw model induces left-right sneutrino mixing and sneutrino-antisneutrino mixing [141] (4.3), in general leading to a 12×12 sneutrino mass matrix. Such mixings are suppressed by the Majorana mass scale M_R of the right-handed neutrinos, and can be neglected if M_R is large as is always the case in our work. The same is true for the right-handed sneutrinos. They do not directly contribute to low energy processes.

B.5 Vertices

Listed are all vertices, taken from [100], used in the calculation of our signal processes. P_L and P_R are the chirality projection operators,

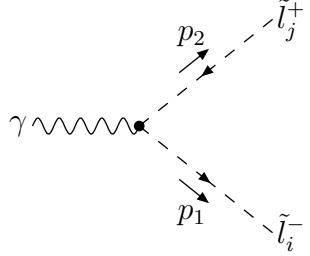
$$P_L = \frac{1}{2}(1 - \gamma_5), \quad P_R = \frac{1}{2}(1 + \gamma_5). \quad (\text{B.24})$$

Standard model vertices



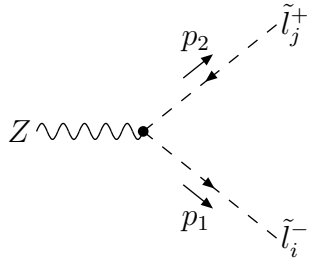
with the coupling strength $g = \frac{e}{\sin\theta_W}$ and $g_V = -\frac{1}{2} + 2\sin^2\theta_W$, $g_A = -\frac{1}{2}$.

Slepton-slepton-gauge boson The definition of the momentum flow of the scalar particles is crucial in these vertices. We choose the momentum direction to be equal with the particle arrow and opposite to the antiparticle arrow, so the momenta always flow out of the vertex in the following cases.



A Feynman diagram showing a photon (γ) represented by a wavy line on the left, meeting a vertex. From the vertex, two dashed lines representing sleptons emerge. The upper dashed line is labeled \tilde{l}_j^+ and has an arrow pointing away from the vertex with momentum p_2 . The lower dashed line is labeled \tilde{l}_i^- and has an arrow pointing towards the vertex with momentum p_1 .

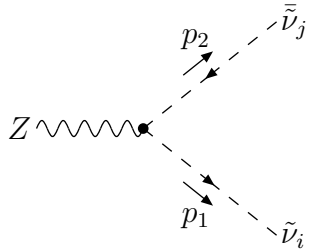
$$+ie\delta_{ij}(p_1 - p_2)^\mu$$



A Feynman diagram showing a Z boson represented by a wavy line on the left, meeting a vertex. From the vertex, two dashed lines representing sleptons emerge. The upper dashed line is labeled \tilde{l}_j^+ and has an arrow pointing away from the vertex with momentum p_2 . The lower dashed line is labeled \tilde{l}_i^- and has an arrow pointing towards the vertex with momentum p_1 .

$$-i\frac{g}{c_W}z_{ij}(p_1 - p_2)^\mu$$

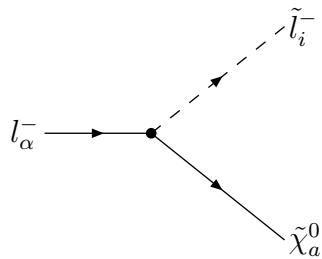
$$\text{with } z_{ij} = -\frac{1}{2}\sum_{k=1}^3(U_{\tilde{l}})_{ik}(U_{\tilde{l}})_{jk} + s_W^2\delta_{ij}$$



A Feynman diagram showing a Z boson represented by a wavy line on the left, meeting a vertex. From the vertex, two dashed lines representing sneutrinos emerge. The upper dashed line is labeled $\tilde{\nu}_j$ and has an arrow pointing away from the vertex with momentum p_2 . The lower dashed line is labeled $\tilde{\nu}_i$ and has an arrow pointing towards the vertex with momentum p_1 .

$$-i\frac{g}{2c_W}\delta_{ij}(p_1 - p_2)^\mu$$

Charged lepton-charged slepton-neutralino



A Feynman diagram showing a charged lepton (l_α^-) represented by a solid line on the left, meeting a vertex. From the vertex, two dashed lines emerge. The upper dashed line is labeled \tilde{l}_i^- and has an arrow pointing away from the vertex. The lower dashed line is labeled $\tilde{\chi}_a^0$ and has an arrow pointing towards the vertex.

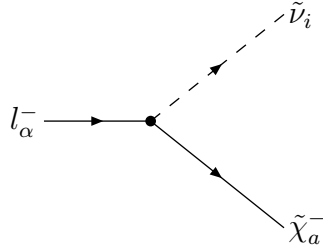
$$-\sqrt{2}ie(N_{i\alpha,a}^L P_L + N_{i\alpha,a}^R P_R)$$

with

$$N_{i\alpha,a}^L = \frac{m_{l_\alpha} N_{a3}^*}{2m_W s_W c_\beta} (U_{\tilde{l}})_{i(\alpha+3)} - \frac{N_{a1}^* t_W + N_{a2}^*}{2s_W} (U_{\tilde{l}})_{i\alpha} \quad (\text{B.25})$$

$$N_{i\alpha,a}^R = \frac{N_{a1}}{c_W} (U_{\tilde{l}})_{i(\alpha+3)} + \frac{m_{l_\alpha} N_{a3}}{2m_W s_W c_\beta} (U_{\tilde{l}})_{i\alpha}, \quad (\text{B.26})$$

Charged lepton-sneutrino-chargino



$$-\sqrt{2}ie (C_{i\alpha,a}^L P_L + C_{i\alpha,a}^R P_R)$$

with

$$C_{i\alpha,a}^L = \frac{(\mathcal{O}_2)_{a1}}{\sqrt{2}s_W} (\mathbf{U}_{\tilde{\nu}})_{i\alpha} \quad (\text{B.27})$$

$$C_{i\alpha,a}^R = -\frac{m_{l_\alpha} (\mathcal{O}_1)_{a2}}{2m_W c_\beta s_W} (\mathbf{U}_{\tilde{\nu}})_{i\alpha} \quad (\text{B.28})$$

Appendix C

Renormalization Group Equations

Throughout this chapter, the logarithmic scale variable t is defined as

$$t = \frac{1}{16\pi^2} \ln \left(\frac{\mu}{\mu_0} \right), \quad (\text{C.1})$$

in order to get rid of factors $16\pi^2$. μ is the running scale whereas μ_0 is an arbitrary base scale. In our numerical calculation, we used $\mu_0 = m_Z$. The following RGEs are taken from [142], including the sign conventions for the gaugino mass terms and trilinear couplings. The SUSY scale, i.e. the scale above which the sparticle degrees of freedom are treated as active, is defined as [138]

$$M_{\text{SUSY}} = \sqrt{m_{t_1} m_{t_2}}, \quad (\text{C.2})$$

the geometric mean of the stop masses. This choice minimizes SUSY threshold effects.

C.1 SM

This section shows the full renormalization group equations for the Yukawa coupling matrices Y_e, Y_u, Y_d and gauge couplings g_a ($a = 1, 2, 3$), in the Standard Model to one loop order. These RGEs are used below the SUSY scale and quark mixing effects are neglected. In addition, the top quark is integrated out below m_t .

$$\frac{dY_e}{dt} = Y_e \left[\left(-\frac{9}{4}g_1^2 - \frac{9}{4}g_2^2 + \text{Tr} \left[Y_e^\dagger Y_e + 3Y_u^\dagger Y_u + 3Y_d^\dagger Y_d \right] \right) \mathbb{I} + \frac{3}{2}Y_e^\dagger Y_e \right], \quad (\text{C.3})$$

$$\begin{aligned} \frac{dY_u}{dt} &= Y_u \left[\left(-\frac{17}{20}g_1^2 - \frac{9}{4}g_2^2 - 8g_3^2 + \text{Tr} \left[Y_e^\dagger Y_e + 3Y_u^\dagger Y_u + 3Y_d^\dagger Y_d \right] \right) \mathbb{I} \right. \\ &\quad \left. + \frac{3}{2}Y_u^\dagger Y_u - \frac{3}{2}Y_d^\dagger Y_d \right], \end{aligned} \quad (\text{C.4})$$

$$\begin{aligned} \frac{dY_d}{dt} &= Y_d \left[\left(-\frac{1}{4}g_1^2 - \frac{9}{4}g_2^2 - 8g_3^2 + \text{Tr} \left[Y_e^\dagger Y_e + 3Y_u^\dagger Y_u + 3Y_d^\dagger Y_d \right] \right) \mathbb{I} \right. \\ &\quad \left. + \frac{3}{2}Y_d^\dagger Y_d - \frac{3}{2}Y_u^\dagger Y_u \right], \end{aligned} \quad (\text{C.5})$$

$$\frac{dg_a}{dt} = b_a g_a^3, \quad \text{with} \quad b = \left(\frac{41}{10}, -\frac{19}{6}, -7 \right), \quad a = 1, 2, 3. \quad (\text{C.6})$$

C.2 MSSM

In the following, we give the RG equations of the MSSM. They are used above the SUSY scale M_{SUSY} . The RGEs for the gauge couplings g_a and the gaugino masses \tilde{M}_a are given to two-loop order for greater accuracy.

$$\frac{dY_e}{dt} = Y_e \left[\left(-\frac{9}{5}g_1^2 - 3g_2^2 + \text{Tr} \left[Y_e^\dagger Y_e + 3Y_d^\dagger Y_d \right] \right) \mathbb{I} + 3Y_e^\dagger Y_e \right], \quad (\text{C.7})$$

$$\frac{dY_u}{dt} = Y_u \left[\left(-\frac{13}{15}g_1^2 - 3g_2^2 - \frac{16}{3}g_3^2 + 3 \text{Tr} \left[Y_u^\dagger Y_u \right] \right) \mathbb{I} + 3Y_u^\dagger Y_u + Y_d^\dagger Y_d \right], \quad (\text{C.8})$$

$$\frac{dY_d}{dt} = Y_d \left[\left(-\frac{7}{15}g_1^2 - 3g_2^2 - \frac{16}{3}g_3^2 + \text{Tr} \left[3Y_d^\dagger Y_d + Y_e^\dagger Y_e \right] \right) \mathbb{I} + 3Y_d^\dagger Y_d + Y_u^\dagger Y_u \right], \quad (\text{C.9})$$

$$\frac{dg_a}{dt} = B_a g_a^3 + \frac{1}{16\pi^2} \left(\sum_{b=1}^3 B_{ab} g_b^2 \right) g_a^3, \quad a = 1, 2, 3, \quad (\text{C.10})$$

$$\frac{d\tilde{M}_a}{dt} = B_a g_a^2 \tilde{M}_a + \frac{2}{16\pi^2} g_a^2 \sum_{b=1}^3 B_{ab} g_b^2 (\tilde{M}_a + \tilde{M}_b), \quad a = 1, 2, 3, \quad (\text{C.11})$$

with

$$B = \left(\frac{33}{5}, 1, -3 \right), \quad \mathbf{B} = \begin{pmatrix} 199/25 & 27/5 & 88/5 \\ 9/5 & 25 & 24 \\ 11/5 & 9 & 14 \end{pmatrix}.$$

The RGEs for the soft SUSY breaking mass contributions $\mathbf{m}_L^2, \mathbf{m}_e^2, \mathbf{m}_Q^2, \mathbf{m}_u^2, \mathbf{m}_d^2, m_{h_u}^2, m_{h_d}^2$ are

$$\begin{aligned} \frac{d\mathbf{m}_L^2}{dt} &= \mathbf{m}_L^2 Y_e^\dagger Y_e + Y_e^\dagger Y_e \mathbf{m}_L^2 + 2 (Y_e^\dagger \mathbf{m}_e^2 Y_e + m_{h_d}^2 Y_e^\dagger Y_e) \\ &\quad - \left(\frac{6}{5}g_1^2 |\tilde{M}_1|^2 + 6g_2^2 |\tilde{M}_2|^2 + \frac{3}{5}g_1^2 S \right) \mathbb{I}, \end{aligned} \quad (\text{C.12})$$

$$\begin{aligned} \frac{d\mathbf{m}_e^2}{dt} &= 2 (\mathbf{m}_e^2 Y_e Y_e^\dagger + Y_e Y_e^\dagger \mathbf{m}_e^2) + 4 (Y_e \mathbf{m}_L^2 Y_e^\dagger + m_{h_d}^2 Y_e Y_e^\dagger + \mathbf{A}_e \mathbf{A}_e^\dagger) \\ &\quad - \left(\frac{24}{5}g_1^2 |\tilde{M}_1|^2 - \frac{6}{5}g_1^2 S \right) \mathbb{I}, \end{aligned} \quad (\text{C.13})$$

$$\begin{aligned}
\frac{dm_{\tilde{Q}}^2}{dt} &= m_{\tilde{Q}}^2 Y_u^\dagger Y_u + Y_u^\dagger Y_u m_{\tilde{Q}}^2 + m_{\tilde{Q}}^2 Y_d^\dagger Y_d + Y_d^\dagger Y_d m_{\tilde{Q}}^2 \\
&+ 2 \left(Y_d^\dagger m_{\tilde{d}}^2 Y_d + m_{\tilde{h}_d}^2 Y_d^\dagger Y_d + A_d^\dagger A_d + Y_u^\dagger m_{\tilde{u}}^2 Y_u + m_{\tilde{h}_u}^2 Y_u^\dagger Y_u + A_u^\dagger A_u \right) \\
&- \left(\frac{2}{15} g_1^2 |\tilde{M}_1|^2 + 6g_2^2 |\tilde{M}_2|^2 + \frac{32}{3} g_3^2 |\tilde{M}_3|^2 + \frac{3}{5} g_1^2 S \right) \mathbb{I},
\end{aligned} \tag{C.14}$$

$$\begin{aligned}
\frac{dm_{\tilde{u}}^2}{dt} &= 2 \left(m_{\tilde{u}}^2 Y_u^\dagger Y_u + Y_u^\dagger Y_u m_{\tilde{u}}^2 \right) + 4 \left(Y_u m_{\tilde{Q}}^2 Y_u^\dagger + m_{\tilde{h}_u}^2 Y_u Y_u^\dagger + A_u A_u^\dagger \right) \\
&- \left(\frac{32}{15} g_1^2 |\tilde{M}_1|^2 + \frac{32}{3} g_3^2 |\tilde{M}_3|^2 + \frac{4}{5} g_1^2 S \right) \mathbb{I},
\end{aligned} \tag{C.15}$$

$$\begin{aligned}
\frac{dm_{\tilde{d}}^2}{dt} &= 2 \left(m_{\tilde{d}}^2 Y_d^\dagger Y_d + Y_d^\dagger Y_d m_{\tilde{d}}^2 \right) + 4 \left(Y_d m_{\tilde{Q}}^2 Y_d^\dagger + m_{\tilde{h}_d}^2 Y_d Y_d^\dagger + A_d A_d^\dagger \right) \\
&- \left(\frac{8}{15} g_1^2 |\tilde{M}_1|^2 + \frac{32}{3} g_3^2 |\tilde{M}_3|^2 + \frac{2}{5} g_1^2 S \right) \mathbb{I},
\end{aligned} \tag{C.16}$$

$$\begin{aligned}
\frac{dm_{\tilde{h}_d}^2}{dt} &= 6 \text{Tr} \left[m_{\tilde{Q}}^2 Y_d^\dagger Y_d + Y_d^\dagger m_{\tilde{d}}^2 Y_d + m_{\tilde{h}_d}^2 Y_d^\dagger Y_d + A_d^\dagger A_d \right] \\
&+ 2 \text{Tr} \left[m_{\tilde{L}}^2 Y_e^\dagger Y_e + Y_e^\dagger m_{\tilde{e}}^2 Y_e + m_{\tilde{h}_1}^2 Y_e^\dagger Y_e + A_e^\dagger A_e \right] \\
&- \frac{6}{5} g_1^2 |\tilde{M}_1|^2 - 6g_2^2 |\tilde{M}_2|^2 - \frac{3}{5} g_1^2 S,
\end{aligned} \tag{C.17}$$

$$\begin{aligned}
\frac{dm_{\tilde{h}_u}^2}{dt} &= 6 \text{Tr} \left[m_{\tilde{Q}}^2 Y_u^\dagger Y_u + Y_u^\dagger m_{\tilde{u}}^2 Y_u + m_{\tilde{h}_u}^2 Y_u^\dagger Y_u + A_u^\dagger A_u \right] \\
&- \frac{6}{5} g_1^2 |\tilde{M}_1|^2 - 6g_2^2 |\tilde{M}_2|^2 - \frac{3}{5} g_1^2 S,
\end{aligned} \tag{C.18}$$

where S is a shorthand for

$$S = \text{Tr} \left[m_{\tilde{Q}}^2 + m_{\tilde{d}}^2 - m_{\tilde{u}}^2 - m_{\tilde{L}}^2 + m_{\tilde{e}}^2 \right] - m_{\tilde{h}_d}^2 + m_{\tilde{h}_u}^2. \tag{C.19}$$

Finally, the RGEs for the soft SUSY-breaking trilinear couplings A_e, A_u, A_d are given as:

$$\begin{aligned}
\frac{dA_e}{dt} &= A_e \left[-\frac{9}{5} g_1^2 - 3g_2^2 + \text{Tr} \left[3Y_d^\dagger Y_d + Y_e^\dagger Y_e \right] \right] \\
&+ 2Y_e \left[\frac{9}{5} g_1^2 \tilde{M}_1 + 3g_2^2 \tilde{M}_2 + \text{Tr} \left[3Y_d^\dagger A_d + Y_e^\dagger A_e \right] \right] \\
&+ 4Y_e Y_e^\dagger A_e + 5A_e Y_e^\dagger Y_e,
\end{aligned} \tag{C.20}$$

$$\begin{aligned}
\frac{dA_u}{dt} &= A_u \left[-\frac{13}{15} g_1^2 - 3g_2^2 - \frac{16}{3} g_3^2 + 3 \text{Tr} \left[Y_u^\dagger Y_u \right] \right] \\
&+ 2Y_u \left[\frac{13}{15} g_1^2 \tilde{M}_1 + 3g_2^2 \tilde{M}_2 + \frac{16}{3} g_3^2 \tilde{M}_3 + 3 \text{Tr} Y_u^\dagger A_u \right] \\
&+ 4Y_u Y_u^\dagger A_u + 5A_u Y_u^\dagger Y_u + 2Y_u Y_d^\dagger A_d + A_u Y_d^\dagger Y_d,
\end{aligned} \tag{C.21}$$

$$\begin{aligned}
\frac{d\mathbf{A}_d}{dt} &= \mathbf{A}_d \left[-\frac{7}{15}g_1^2 - 3g_2^2 - \frac{16}{3}g_3^2 + \text{Tr} \left[3\mathbf{Y}_d^\dagger \mathbf{Y}_d + \mathbf{Y}_e^\dagger \mathbf{Y}_e \right] \right] \\
&+ 2\mathbf{Y}_d \left[\frac{7}{15}g_1^2 \tilde{M}_1 + 3g_2^2 \tilde{M}_2 + \frac{16}{3}g_3^2 \tilde{M}_3 + \text{Tr} \left[3\mathbf{Y}_d^\dagger \mathbf{A}_d + \mathbf{Y}_e^\dagger \mathbf{A}_e \right] \right] \\
&+ 4\mathbf{Y}_d \mathbf{Y}_d^\dagger \mathbf{A}_d + 5\mathbf{A}_d \mathbf{Y}_d^\dagger \mathbf{Y}_d + 2\mathbf{Y}_d \mathbf{Y}_u^\dagger \mathbf{A}_u + \mathbf{A}_d \mathbf{Y}_u^\dagger \mathbf{Y}_u.
\end{aligned} \tag{C.22}$$

C.3 SUSY seesaw

The RGEs for the supersymmetric seesaw model are given below to one-loop order. The method to properly apply them in the case of non-degenerate right-handed neutrinos is given in Section 4.2. The scale dependence of the new additional matrices \mathbf{Y}_ν , $m_{\nu_R}^2$, \mathbf{A}_ν , \mathbf{M} and \mathbf{m}_ν is governed by

$$\frac{d\mathbf{Y}_\nu}{dt} = \mathbf{Y}_\nu \left[\left(-\frac{3}{5}g_1^2 - 3g_2^2 + \text{Tr} \left[3\mathbf{Y}_u^\dagger \mathbf{Y}_u + \mathbf{Y}_\nu^\dagger \mathbf{Y}_\nu \right] \right) \mathbb{I} + 3\mathbf{Y}_\nu^\dagger \mathbf{Y}_\nu + \mathbf{Y}_e^\dagger \mathbf{Y}_e \right], \tag{C.23}$$

$$\frac{dm_{\nu_R}^2}{dt} = 2 \left(m_{\nu_R}^2 \mathbf{Y}_\nu \mathbf{Y}_\nu^\dagger + \mathbf{Y}_\nu \mathbf{Y}_\nu^\dagger m_{\nu_R}^2 \right) + 4 \left(\mathbf{Y}_\nu m_{\nu_R}^2 \mathbf{Y}_\nu^\dagger + m_{\nu_R}^2 \mathbf{Y}_\nu \mathbf{Y}_\nu^\dagger + \mathbf{A}_\nu \mathbf{A}_\nu^\dagger \right), \tag{C.24}$$

$$\begin{aligned}
\frac{d\mathbf{A}_\nu}{dt} &= \mathbf{A}_\nu \left(-\frac{3}{5}g_1^2 - 3g_2^2 + \text{Tr} \left[3\mathbf{Y}_u^\dagger \mathbf{Y}_u + \mathbf{Y}_\nu^\dagger \mathbf{Y}_\nu \right] \right) \\
&+ 2\mathbf{Y}_\nu \left(\frac{3}{5}g_1^2 M_1 + 3g_2^2 M_2 + \text{Tr} \left[3\mathbf{Y}_u^\dagger \mathbf{A}_u + \mathbf{Y}_\nu^\dagger \mathbf{A}_\nu \right] \right) \\
&+ 4\mathbf{Y}_\nu^\dagger \mathbf{Y}_\nu \mathbf{A}_\nu + 5\mathbf{A}_\nu \mathbf{Y}_\nu^\dagger \mathbf{Y}_\nu + 2\mathbf{Y}_\nu \mathbf{Y}_e^\dagger \mathbf{A}_e + \mathbf{A}_\nu \mathbf{Y}_e^\dagger \mathbf{Y}_e,
\end{aligned} \tag{C.25}$$

$$\frac{d\mathbf{M}}{dt} = 2(\mathbf{Y}_\nu^\dagger \mathbf{Y}_\nu) \mathbf{M} + 2\mathbf{M} (\mathbf{Y}_\nu \mathbf{Y}_\nu^\dagger)^\text{T}, \tag{C.26}$$

$$\begin{aligned}
\frac{d\mathbf{m}_\nu}{dt} &= -\frac{3}{2}(\mathbf{Y}_e^\dagger \mathbf{Y}_e)^\text{T} \mathbf{m}_\nu - \frac{3}{2} \mathbf{m}_\nu (\mathbf{Y}_e^\dagger \mathbf{Y}_e) \\
&+ \left(2 \text{Tr} \left[\mathbf{Y}_e^\dagger \mathbf{Y}_e + 3\mathbf{Y}_u^\dagger \mathbf{Y}_u + 3\mathbf{Y}_d^\dagger \mathbf{Y}_d \right] - 3g_2^2 + \lambda_h \right) \mathbf{m}_\nu,
\end{aligned} \tag{C.27}$$

for $\mu < M_{\text{SUSY}}$, and

$$\begin{aligned}
\frac{d\mathbf{m}_\nu}{dt} &= (\mathbf{Y}_e^\dagger \mathbf{Y}_e)^\text{T} \mathbf{m}_\nu + \mathbf{m}_\nu (\mathbf{Y}_e^\dagger \mathbf{Y}_e) + (\mathbf{Y}_\nu^\dagger \mathbf{Y}_\nu)^\text{T} \mathbf{m}_\nu + \mathbf{m}_\nu (\mathbf{Y}_\nu^\dagger \mathbf{Y}_\nu) \\
&+ \left(2 \text{Tr} \left[3\mathbf{Y}_u^\dagger \mathbf{Y}_u + \mathbf{Y}_\nu^\dagger \mathbf{Y}_\nu \right] - \frac{6}{5}g_1^2 - 6g_2^2 \right) \mathbf{m}_\nu,
\end{aligned} \tag{C.28}$$

for $\mu > M_{\text{SUSY}}$. λ_h is the Higgs quartic self-coupling, in the MSSM given by $\lambda_h = \frac{1}{4}(g_1^2 + g_2^2)$. The following quantities are modified due to additional right-handed neutrino corrections:

$$\frac{dY_e}{dt} = \left. \frac{dY_e}{dt} \right|_{\text{MSSM}} + Y_e Y_\nu^\dagger Y_\nu, \quad (\text{C.29})$$

$$\frac{dY_u}{dt} = \left. \frac{dY_u}{dt} \right|_{\text{MSSM}} + Y_u \text{Tr} [Y_\nu^\dagger Y_\nu], \quad (\text{C.30})$$

$$\frac{dm_{\tilde{L}}^2}{dt} = \left. \frac{dm_{\tilde{L}}^2}{dt} \right|_{\text{MSSM}} + m_{\tilde{L}}^2 Y_\nu^\dagger Y_\nu + Y_\nu^\dagger Y_\nu m_{\tilde{L}}^2 + 2 (Y_\nu^\dagger m_{\tilde{\nu}_R}^2 Y_\nu + m_{h_u}^2 Y_\nu^\dagger Y_\nu + A_\nu^\dagger A_\nu), \quad (\text{C.31})$$

$$\frac{dm_{h_u}^2}{dt} = \left. \frac{dm_{h_u}^2}{dt} \right|_{\text{MSSM}} + 2 \text{Tr} [m_{\tilde{L}}^2 Y_\nu^\dagger Y_\nu + Y_\nu^\dagger m_{\tilde{\nu}_R}^2 Y_\nu + m_{h_2}^2 Y_\nu^\dagger Y_\nu + A_\nu^\dagger A_\nu], \quad (\text{C.32})$$

$$\frac{dA_e}{dt} = \left. \frac{dA_e}{dt} \right|_{\text{MSSM}} + 2Y_e Y_\nu^\dagger A_\nu + A_e Y_\nu^\dagger Y_\nu. \quad (\text{C.33})$$

Below their mass scale, the heavy Majorana neutrinos are integrated out, which effectively means that Y_ν and A_ν are zero in this regime.

Appendix D

Processes

Given below are the amplitudes for the processes studied in this work. The vertex factors $N^{R/L}$ and $C^{R/L}$ corresponding to neutralino/charged slepton and chargino/sneutrino vertices are given in Appendix B.5.

D.1 $l_i \rightarrow l_j \gamma$

The amplitude for the process $l_i^-(1) \rightarrow l_j(2)^- \gamma(3)$ is [20, 48]

$$\mathcal{M}_{ij} = iem_{l_i} \bar{u}_2 \epsilon_\mu^* \sigma^{\mu\nu} q_\nu (A_{ij}^L P_L + A_{ij}^R P_R) u_1, \quad (\text{D.1})$$

where $\sigma_{\alpha\beta} = \frac{i}{2} [\gamma_\alpha, \gamma_\beta]$, q is the photon momentum and ϵ is the polarization vector of the photon. In the limit of a massless final lepton, $m_{l_j} = 0$, this yields the decay rate [20, 48]

$$\Gamma(l_i^- \rightarrow l_j^- \gamma) = \frac{e^2}{16\pi} m_{l_i}^5 (|A_{ij}^L|^2 + |A_{ij}^R|^2). \quad (\text{D.2})$$

The coefficients $A_{ij}^{L,R}$ are determined by calculating the photon penguin diagrams shown in Fig. 3.1 with charginos/sneutrinos or neutralinos/charged sleptons in the loop [20, 45, 48]:

$$32\pi^2 A_{ij}^L = \sum_{k=1}^6 \sum_{a=1}^4 \frac{1}{m_{l_k}^2} \left(N_{jk,a}^L N_{ik,a}^{L*} F_1^N \left(\frac{m_{\tilde{\chi}_a^0}^2}{m_{l_k}^2} \right) + \frac{m_{\tilde{\chi}_a^0}}{m_{l_i}} N_{jk,a}^L N_{ik,a}^{R*} F_2^N \left(\frac{m_{\tilde{\chi}_a^0}^2}{m_{l_k}^2} \right) \right) \\ - \sum_{k=1}^3 \sum_{a=1}^2 \frac{1}{m_{\tilde{\nu}_k}^2} \left(C_{jk,a}^L C_{ik,a}^{L*} F_1^C \left(\frac{m_{\tilde{\chi}_a^-}^2}{m_{\tilde{\nu}_k}^2} \right) + \frac{m_{\tilde{\chi}_a^-}}{m_{l_i}} C_{jk,a}^L C_{ik,a}^{R*} F_2^C \left(\frac{m_{\tilde{\chi}_a^-}^2}{m_{\tilde{\nu}_k}^2} \right) \right), \quad (\text{D.3})$$

$$A_{ij}^R = A_{ij}^L \Big|_{L \leftrightarrow R}, \quad (\text{D.4})$$

with

$$F_1^N(x) = \frac{1 - 6x + 3x^2 + 2x^3 - 6x^2 \ln x}{6(1-x)^4}, \quad (\text{D.5})$$

$$F_2^N(x) = \frac{1 - x^2 + 2x \ln x}{(1-x)^3}, \quad (\text{D.6})$$

$$F_1^C(x) = \frac{2 + 3x - 6x^2 + x^3 + 6x \ln x}{6(1-x)^4}, \quad (\text{D.7})$$

$$F_2^C(x) = \frac{-3 + 4x - x^2 - 2 \ln x}{(1-x)^3}. \quad (\text{D.8})$$

D.2 $e^+e^- \rightarrow \tilde{l}_j^+ \tilde{l}_i^-$

The amplitude for the process $e^+(1)e^-(2) \rightarrow \tilde{l}_j^+(3)\tilde{l}_i^-(4)$ is given by [99]:

$$\begin{aligned} \mathcal{M}_{ij} &= \mathcal{M}_{ij}^s + \mathcal{M}_{ij}^t, \\ \mathcal{M}_{ij}^s &= \bar{v}_1 \gamma_\mu (p_3 - p_4)^\mu \left[\frac{e^2 \delta_{ij}}{s} + \frac{e^2 z_{ij}}{2c_W^2} \frac{1}{s - M_Z^2} (g_V - g_A \gamma_5) \right] u_2, \\ \mathcal{M}_{ij}^t &= -\bar{v}_1 \frac{e^2}{2} \sum_{a=1}^4 \left[(N_{j1,a}^{L*} P_R + N_{j1,a}^{R*} P_L) \frac{\not{p} + m_{\tilde{\chi}_a^0}}{t - m_{\tilde{\chi}_a^0}^2} (N_{i1,a}^L P_L + N_{i1,a}^R P_R) \right] u_2. \end{aligned} \quad (\text{D.9})$$

In comparison to the slepton and neutralino masses, and to the center of mass energy of a linear collider the masses of the initial and final state leptons can be neglected regarding the process kinematics. In terms of the Mandelstam variables $s = (p_1 + p_2)^2$, $t = (p_1 - p_3)^2$, $u = (p_1 - p_4)^2$ the helicity amplitudes $\mathcal{M}_{ij}(h_{e^-}, h_{e^+})$ ($h = \pm 1$) can be written as

$$\begin{aligned} \mathcal{M}_{ij}(+, +) &= -2ie^2 \sqrt{s} \sum_{a=1}^4 m_{\tilde{\chi}_a^0} \frac{N_{i1,a}^R N_{j1,a}^{L*}}{t - m_{\tilde{\chi}_a^0}^2}, \\ \mathcal{M}_{ij}(-, -) &= -2ie^2 \sqrt{s} \sum_{a=1}^4 m_{\tilde{\chi}_a^0} \frac{N_{i1,a}^L N_{j1,a}^{R*}}{t - m_{\tilde{\chi}_a^0}^2}, \\ \mathcal{M}_{ij}(+, -) &= -2ie^2 \sqrt{tu - p_3^2 p_4^2} \left(\frac{\delta_{ij}}{s} + \frac{1}{c_W^2} \frac{z_{ij}}{s - m_Z^2} + \sum_{a=1}^4 \frac{N_{i1,a}^R N_{j1,a}^{R*}}{t - m_{\tilde{\chi}_a^0}^2} \right), \\ \mathcal{M}_{ij}(-, +) &= +2ie^2 \sqrt{tu - p_3^2 p_4^2} \left(\frac{\delta_{ij}}{s} + \frac{s_W^2 - 1/2}{s_W^2 c_W^2} \frac{z_{ij}}{s - m_Z^2} + \sum_{a=1}^4 \frac{N_{i1,a}^L N_{j1,a}^{L*}}{t - m_{\tilde{\chi}_a^0}^2} \right). \end{aligned} \quad (\text{D.10})$$

Arbitrarily polarized beams are described by polarizations P_{e^-} and $P_{e^+} \in [-1, 1]$ of the incoming electrons and positrons, respectively. A polarization of $P_{e^-} = -1(+1)$ corresponds to a beam that entirely consists of particles with helicities $-1/2(+1/2)$. In the limit of massless fermions, which is appropriate in our case, a negative (positive) electron helicity

corresponds to left-handed (right-handed) chirality. For positrons, this relation is reversed: negative (positive) helicity \leftrightarrow right-h. (left-h.) chirality.

The squared amplitude for an arbitrarily polarized beams is generally given by

$$|\mathcal{M}|^2(P_{e^-}, P_{e^+}) = \frac{1}{4} \sum_{h_{e^\pm} = -1, 1} (1 + h_{e^-} P_{e^-})(1 + h_{e^+} P_{e^+}) |\mathcal{M}(h_{e^-}, h_{e^+})|^2. \quad (\text{D.11})$$

D.3 $e^-e^- \rightarrow \tilde{l}_i^- \tilde{l}_j^-$

Analogously, the amplitude for the process $e^-e^- \rightarrow \tilde{l}_i^- \tilde{l}_j^-$ reads [104]:

$$\begin{aligned} \mathcal{M}_{ij} = & -\bar{u}_1 \frac{e^2}{2} \sum_{a=1}^4 \left[(N_{j1,a}^L P_L + N_{j1,a}^R P_R) \frac{C^{-1}(\not{t} + m_{\tilde{\chi}_a^0})}{t - m_{\tilde{\chi}_a^0}^2} (N_{i1,a}^L P_L + N_{i1,a}^R P_R) \right] u_2 \\ & + (t \rightarrow u, i \leftrightarrow j), \end{aligned} \quad (\text{D.12})$$

where C is the charge conjugation operator, satisfying $C^\dagger = C^{-1}$, $C^T = -C$. This leads to helicity amplitudes $\mathcal{M}_{ij}(h_{e^-}, h_{e^-})$,

$$\begin{aligned} \mathcal{M}_{ij}(+, +) &= 2ie^2 \sqrt{s} \sum_{a=1}^4 m_{\tilde{\chi}_a^0} \frac{N_{i1,a}^R N_{j1,a}^R}{t - m_{\tilde{\chi}_a^0}^2} + (t \leftrightarrow u, i \leftrightarrow j), \\ \mathcal{M}_{ij}(-, -) &= 2ie^2 \sqrt{s} \sum_{a=1}^4 m_{\tilde{\chi}_a^0} \frac{N_{i1,a}^L N_{j1,a}^L}{t - m_{\tilde{\chi}_a^0}^2} + (t \leftrightarrow u, i \leftrightarrow j), \\ \mathcal{M}_{ij}(+, -) &= 2ie^2 \sqrt{tu - p_3^2 p_4^2} \sum_{c=1}^4 \frac{N_{i1,a}^R N_{j1,a}^L}{t - m_{\tilde{\chi}_a^0}^2} - (t \leftrightarrow u, i \leftrightarrow j), \\ \mathcal{M}_{ij}(-, +) &= -2ie^2 \sqrt{tu - p_3^2 p_4^2} \sum_{c=1}^4 \frac{N_{i1,a}^L N_{j1,a}^R}{t - m_{\tilde{\chi}_a^0}^2} - (t \leftrightarrow u, i \leftrightarrow j). \end{aligned} \quad (\text{D.13})$$

D.4 $\tilde{l}_i^\pm \rightarrow l_\alpha^\pm \tilde{\chi}_a^0$

The amplitude for the decay $\tilde{l}_i^-(1) \rightarrow l_\alpha^-(2) \tilde{\chi}_a^0(3)$ is [99]

$$\mathcal{M}_i^- = -\frac{e}{\sqrt{2}} \bar{u}_2 [N_{i\alpha,a}^L P_L + N_{i\alpha,a}^R P_R] v_3, \quad (\text{D.14})$$

or in helicity form, $\mathcal{M}_i^-(h_{l_\alpha^-})$, summed over the helicity of the outgoing neutralino,

$$\begin{aligned} \mathcal{M}_i^-(+) &= 2ie N_{i\alpha,a}^R \sqrt{p_2 \cdot p_3}, \\ \mathcal{M}_i^-(-) &= 2ie N_{i\alpha,a}^L \sqrt{p_2 \cdot p_3}. \end{aligned} \quad (\text{D.15})$$

The helicity amplitudes for $\tilde{l}_i^+ \rightarrow l_\alpha^+ \tilde{\chi}_a^0$ can be obtained from (D.15) by substituting $N^{R/L} \rightarrow (N^{L/R})^*$.

Bibliography

- [1] Nabeshima Naoshige, Japanese Daimyo (feudal lord), 1538-1618, the quote is from his famous wall inscriptions.
- [2] R. Davis, *Prog. Part. Nucl. Phys.* **32**, 13 (1994).
- [3] B. T. Cleveland *et al.*, *Astrophys. J.* **496**, 505 (1998).
- [4] SAGE, J. N. Abdurashitov *et al.*, *Phys. Rev.* **C60**, 055801 (1999), [astro-ph/9907113].
- [5] GNO, C. M. Cattadori, *Nucl. Phys. Proc. Suppl.* **110**, 311 (2002).
- [6] GALLEX, W. Hampel *et al.*, *Phys. Lett.* **B447**, 127 (1999).
- [7] GNO, M. Altmann *et al.*, *Phys. Lett.* **B490**, 16 (2000), [hep-ex/0006034].
- [8] Super-Kamiokande, S. Fukuda *et al.*, *Phys. Lett.* **B539**, 179 (2002), [hep-ex/0205075].
- [9] SNO, Q. R. Ahmad *et al.*, *Phys. Rev. Lett.* **89**, 011301 (2002), [nucl-ex/0204008].
- [10] SNO, Q. R. Ahmad *et al.*, *Phys. Rev. Lett.* **89**, 011302 (2002), [nucl-ex/0204009].
- [11] SNO, S. N. Ahmed *et al.*, *Phys. Rev. Lett.* **92**, 181301 (2004), [nucl-ex/0309004].
- [12] Super-Kamiokande, Y. Fukuda *et al.*, *Phys. Rev. Lett.* **81**, 1562 (1998), [hep-ex/9807003].
- [13] MACRO, A. Surdo, *Nucl. Phys. Proc. Suppl.* **110**, 342 (2002).
- [14] Soudan 2, M. Sanchez *et al.*, *Phys. Rev.* **D68**, 113004 (2003), [hep-ex/0307069].
- [15] KamLAND, K. Eguchi *et al.*, *Phys. Rev. Lett.* **90**, 021802 (2003), [hep-ex/0212021].
- [16] K2K, M. H. Ahn *et al.*, *Phys. Rev. Lett.* **90**, 041801 (2003), [hep-ex/0212007].
- [17] M. Gell-Mann, P. Ramond and R. Slansky, Print-80-0576 (CERN).
- [18] T. Yanagida, In Proceedings of the Workshop on the Baryon Number of the Universe and Unified Theories, Tsukuba, Japan, 13-14 Feb 1979.
- [19] R. N. Mohapatra and G. Senjanovic, *Phys. Rev. Lett.* **44**, 912 (1980).

-
- [20] J. Hisano, T. Moroi, K. Tobe and M. Yamaguchi, *Phys. Rev.* **D53**, 2442 (1996), [hep-ph/9510309].
- [21] J. Hisano and D. Nomura, *Phys. Rev.* **D59**, 116005 (1999), [hep-ph/9810479].
- [22] J. A. Casas and A. Ibarra, *Nucl. Phys.* **B618**, 171 (2001), [hep-ph/0103065].
- [23] R. Barbieri, L. J. Hall and A. Strumia, *Nucl. Phys.* **B445**, 219 (1995), [hep-ph/9501334].
- [24] G. K. Leontaris and N. D. Tracas, *Phys. Lett.* **B431**, 90 (1998), [hep-ph/9803320].
- [25] W. Buchmuller, D. Delepine and F. Vissani, *Phys. Lett.* **B459**, 171 (1999), [hep-ph/9904219].
- [26] M. E. Gomez, G. K. Leontaris, S. Lola and J. D. Vergados, *Phys. Rev.* **D59**, 116009 (1999), [hep-ph/9810291].
- [27] S. F. King and M. Oliveira, *Phys. Rev.* **D60**, 035003 (1999), [hep-ph/9804283].
- [28] W. Buchmuller, D. Delepine and L. T. Handoko, *Nucl. Phys.* **B576**, 445 (2000), [hep-ph/9912317].
- [29] J. L. Feng, Y. Nir and Y. Shadmi, *Phys. Rev.* **D61**, 113005 (2000), [hep-ph/9911370].
- [30] J. Sato and K. Tobe, *Phys. Rev.* **D63**, 116010 (2001), [hep-ph/0012333].
- [31] D. F. Carvalho, M. E. Gomez and S. Khalil, *JHEP* **07**, 001 (2001), [hep-ph/0101250].
- [32] J. Sato, K. Tobe and T. Yanagida, *Phys. Lett.* **B498**, 189 (2001), [hep-ph/0010348].
- [33] S. Davidson and A. Ibarra, *JHEP* **09**, 013 (2001), [hep-ph/0104076].
- [34] P. Ciafaloni, A. Romanino and A. Strumia, *Nucl. Phys.* **B458**, 3 (1996), [hep-ph/9507379].
- [35] J. Hisano, T. Moroi, K. Tobe and M. Yamaguchi, *Phys. Lett.* **B391**, 341 (1997), [hep-ph/9605296].
- [36] J. Hisano, D. Nomura, Y. Okada, Y. Shimizu and M. Tanaka, *Phys. Rev.* **D58**, 116010 (1998), [hep-ph/9805367].
- [37] J. Hisano, D. Nomura and T. Yanagida, *Phys. Lett.* **B437**, 351 (1998), [hep-ph/9711348].
- [38] S. Baek, N. G. Deshpande, X. G. He and P. Ko, *Phys. Rev.* **D64**, 055006 (2001), [hep-ph/0104141].
- [39] G. Barenboim, K. Huitu and M. Raidal, *Phys. Rev.* **D63**, 055006 (2001), [hep-ph/0005159].

-
- [40] S. Lavignac, I. Masina and C. A. Savoy, Phys. Lett. **B520**, 269 (2001), [hep-ph/0106245].
- [41] A. Kageyama, S. Kaneko, N. Shimoyama and M. Tanimoto, Phys. Rev. **D65**, 096010 (2002), [hep-ph/0112359].
- [42] D. F. Carvalho, J. R. Ellis, M. E. Gomez and S. Lola, Phys. Lett. **B515**, 323 (2001), [hep-ph/0103256].
- [43] J. R. Ellis and S. Lola, Phys. Lett. **B458**, 310 (1999), [hep-ph/9904279].
- [44] J. R. Ellis, M. E. Gomez, G. K. Leontaris, S. Lola and D. V. Nanopoulos, Eur. Phys. J. **C14**, 319 (2000), [hep-ph/9911459].
- [45] Y. Okada, K.-i. Okumura and Y. Shimizu, Phys. Rev. **D61**, 094001 (2000), [hep-ph/9906446].
- [46] J. R. Ellis, J. Hisano, S. Lola and M. Raidal, Nucl. Phys. **B621**, 208 (2002), [hep-ph/0109125].
- [47] S. T. Petcov, S. Profumo, Y. Takanishi and C. E. Yaguna, Nucl. Phys. **B676**, 453 (2004), [hep-ph/0306195].
- [48] A. Redelbach, PhD thesis, University of Würzburg, 2004.
- [49] N. Arkani-Hamed, H.-C. Cheng, J. L. Feng and L. J. Hall, Phys. Rev. Lett. **77**, 1937 (1996), [hep-ph/9603431].
- [50] N. V. Krasnikov, Phys. Lett. **B388**, 783 (1996), [hep-ph/9511464].
- [51] N. Arkani-Hamed, J. L. Feng, L. J. Hall and H.-C. Cheng, Nucl. Phys. **B505**, 3 (1997), [hep-ph/9704205].
- [52] H.-C. Cheng, hep-ph/9712427.
- [53] M. Hirouchi and M. Tanaka, Phys. Rev. **D58**, 032004 (1998), [hep-ph/9712532].
- [54] J. L. Feng, Int. J. Mod. Phys. **A13**, 2319 (1998), [hep-ph/9803319].
- [55] J. Hisano, M. M. Nojiri, Y. Shimizu and M. Tanaka, Phys. Rev. **D60**, 055008 (1999), [hep-ph/9808410].
- [56] D. Nomura, Phys. Rev. **D64**, 075001 (2001), [hep-ph/0004256].
- [57] M. Dine, Y. Grossman and S. Thomas, eConf **C010630**, P332 (2001), [hep-ph/0111154].
- [58] M. Cannoni, S. Kolb and O. Panella, Phys. Rev. **D68**, 096002 (2003), [hep-ph/0306170].

-
- [59] J. Cao, Z. Xiong and J. M. Yang, Eur. Phys. J. **C32**, 245 (2004), [hep-ph/0307126].
- [60] W. Porod and W. Majerotto, Phys. Rev. **D66**, 015003 (2002), [hep-ph/0201284].
- [61] F. Deppisch, H. Pas, A. Redelbach, R. Ruckl and Y. Shimizu, Phys. Rev. **D69**, 054014 (2004), [hep-ph/0310053].
- [62] F. Deppisch, J. Kalinowski, H. Pas, A. Redelbach and R. Ruckl, hep-ph/0401243.
- [63] F. Deppisch, H. Pas, A. Redelbach and R. Ruckl, hep-ph/0403212.
- [64] E. . Wali, K. C., Grand Unification. Proceedings, 8th Workshop, Syracuse, USA, April 16-18, 1987, Singapore, Singapore: World Scientific (1988) 451p.
- [65] A. D. Sakharov, Pisma Zh. Eksp. Teor. Fiz. **5**, 32 (1967).
- [66] L. E. Ibanez and G. G. Ross, Phys. Lett. **B110**, 215 (1982).
- [67] S. Dimopoulos, S. Raby and F. Wilczek, Phys. Rev. **D24**, 1681 (1981).
- [68] N. Sakai, Zeit. Phys. **C11**, 153 (1981).
- [69] C. Giunti, C. W. Kim and U. W. Lee, Mod. Phys. Lett. **A6**, 1745 (1991).
- [70] P. Langacker and M.-x. Luo, Phys. Rev. **D44**, 817 (1991).
- [71] H. Pagels and J. R. Primack, Phys. Rev. Lett. **48**, 223 (1982).
- [72] S. P. Martin, hep-ph/9709356.
- [73] L. Girardello and M. T. Grisaru, Nucl. Phys. **B194**, 65 (1982).
- [74] K. Inoue, A. Kakuto, H. Komatsu and S. Takeshita, Prog. Theor. Phys. **71**, 413 (1984).
- [75] D. J. H. Chung *et al.*, hep-ph/0312378.
- [76] J. Polonyi, Hungary Central Inst Res - KFKI-77-93 (77,REC.JUL 78) 5p.
- [77] H. P. Nilles, Phys. Lett. **B115**, 193 (1982).
- [78] H. P. Nilles, Nucl. Phys. **B217**, 366 (1983).
- [79] M. Battaglia *et al.*, Eur. Phys. J. **C22**, 535 (2001), [hep-ph/0106204].
- [80] N. Ghodbane and H.-U. Martyn, hep-ph/0201233.
- [81] Particle Data Group, K. Hagiwara *et al.*, Phys. Rev. **D66**, 010001 (2002).
- [82] MECO, M. Hebert, Nucl. Phys. **A721**, 461 (2003).
- [83] CLEO, S. Ahmed *et al.*, Phys. Rev. **D61**, 071101 (2000), [hep-ex/9910060].

-
- [84] Belle, K. Abe *et al.*, Phys. Rev. Lett. **92**, 171802 (2004), [hep-ex/0310029].
- [85] MEG experiment home page, <http://meg.psi.ch>.
- [86] BELLE, K. Inami, T. Hokuue and T. Ohshima, eConf **C0209101**, TU11 (2002), [hep-ex/0210036].
- [87] F. Deppisch, H. Paes, A. Redelbach, R. Ruckl and Y. Shimizu, Eur. Phys. J. **C28**, 365 (2003), [hep-ph/0206122].
- [88] T. S. Kosmas, A. Faessler, F. Simkovic and J. D. Vergados, Phys. Rev. **C56**, 526 (1997), [nucl-th/9704021].
- [89] H. C. Chiang, E. Oset, T. S. Kosmas, A. Faessler and J. D. Vergados, Nucl. Phys. **A559**, 526 (1993).
- [90] MECO experiment home page, <http://meco.ps.uci.edu>.
- [91] W. Ootani, Prepared for 3rd Workshop on Neutrino Oscillations and Their Origin (NOON 2001), Kashiwa, Japan, 5-8 Dec 2001.
- [92] J. Aysto *et al.*, hep-ph/0109217.
- [93] T. S. Kosmas, Nucl. Phys. **A683**, 443 (2001).
- [94] T. S. Kosmas, Nucl. Instrum. Meth. **A503**, 247 (2001), [nucl-th/0108045].
- [95] T. S. Kosmas, Prog. Part. Nucl. Phys. **48**, 307 (2002).
- [96] K. Yoshimura, talk at the 3rd Workshop on Neutrino Oscillations and their Origin (NOON2001), 2001, ICRR, Univ. of Tokyo, Kashiwa, Japan, to appear in the proceedings.
- [97] B. C. Regan, E. D. Commins, C. J. Schmidt and D. DeMille, Phys. Rev. Lett. **88**, 071805 (2002).
- [98] S. K. Lamoreaux, nucl-ex/0109014.
- [99] F. Deppisch, Master's thesis, University of Würzburg, 2000.
- [100] J. Rosiek, hep-ph/9511250.
- [101] A. Pukhov *et al.*, hep-ph/9908288.
- [102] R. Becker and C. Vander Velde, Prepared for Working Group on e+ e- Collisions at 500-GeV: The Physics Potential, Munich, Germany, 20 Nov 1992.
- [103] F. Deppisch, H. U. Martyn, H. Paes and R. Rueckl, (2004), talk given by Rueckl, R. at the Linear Collider workshop 2004, Paris, to appear in the proceedings.

-
- [104] A. Redelbach, Master's thesis, University of Würzburg, 2000.
- [105] J. Gluza and M. Zralek, Phys. Lett. **B362**, 148 (1995), [hep-ph/9507269].
- [106] A. Freitas *et al.*, hep-ph/0211108.
- [107] B. C. Allanach *et al.*, hep-ph/0407067.
- [108] K. Fujii, T. Tsukamoto and M. M. Nojiri, Prog. Theor. Phys. Suppl. **123**, 203 (1996), [hep-ph/9511338].
- [109] H. U. Martyn, hep-ph/0002290.
- [110] S. Antusch, J. Kersten, M. Lindner and M. Ratz, Phys. Lett. **B538**, 87 (2002), [hep-ph/0203233].
- [111] R. N. Mohapatra and P. B. Pal, *Massive Neutrinos in Physics and Astrophysics*, World Scientific Lecture Notes in Physics Vol. 60, 2 ed. (World Scientific, 1998).
- [112] D. N. Spergel *et al.*, Astrophys. J. Suppl. **148**, 175 (2003), [astro-ph/0302209].
- [113] SDSS, M. Tegmark *et al.*, Phys. Rev. **D69**, 103501 (2004), [astro-ph/0310723].
- [114] P. Di Bari, hep-ph/0406115.
- [115] M. Fukugita and T. Yanagida, Phys. Lett. **B174**, 45 (1986).
- [116] W. Buchmuller and M. Plumacher, Phys. Rept. **320**, 329 (1999), [hep-ph/9904310].
- [117] V. A. Kuzmin, V. A. Rubakov and M. E. Shaposhnikov, Phys. Lett. **B155**, 36 (1985).
- [118] W. Buchmuller and M. Plumacher, Int. J. Mod. Phys. **A15**, 5047 (2000), [hep-ph/0007176].
- [119] W. Buchmuller, P. Di Bari and M. Plumacher, Nucl. Phys. **B643**, 367 (2002), [hep-ph/0205349].
- [120] S. Davidson and A. Ibarra, Phys. Lett. **B535**, 25 (2002), [hep-ph/0202239].
- [121] M. Y. Khlopov and A. D. Linde, Phys. Lett. **B138**, 265 (1984).
- [122] J. R. Ellis, J. E. Kim and D. V. Nanopoulos, Phys. Lett. **B145**, 181 (1984).
- [123] M. Kawasaki, K. Kohri and T. Moroi, Phys. Rev. **D63**, 103502 (2001), [hep-ph/0012279].
- [124] M. Maltoni, T. Schwetz, M. A. Tortola and J. W. F. Valle, hep-ph/0405172.
- [125] V. D. Barger, D. Marfatia and B. P. Wood, Phys. Lett. **B498**, 53 (2001), [hep-ph/0011251].

-
- [126] P. Huber, M. Lindner, M. Rolinec, T. Schwetz and W. Winter, hep-ph/0403068.
- [127] CHOOZ, M. Apollonio *et al.*, Phys. Lett. **B466**, 415 (1999), [hep-ex/9907037].
- [128] MINOS Technical Design Report, http://www.hep.anl.gov/ndk/hypertext/minos_tdr.html.
- [129] H. Minakata and H. Nunokawa, Phys. Lett. **B504**, 301 (2001), [hep-ph/0010240].
- [130] C. Lunardini and A. Y. Smirnov, Phys. Rev. **D63**, 073009 (2001), [hep-ph/0009356].
- [131] V. Barger, D. Marfatia and B. P. Wood, Phys. Lett. **B532**, 19 (2002), [hep-ph/0202158].
- [132] J. J. Gomez-Cadenas, Nucl. Phys. Proc. Suppl. **99B**, 304 (2001), [hep-ph/0105298].
- [133] W. Rodejohann, hep-ph/0203214.
- [134] H. Paes and T. J. Weiler, Phys. Rev. **D63**, 113015 (2001), [hep-ph/0101091].
- [135] KATRIN, A. Osipowicz *et al.*, hep-ex/0109033.
- [136] H. V. Klapdor-Kleingrothaus, A. Dietz, H. L. Harney and I. V. Krivosheina, Mod. Phys. Lett. **A16**, 2409 (2001), [hep-ph/0201231].
- [137] Philip K. Dick, American author, 1928-1982, consistently explored the nature of reality and humanity in his novels.
- [138] B. C. Allanach, Comput. Phys. Commun. **143**, 305 (2002), [hep-ph/0104145].
- [139] H. E. Haber and G. L. Kane, Phys. Rept. **117**, 75 (1985).
- [140] J. F. Gunion and H. E. Haber, Nucl. Phys. **B272**, 1 (1986).
- [141] Y. Grossman and H. E. Haber, Phys. Rev. Lett. **78**, 3438 (1997), [hep-ph/9702421].
- [142] S. P. Martin and M. T. Vaughn, Phys. Rev. **D50**, 2282 (1994), [hep-ph/9311340].

Lebenslauf (April 2005)

Persönliche Daten

Name: Frank Franz Deppisch (Dr. rer. nat.)
Geboren: 27. März 1975 in Ochsenfurt
Nationalität: Deutsch
Ehestand: Ledig
Vater: Kurt Deppisch
Mutter: Hildegard Deppisch, geb. Hamm

Adresse

Anschrift: Institut für Theoretische Physik und Astrophysik,
Universität Würzburg, Am Hubland, D-97074 Würzburg
Telefon: 0931-888-5730
Fax: 0931-888-4604
E-mail: deppisch@physik.uni-wuerzburg.de (Universität)
FrankDeppisch@gmx.de (Privat)

Beruflicher Werdegang

- **Januar 2001 - Mai 2005:** wissenschaftlicher Mitarbeiter/Stipendiat,
Universität Würzburg
- **Mai - November 2003:** Marie Curie fellow,
IFIC, Universität Valencia, Spanien

Ausbildung

- **Promotion Physik**
Universität Würzburg, 2005
Note: sehr gut
- **Diplom Physik**
Universität Würzburg, 2000
Prüfungsfächer: Theoretische und Experimentelle Physik,

Computational Physics, Astronomie
Note: sehr gut

- **Abitur**

Röntgen-Gymnasium Würzburg, 1995
Prüfungsfächer: Physik, Mathematik, Französisch, Geschichte
Note: 1,6

- **Mittlere Reife**

Staatliche Realschule Ochsenfurt, 1991
Note: 1,6

Doktorarbeit

Titel: Towards a reconstruction of the SUSY seesaw model
Online: <ftp://ftp.physik.uni-wuerzburg.de/pub/dissertation/deppisch.pdf>
Betreuer: Prof. R. Rückl, Institut für Theoretische Physik, Universität Würzburg
Note: sehr gut

Diplomarbeit

Titel: Calculation of lepton flavor violating SUSY processes at e^+e^- colliders
Online: <ftp://ftp.physik.uni-wuerzburg.de/pub/diplom/deppisch.ps.gz>
Betreuer: Prof. R. Rückl, Institut für Theoretische Physik, Universität Würzburg
Note: sehr gut

Stipendien

1. Promotionsstipendium des Freistaats Bayern
(August 2002 - Mai 2003)
2. Marie Curie Stipendium der EU am IFIC, Universität Valencia
(Mai - November 2003)
3. Promotionsstipendium des Freistaats Bayern
(Dezember 2003 - Juli 2004)

Lehraktivitäten

- Übungsleiter an der Universität Würzburg für
 - Theoretische Mechanik (2001, 2004)
 - Theoretische Elektrodynamik (2001/2002)
 - Statistische und Theoretische Thermodynamik (2002/2003)

- Beisitzer bei Diplomprüfungen
Universität Würzburg (2001 - 2005)

Computing Mathematica, UNIX/Linux, Windows, C/C++, L^AT_EX, DirectX, CompHEP, SVN

Sprachen Muttersprache Deutsch, Englisch (fließend), Französisch, Spanisch

Wissenschaftliche Besuche

1. Instituto de Fisica Corpuscular, Universität Valencia, Spanien, März 2004, November 2004

Wissenschaftliche Vorträge

1. Towards a reconstruction of the SUSY seesaw model
Promotionskolloquium, Universität Würzburg, 17. März 2005
2. Towards a reconstruction of the SUSY seesaw model
Teilchenphysikseminar, Universität Würzburg, 6. November 2004
3. SUSY-Seesaw und LFV an Linearbeschleunigern
Teilchenphysikseminar, IFIC, Valencia, Spanien, 5. Juni 2003
4. SUSY-Seesaw und LFV an Linearbeschleunigern
Frühjahrstagung der Deutschen Physikalischen Gesellschaft, Aachen, 10.-13. März 2003
5. SUSY-Seesaw-Mechanismus and geladene Lepton-Flavour-Verletzung
Herbstschule für Hochenergiephysik, Maria Laach, 3.-13. September 2002
6. Test der Majoranamassen-Skala rechtshändiger Neutrinos an zukünftigen Beschleunigern
66. Tagung der Deutschen Physikalischen Gesellschaft, Leipzig, 18-22. März 2002
7. Lepton-Flavour verletzende Prozesse in supersymmetrischen Modellen
Adriatic School on Particle Physics and Physics Informatics, Split, Kroatien, 11.-21. September 2001
8. Berechnung Lepton-Flavour verletzende SUSY-Prozesse an e^+e^- -Beschleunigern
Teilchenphysikseminar, Universität Würzburg, 25. Januar 2001

Publikationen

Zeitschriften- und Buchbeiträge

- 1) Physics interplay of the LHC and the ILC
G. Weiglein *et al.* [LHC/LC Study Group],
submitted to Phys. Rept.,
arXiv:hep-ph/0410364
- 2) Double beta decay versus cosmology: Majorana CP phases and nuclear matrix elements
F. Deppisch, H. Päs, J. Suhonen,
submitted to Phys. Rev. D,
arXiv:hep-ph/0409306
- 3) Enhanced lepton flavor violation in the supersymmetric inverse seesaw model
F. Deppisch, J.W.F. Valle,
submitted to Phys. Rev. D,
arXiv:hep-ph/0406040
- 4) Supersymmetric lepton flavor violation at the LHC and LC
F. Deppisch, J. Kalinowski, H. Päs, A. Redelbach, R. Rückl,
<http://www.ipp.dur.ac.uk/~georg/lhc/lc>,
e-Print Archiv: hep-ph/0401243
- 5) The SUSY seesaw model and lepton flavor violation at a future electron positron linear collider
F. Deppisch, H. Päs, A. Redelbach, R. Rückl, Y. Shimizu,
Phys. Rev. D **69**, 054014 (2004),
e-Print Archiv: hep-ph/0310053
- 6) Probing the Majorana mass scale of right-handed neutrinos in mSUGRA
F. Deppisch, H. Päs, A. Redelbach, R. Rückl, Y. Shimizu,
Eur. Phys. J. C **28**, 365 (2003),
e-Print Archiv: hep-ph/0206122

Veröffentlichte Kongress- und Posterbeiträge

- 7) Slepton flavor violation
F. Deppisch, H. U. Martyn, H. Päs, A. Redelbach and R. Rückl,
Talk given at International Conference on Linear Colliders (LCWS 04),
Paris, France, 19-24 Apr 2004,
arXiv:hep-ph/0408140
- 8) Lepton flavor violation in the SUSY seesaw model: an update
F. Deppisch, H. Päs, A. Redelbach, R. Rückl,
9th Adriatic Meeting, Dubrovnik, Croatia, 4-14 Sep 2003,
e-Print Archiv: hep-ph/0403212

9) Neutrino oscillations, SUSY seesaw mechanism and charged lepton flavor violation
F. Deppisch, H. Päs, A. Redelbach, R. Rückl, Y. Shimizu,
in Proc. *RADCOR 2002 - 6th International Symposium on Radiative Corrections*,
Kloster Banz, Germany, September 8-13, 2002,
Nucl. Phys. Proc. Suppl. **116** 316 (2003),
Auch in: *Staffelstein 2002, Application of quantum field theory in phenomenology* 316-
320,
e-Print Archiv: hep-ph/0211138

10) LFV constraints on the Majorana mass scale in mSUGRA
F. Deppisch, H. Päs, A. Redelbach, R. Rückl, Y. Shimizu,
in Proc. *SUSY02 - 10th International Conference on Supersymmetry and Unification
of Fundamental Interactions*, 1012-1017, DESY, Hamburg, June 17-23, 2002,
e-Print Archiv: hep-ph/0210407

